



**Study and discovery of TASK–potassium channel modulators:
A theoretical and experimental approach.**

by

DAVID MAURICIO RAMÍREZ SÁNCHEZ

This thesis is submitted for the degree of
Ph.D. in Applied Sciences

Supervisor: **Dr. Wendy González**

Co-supervisors: **Dr. Julio Caballero**

Dr. Niels Decher

Talca, Chile

November 2016


UNIVERSIDAD DE TALCA

**AUTORIZACIÓN PARA LA PUBLICACIÓN
DE MEMORIAS DE PREGRADO Y TESIS DE POSTGRADO**

Yo, **David Mauricio Ramírez Sánchez**, cédula de Identidad N° 24300408-k, autor de la memoria o tesis que se señala a continuación, **SI** autorizo a la Universidad de Talca para publicar en forma total o parcial, tanto en formato papel y/o electrónico, copias de mi trabajo.
Esta autorización se otorga en el marco de la Ley N° 20.435 que modifica la Ley N° 17.336 sobre Propiedad Intelectual, con carácter gratuito y no exclusivo para la Universidad.

Título de la memoria o tesis:	Study and discovery of TASK-potassium channel modulators: A theoretical and experimental approach
Unidad Académica:	Facultad de Ingeniería e Instituto de Química de Recursos Naturales
Carrera o Programa:	Doctorado en Ciencias Aplicadas
Título y/o grado al que se opta:	Doctor en Ciencias Aplicadas
Nota de calificación	7

Timbre Escuela

Firma de Alumno	
Rut:	<u>24300408 - K</u>
Fecha:	<u>Sep / 06 / 2018</u>

Study and discovery of TASK–potassium channels modulators:**A theoretical and experimental approach.**

Two-pore domain potassium (K_{2p}) channels underlie the background K^+ currents in mammalian cells; these can be segregated into six subfamilies based on their structure and functional properties. The acid-sensitive TASK-1 and TASK-3 channels belong to the TASK subfamily. TASK channels contribute to the central respiratory chemosensitivity and are also relevant for neuronal excitability. TASK-3 is an oncogenic potassium channel and it is overexpressed in breast and ovarian tumors. Development of compounds that selectively modulate K_{2p} channels such as TASK-1 and TASK-3 is crucial to assess the efficacy of therapies targeting these interesting proteins.

In the present work several computational methodologies such as homology modeling, molecular dynamics simulations, virtual screening, docking, binding free energy calculation, etc.; as well as electrophysiological techniques like such as two electrode voltage clamp (TEVC) and Fluorometric imaging plate reader – Membrane potential assay (FLIPR–MPA) were employed to: 1) understand why potassium voltage-gated channel ($Kv1.5$) blockers preferentially inhibit TASK-1 channels. Our results described how $Kv1.5$ blockers, like AVE0118 and AVE1231, which are promising drugs against atrial fibrillation or obstructive sleep apnea, are in fact potent TASK-1 blockers. Accordingly, the TASK-1 channels blockage by these compounds might contribute to the clinical effectiveness of these drugs. 2) To study the role of the fenestrations (side-opening facing the membrane) in the binding of A1899 to TASK-1 potassium channel; our results showed that A1899 binds tightly to structures with open fenestrations and demonstrated that A1899 cannot travel from the membrane through the fenestrations to reach the binding site. Finally, 3) to structure-based discovered novel TASK-3 modulators; our results allowed the identification of two lead ligands showing inhibition of 40.6 μM and 43.1 μM against TASK-3. For this reason, the conserved pharmacophore described in this work, and the novel chemical characteristics of this chemical class makes them good candidates for future development into highly potent TASK-3 modulators through medical chemistry optimization.

In this work we present findings regarding the understanding of the structural mechanism of TASK channels blockage through a theoretical–experimental approach. This gained knowledge will allow us to propose novel modulators that might aid unraveling the physiological functions of TASK channels in their sites of expression in native organs and cells.

Estudio y Diseño de Moduladores de Canales de Potasio – TASK.**Aproximación Teórico – Experimental.**

Los canales de potasio de dos dominios de poro (K_{2p}) son responsables de fugas de corrientes en células de mamíferos. Estos canales se pueden categorizar en seis subfamilias basados en su estructura y función. Los canales sensibles a pH, TASK-1 y TASK-3 pertenecen a la familia TASK; estos canales contribuyen a la quimiosensibilidad y son relevantes en la excitabilidad neuronal. TASK-3, particularmente, es un oncogén y se encuentra sobre-expresado en cáncer de seno y de ovario. El desarrollo de nuevos compuestos que modulen selectivamente canales K_{2p} como TASK-1 y TASK-3 es fundamental para evaluar la eficacia de las terapias dirigidas a estas interesantes proteínas.

En el presente trabajo se emplearon múltiples metodologías computacionales como modelamiento por comparación, simulaciones de dinámica molecular, cribado virtual, acoplamiento molecular, cálculo de energía libre, etc.; así como también técnicas experimentales (electrofisiología) para: 1) comprender por qué ciertos bloqueadores de canales de potasio dependientes de voltaje (Kv1.5) inhiben preferencialmente los canales TASK-1. Nuestros resultados describen cómo los bloqueadores de Kv1.5, como AVE0118 y AVE1231, los cuales son potenciales fármacos contra fibrilación atrial o apnea obstructiva del sueño, son potentes bloqueadores de canales TASK-1. Por consiguiente, el bloqueo de TASK-1 por estos compuestos podría contribuir en la mejora de la efectividad clínica de estos fármacos. 2) Estudiar el rol de las fenestraciones (cavidades laterales hacia la membrana) en el modo de unión del bloqueador A1899 en canal de potasio TASK-1; nuestros resultados mostraron que A1899 se une fuertemente a estructuras con las fenestraciones abiertas, también revelan que A1899 no accede al sitio de unión desde la membrana por medio de las fenestraciones. Finalmente, 3) desarrollar nuevos moduladores de TASK-3 basados en la estructura de bloqueadores reportados; nuestros resultados nos permitieron identificar dos ligandos con actividad inhibitoria de $40.6 \mu M$ y $43.1 \mu M$ contra TASK-3. El farmacóforo conservado descrito en este trabajo, y las características químicas de estos nuevos compuestos los convierten en buenos candidatos para el futuro desarrollo de potentes moduladores de TASK-3 mediante optimización usando química medicinal.

En este trabajo se presentan resultados que permiten la comprensión del mecanismo estructural del bloqueo de canales TASK mediante una aproximación teórico-experimental. Este conocimiento permite proponer nuevos moduladores que podrían ayudar a entender las funciones fisiológicas de estos canales en sus sitios de expresión en órganos y células.

DEDICATION

This dissertation is lovingly dedicated to my mother, her support, encouragement, and constant love have sustained me throughout my life; to my brother, who has been a constant source of inspiration in professional and personal stage; to my family who have always loved me unconditionally and whose good examples have taught me to work hard for the things I aspire to achieve; and to my love, Claudia, who has been a constant source of support and encouragement during the challenges of life. I am truly thankful for having you in my life.

ACKNOWLEDGEMENTS

I am deeply indebted to my adviser Wendy González for her fundamental role in my doctoral research. Wendy provided me with every bit of guidance, assistance, and expertise I needed during my studies; she gave me the freedom to develop and explain my ideas, but always guided me to achieve all the goals proposed. In addition to our academic partnership, I truly admire her dedication and commitment in both, professional and personal fields.

I would like to thank the Center for Bioinformatics and Molecular Simulation at the Universidad de Talca, especially Julio Caballero and Jans Alzate, for the substantial influence that they have had on my research. I gratefully acknowledge the members of my Ph.D. committee for their time and valuable feedback in this work. Among many other things, I am thankful to Niels Decher due to all his contributions in this research and for inviting me to improve my knowledge and get to know his Lab at the University of Marburg, as well as our fruitful collaboration there. I would like to express my sincere gratitude to Claudia Daza for her assistance with the English revision of this manuscript.

Finally, I would like to thank my friends in the Center for Bioinformatics and Molecular Simulation and the Universidad de Talca as well as everyone that I met in Chile during my doctoral studies, I am sure we will be friends for several years.

CONTENTS

1. Introduction.	1
2. State of Art.	3
2.1. Overview.	3
2.2. K _{2P} channels topology and structure.	5
2.3. TASK subfamily physiology.	9
2.4. TASK channels pharmacology.	10
3. Hypothesis.	13
4. Objectives.	14
5. Chapter I: Kv1.5 blockers preferentially inhibit TASK-1 channels: TASK-1 as a target against atrial fibrillation and obstructive sleep apnea?	15
5.1. Introduction.	15
5.2. Materials and Methods.	17
5.3. Results.	18
5.4. Discussion.	27
5.5. Future work.	31
5.6. Scientific production.	32
6. Chapter II: Side fenestration provide and ‘anchor’ for stable binding of A1899 to the pore of TASK-1 potassium channels.	33
6.1. Introduction.	33
6.2. Materials and Methods.	35
6.3. Results.	40
6.4. Discussion.	51
6.5. Future work.	54
6.6. Scientific production.	55
7. Chapter III: Structure-based discovery of potential two-pore domain potassium channels TASK-3 modulators.	56
7.1. Introduction.	56
7.2. Materials and Methods.	59
7.3. Results.	65
7.4. Discussion.	77
7.5. Future work.	81
7.6. Scientific production.	82
8. Chapter IV: Additional Studies.	83
9. Concluding Remarks.	91
10. References.	93
11. Appendix A: Abbreviations and acronyms.	108
12. Appendix B: Supplemental information of Chapter II.	111
13. Appendix C: Supplemental information of Chapter III.	123

LIST OF FIGURES

Figure 1. K_{2P} subfamilies in <i>Homo sapiens</i> .	4
Figure 2. K_{2P} channels topology.	5
Figure 3. Architecture of K_{2P} channels.	6
Figure 4. Chemical structures of Kv1.5 blockers and their affinity for Kv1.5 and TASK-1.	19
Figure 5. Sequence alignment and cartoon illustrating the drug binding site of Kv1.5 and TASK-1.	21
Figure 6. The drug binding sites of Kv1.5 and TASK-1 illustrated in pore homology models.	23
Figure 7. Diameter of the cytosolic opening to the central cavity and analysis of the frequency-dependent inhibition of Kv1.5 and TASK-1.	25
Figure 8. Common pharmacophore for the TASK-1 blockers AVE0118, S20951 (A1899), S9947, AVE1231 (A293), and MSD-D.	26
Figure 9. Characterization of the side fenestration in TASK-1 models.	41
Figure 10. Ordering of A1899 docking solutions in TASK-1 by cluster analyses.	44
Figure 11. Ordering A1899 poses of significant clusters by their free binding energy.	45
Figure 12. Contacts of A1899 with residues of the TASK-1 binding site and the nature of the chemical interaction.	47
Figure 13. Redefined binding mode of A1899 in TASK-1 includes residues that contribute to the side fenestrations.	48
Figure 14. A1899 stabilizes the pen fenestration of TASK-1.	49
Figure 15. A1899 does not pass the side fenestration to reach the binding site.	50
Figure 16. RMSD for backbones of TASK-3 models during MD simulations.	66
Figure 17. Fenestration states in T3trCO.	67
Figure 18. Common e-Pharmacophore for the TASK-3 reported blockers $_K$ -THPP, A1899, Doxapram, Loratadine and L-703,606.	69
Figure 19. Biological activity validation.	71
Figure 20. DR6 binding mode.	73
Figure 21. DR17 binding mode.	75
Scheme 1. Systematic representation of the workflow to identify TASK-3 modulators.	58

LIST OF TABLES

Table 1. Nomenclature of the TASK-1 homology models.	36
Table 2. TASK-1 residues in the fenestration (F) and the Pore during the MDs – HOLE results.	42
Table 3. Significant clusters in TASK-1 models.	43
Table 4. Nomenclature of the TASK-3 homology models.	59
Table 5. Reported TASK-3 modulators.	61
Table 6. e-Pharmacophore hypotheses.	69
Table 7. Ligands hits interacting with TASK-3 homology models.	70
Table 8. Location of the interacting residues of DR6 and DR17 in TASK-3 models.	72
Table 9. Physicochemical descriptor calculated by QikProp simulation.	76
Table 10. Pharmacokinetics properties predicted by QikProp simulation.	77

1. INTRODUCTION

Ion channels are biological targets of many pharmacological therapies. Worldwide sales of ion channel-targeted drugs are estimated to be approximately US\$ 12 billion per year, and there is a reason for cautious optimism for the future of ion channel drug discovery: nowadays about 60 ion channel modulators have entered Phase II/III of clinical studies (Wickenden, et al., 2012). Only 10% of these modulators in Phase II/III target a potassium channel (K^+), and none of them target a leak channel such as two-pore domain K^+ channels (K_{2p}).

K_{2p} channels have been widely studied since the gene family KCNK – those that codify the K_{2p} channels- was described (Goldstein et al., 2001), giving an insight into the understanding of the physiological role of these ion channels. These channels form dimers of pore-forming subunits that produce background conductances which are finely regulated by a range of natural and chemical effectors. The TASK subfamily (*tandem of pore domains in a weak inwardly rectifying K^+ channel [TWIK]-related acid-sensitive K^+ channel*) is integrated by 3 members (TASK-1, -3 and -5) (Cotten 2013b). TASK-1 and -3 channels play an important role in physiological conditions and exhibit high sensitivity to extracellular pH changes (between 6 and 7) (Rajan et al. 2000; González et al. 2013; Zúñiga et al. 2011).

TASK channels have been associated to several physiological processes in the cardiovascular system (Putzke et al. 2007), central nervous system (Budde et al. 2008) and the adrenal gland (Czirják et al., 2000). Additionally, these channels are involved in the peripheral chemosensory control of breathing (Trapp et al., 2008) and in the regulation of the immune system (Meuth et al. 2008). TASK-1 is an important modulator of multiple sclerosis (Bittner et al. 2010) and influence the T lymphocyte effector functions (Meuth et al. 2008). Besides, TASK-1 is present in many different tissues (pancreas, placenta, kidney, lung, liver, ovary, prostate, and small intestine), where contributes to maintain the resting membrane potential (Lesage & Lazdunski 2000). This modulation appears to be important

in a number of physiological contexts, including the transmission and anesthetic regulation of neuronal activity (Talley & Bayliss 2002). TASK-1 and TASK-3 have been verified as oncogenes (Huang et al., 2014). TASK-3 overexpression accelerates human tumor formation such as in ovarian (Innamaa et al. 2013) and breast tumors (Mu et al. 2003). TASK-3 is fundamental in various cellular functions including the modulation of aldosterone secretion in the adrenal cortex (Guagliardo et al. 2012). For these reasons, the rational drug design targeting TASK-1 and -3 channels might have influence in the pharmaceutical therapy of several pathogenic conditions related with the cardiovascular and the central nervous systems.

In the present work several theoretical (homology modeling, virtual screening, docking, molecular dynamics simulation, binding free energy, etc.) and experimental (Two Electrode Voltage Clamp (TEVC) and Fluorometric imaging plate reader – Membrane potential assay (FLIPR–MPA) approaches were employed to: 1) understand why some potassium voltage-gated (Kv1.5) channel blockers preferentially inhibit TASK-1 channels; 2) to comprehend the role of the side-fenestrations (open cavities facing the membrane) for the binding of the blocker A1899 to TASK-1; and 3) to rational drug design novel TASK-3 modulators.

2.1. Overview

Two-pore domain potassium channels (K_{2p}) mediate background K^+ conductance, which control the excitability of the cells. The human genome contains 15 KCNK genes coding proteins able to form K_{2p} channels (González et al., 2015). These are subdivided into 6 subfamilies (TWIK, TREK, TASK, TALK, THIK, and TRESK) on the basis of their sequence similarities and functional properties (Fig. 1). The members of TASK (TWIK-related Acid Sensitive K^+ channels) subfamily such as TASK-1 and TASK-3 are inhibited by extracellular acidification (O'Connell et al., 2002). They share 55-60% sequence identity within different mammalian species (Bayliss & Barrett 2009). The remarkable difference between both channel sequences is: TASK-1 (K70 and M247) and TASK-3 (E70 and L247). These residues are involved in the binding site of blocking compounds (Clarke et al., 2008; Czirják & Enyedi, 2003; Streit et al., 2011).

Currently, multiple nomenclatures for human two-pore domain potassium channels are in use. The Human Genome Organization (Gray et al. 2012; HUGO 2014) use the gene names (KCNK) preceded by a number reflecting the discovery order of each one of the genes. The International Union of Basic and Clinical Pharmacology (IUPHAR 2014) adopted a very similar scheme for naming the cognate channels, replacing the KCNK with K_{2p} prefix. A third naming scheme (most popular) employs a set of acronyms based on salient physiological or pharmacological properties. The acronyms are as follows: **TWIK**: *Tandem of P domains in a Weak Inwardly rectifying K^+ channel*; **THIK**: *Tandem pore domain Halothane Inhibited K^+ channel*; **TREK**: *TWIK-Related K^+ channel gene*; **TRAAK**, *TWIK-Related Arachidonic Acid stimulated K^+ channel*; **TASK**: *TWIK-related Acid Sensitive K^+ channel*; **TALK**, *TWIK-related Alkaline pH activated K^+ channel* and **TRESK**, *TWIK-Related Spinal cord K^+ channel* (Bayliss & Barrett, 2009; Talley, et al., 2003). The third naming scheme (acronyms) will be used in the present work.

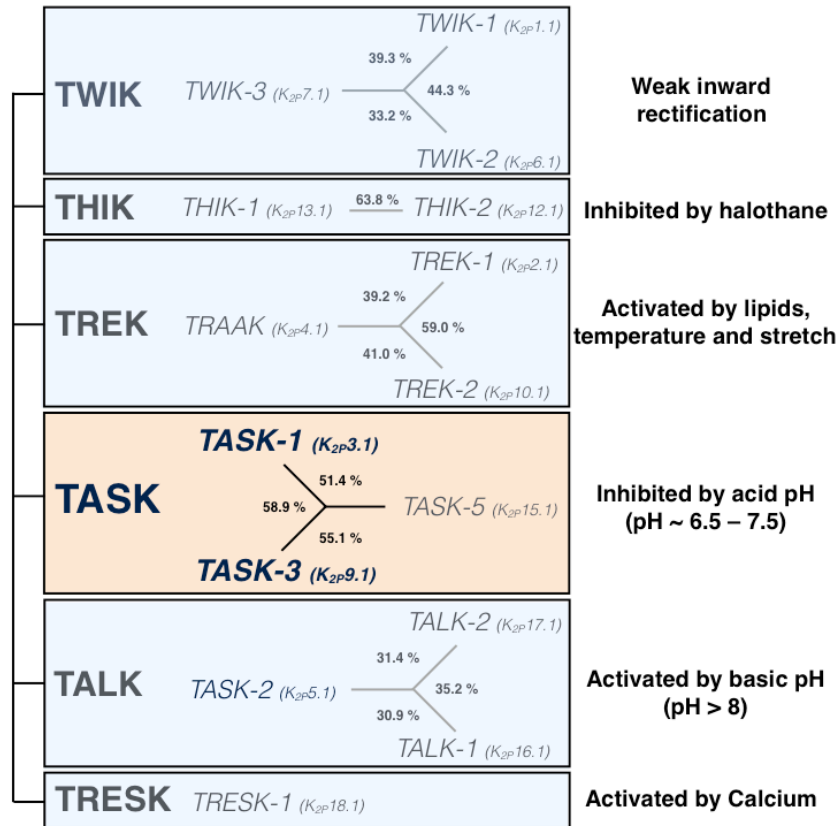


Figure 1. K_{2P} subfamilies in *Homo sapiens*. The 15 know human K_{2P}-genes are placed into six subgroups; the % sequence identity is given for the members of the subfamilies. (Taken and adapted from Bayliss & Barrett, 2009).

K_{2P} channels have been identified in mammals, plants, and other organism. In plants for instance, the genome of the model plant *Arabidopsis thaliana* harbors five genes coding for K_{2P} channels (TPK1-5, for tandem-pore K⁺, named here as AtTPKs). Orthologs of AtTPKs are found in all higher plants sequenced so far. In contrast, in algae, they have only been found in the chlorophyte *Ostreococcus* (Voelker et al. 2010). Although AtTPKs share their topology with human K_{2P} channels, their sequence identities and similarities are low, varying between 5.9% and 18.9% for identity and 12.1% and 31.7% for similarity (González et al. 2015). In this regard, our group was wondering which are the similarities and differences between K_{2P} channels in plants and animals in terms of their physiology? And, what is the nature of the last common ancestor (LCA) of these two groups of proteins? In order to answer these questions, we reviewed and presented physiological, structural, and phylogenetic evidence, which discards the hypothesis proposing that the

duplication and fusion that gave rise to the K_{2P} channels occurred in a prokaryote LCA. Conversely, we argue that the K_{2P} LCA was most likely an eukaryote organism. Our findings showed that comparative studies on animal and plant K_{2P} channels will move the field forward and will broaden our knowledge regarding the evolution, physiological role, and molecular mechanisms of the regulation of these fascinating classes of ion channels in all branches of the tree of life (González et al. 2015).

2.2. K_{2P} channels topology and structure

The name of the family, “two-pore domain” potassium channels, describes the unique topology of the K^+ channel subunits. Each subunit contains two pore-forming domains (P1, P2), four transmembrane segments (M1-M4) and one extended extracellular loop between M1 and P1 (Fig. 3A) (Bayliss & Barrett 2009). The N- and C-terminal domains are exposed to the cytoplasmic space (Lesage & Lazdunski 2000). In contrast to the other K^+ channel families characterized by one pore domain *per* subunit, like Kv1.3 (Sabogal-Arango et al., 2014). The N- and C-terminal domains of K_{2P} channels are exposed to the cytoplasmic space (Lesage & Lazdunski 2000) (Fig. 3A). Both pore regions (P1, P2) have the conserved **TXGXXG** motif, known to form the selectivity filter, a signature sequence characteristic for all potassium-selective channels (O’Connell et al. 2002), where X denotes a hydrophobic amino acid (Fig. 3B).

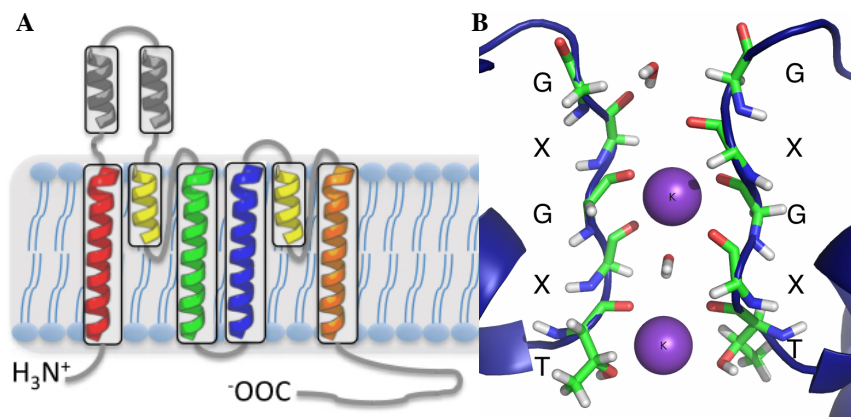


Figure 2. K_{2P} channels topology. **A.** Each subunit contains two pore forming domains: P1 and P2 (yellow); four transmembrane segments: M1 (red), M2 (green), M3 (blue) and M4 (orange); and one extended extracellular loop between M1 and P1 (gray). **B.** Conserved **TXGXXG** motif present in selective K^+ channels.

The recently released K_{2P} channels crystals allow to describe the unique topology and structure of these ion channels and also to understand how and why K_{2P} channels have different conformations in the membrane. The first K_{2P} channel crystals were deposited in the PDB in 2012 by Miller & Long (Miller & Long 2012) and by Brohawn et al. (Brohawn et al. 2012). They obtained the 3D structure of TWIK-1 (PDB ID: 3UKM) and TRAAK (PDB ID: 3UM7) respectively. These crystals revealed a unique cap structure formed by the two large extracellular linkers from the M1 to the pore loop (M1-P1 linker) (Goldstein et al. 2016); this cap forms two extracellular ion pathway (EIP) at both sides of the SF entrance (Fig. 3). The crystals channels also showed two open cavities facing the membrane known as side-fenestrations; these fenestrations are also present in other ion channels like the voltage-gated sodium channel (Kaczmarek & Corry 2014; Payandeh et al. 2012) and are one of the main research topic in rational drug design targeting K_{2P} channels. Later, in 2013 Brohawn et al. (Brohawn et al. 2013) deposited other TRAAK crystal structure (PDB ID: 4I9W), but this time the conformation of the TRAAK channel was different, with one fenestration opened and the other closed, this structure also revealed a domain-swapped chain connectivity enable by the cap that exchange two opposing outer helices 180° around the channel.

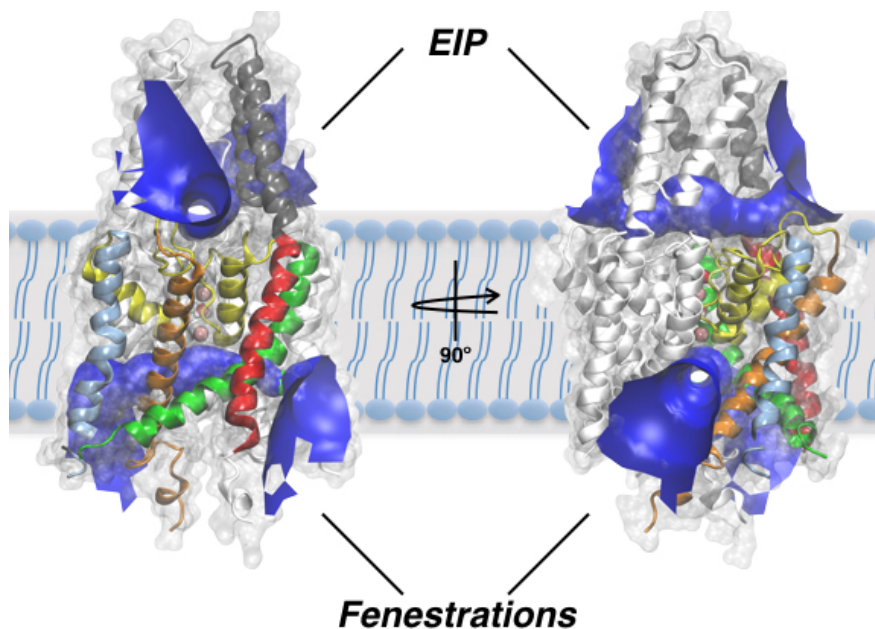


Figure 3. Architecture of K_{2P} channels. Three-dimensional structure of human TWIK-1 channel shown with one subunit colored (according to the topology of Fig. 2). Extracellular ion pathway (EIP) and side-fenestration are shown as blue surface. TWIK-1 is rotated 90° for better representation.

The functional role of the cap is poorly understood and it remains unclear whether the cap of K_{2p} channels assembled in a domain-swapped orientation or not. Recently, our group aimed at the understanding of the structural differences between the K_{2p} channels, which exhibits the cap stabilized by a disulfide-bridge (Lesage et al. 1996; Brohawn et al. 2012; Miller & Long 2012; González et al. 2013; Dong et al. 2015) and the K_{2p} channels that do not contain a disulfide-bridge in the extracellular cap, like TASK-1 and TASK-3. Functional mutagenesis screens together with the structures of crystallized K_{2p} channels as templates were used to build an experimentally validated model of the disulfide-bridge free cap structure of TASK-1. Moreover, we alanine-screened the TRAAK M1-P1 linker to identify residues relevant for homomerization and additionally investigated the role of cysteine residues in the M1-P1 loop of other K_{2p} channels. Our data suggest that the cysteine residues in the cap structure of K_{2p} channels are less important for channel assembly than expected. In particular for TASK-1, using a domain-swapped K_{2p} channel crystal structure as a template for the modeling, we can show that the cap is stabilized by a defined set of hydrophobic intersubunit interactions, which are primarily present near the tip of the cap. Our data indicate that TASK-1 channels might primarily assemble in the domain-swapped orientation, and our functional data obtained with TRAAK could be reconciled with the existence of both channel variants crystallized. We proposed that hydrophobic residues at the inner leaflets of the cap domains can interact with each other and that this way of stabilizing the cap is most likely conserved among K_{2p} channels (Goldstein et al. 2016).

In 2014, Brohawn et al. (Brohawn, et al. 2014) propose a physical mechanism for gating and mechanosensitivity of the human TRAAK channel. In these TRAAK crystal structures (PDBs: 4WFE, 4WFF, 4WFG and 4WFH) the K^+ ion occupancy was associated with the conductance of the K_{2p} channels as well as the conformation of the side-fenestration. The K^+ ions in the TRAAK crystals 4WFE and 4WFG were found at positions S1, S2, S3, S4 at the selectivity filter (SF) and in the inner cavity, but the K^+ ions in the crystals 4WFF and 4WFH were found only at S1, S2, S3 and S4. The crystal structures where K^+ ion was found at the inner cavity have the side-fenestration closed; for this reason, the closed side-fenestration was associated with the “conductive state”, and the open side-fenestration with the “non-conductive state”. It was also described how in the

non-conductive state a lipid acyl chain might access the central cavity through the side-fenestration to sterically block the K^+ ion flux. In the conductive state, conformational changes in the transmembrane helix seal the side-fenestration to prevent lipid access, and allow the ion conduction through the channel; in this proposed mechanism the transmembrane segments M2, M3 and M4 are implicated. Finally, Dong et al. deposited (2013) the structure of TREK-2 (PDB ID: 4BW5) with both fenestrations closed and with the cap in a domain-swapped conformation (Dong et al. 2015); in 2014 they deposited the crystal structure of TREK-1 (PDB ID: 4TWK) with the same conformation (both fenestrations closed and domain-swapped) and in 2015 deposited other 3 crystal structures of TREK-2, all of them with the domain-swapped and both fenestrations opened without ligand (PDB ID: 4XDJ), in complex with norfluoxetine (PDB ID: 4XDK), and in complex with brominated fluoxetine (PDB ID: 4XDL) (Dong et al. 2015). These last structures revealed insights about the binding site of the crystallized ligands and the role of the fenestrations in the binding mode and ion conductivity because the conductive and non-conductive states of TREK-2 were also associated (as it was associated for TRAAK) with the ion occupancy at the selectivity filter. In this study, Dong et al. also studied the coordinated movement of all three involved helices (M2-M4) by Molecular Dynamics simulations (MDs). These simulations exhibit a downward movement of M2, M3, and M4 from the non-conductive state (side-fenestration open) to adopt a conformation similar to the conductive state (side-fenestration closed), thus indicating that movement between states can occur. They described for the very first time (by crystal structures) the binding site of drugs such as norfluoxetine and brominated fluoxetine with a K_{2p} channel. These drugs bind within the side-fenestration but neither ligand extended into the inner cavity to block the ion path directly. The fenestration provides a hydrophobic environment close to the SF in which both ligands promote the non-conductive state (open fenestrations) (Dong et al. 2015). It was also described for TWIK-1 by MDs how the movement of the transmembrane segments to open the fenestrations creates a hydrophobic barrier deep within the inner pore restricting full hydration of the inner cavity and therefore generating an energetic barrier limiting ion permeation through these channels (Aryal, et al., 2014).

2.3. TASK subfamily physiology

The TASK subfamily of K_{2p} channels includes TASK-1, TASK-3 and TASK-5 (Fig. 1) with 394 amino acids (aa) (Duprat et al. 1997), 374 aa (Rajan et al. 2000; Vega-Saenz de Miera et al. 2001) and 330 aa (Kim & Gnatenco 2001) respectively. In humans, TASK-1 shares 58.9% of identity with TASK-3 and 51.4% with TASK-5, TASK-3 shares the 55.1% of identity with TASK-5. In other K_{2p} channels, for instance TREK subgroup, TREK-1, TREK-2 and TRAAK shared between 39.2% and 59.0% of identity; in other subfamilies like TWIK and TALK, the identity is about 44.3% and 35.2% respectively. The sequence conservation between K_{2p} subgroups is comparable to the one between channels from other K^+ channel families like K_v and Kir (Brohawn et al. 2012).

Some studies have demonstrated that TASK-1 and TASK-3 channels participate in the chemical control of breathing due to their intrinsic pH and O_2 sensitivity (Bayliss et al. 2001; Talley et al. 2003). The two channels play an important role in the central nervous system but also in the cardiovascular system (Goldstein et al. 2001). They are involved in the regulation of the immune system (Meuth et al. 2008) and play a role in sensing acidosis and hypoxia in glomus cells of the carotid body (Ortega-Sáenz et al. 2010). Adrenal gland is also a major site for TASK-1 and TASK-3 expression in both rodents and humans. TASK-1 null mice (*task1*^{-/-}) shows hyperaldosteronism, a pathological condition where an excess of aldosterone is produced by the adrenal gland (Heitzmann et al. 2008). TASK-1 and TASK-3 channels are also relevant for neuronal excitability, confirmed by the fact that *task1*^{-/-} and *task3*^{-/-} mice show a substantial decrease in halothane-induced analgesia and immobilization. Both channels are activated by this volatile anesthetic (Talley & Bayliss 2002). Besides, *task3*^{-/-} mice exhibit pronounced sleep disorders and a marked reduction in the sensitivity to the halothane hypnotic effects (Pang et al. 2009).

TASK-1 is present in many different tissues (pancreas, placenta, kidney, lung, liver, ovary, prostate, and small intestine), where contributes to maintain the resting membrane potential (Lesage & Lazdunski 2000). This modulation appears to be important in a number of physiological contexts, including the transmission and anesthetic regulation of neuronal activity (Talley & Bayliss 2002). TASK-3 has also brought considerable attention as a channel involved in carcinogenesis and tumor progression. TASK-3 was verified as an

effective oncogene; its overexpression accelerates breast tumor formation and confers resistance to both hypoxia and serum deprivation (Mu et al. 2003). Point mutations that abolished TASK-3 potassium channel activity abrogate these oncogenic functions (Pei et al. 2003) and TASK-3 blockers caused a significant reduction in cell proliferation and an increase in apoptosis in ovarian cancer cell lines (Innamaa et al. 2013).

2.4. TASK channels pharmacology

TASK channels are insensitive to typical K^+ channel blockers as Cs^+ , tetraethylammonium (TEA) and 4-aminopyridine (4-AP) (Czirják et al. 2000; Meadows & Randall 2001). These channels are regulated by a diversity of molecules as neurotransmitters (Talley et al. 2000), hormones (Czirják et al. 2000) alkaloids (Millar et al. 2000), cannabinoids (Maingret et al. 2001), divalent cations (Czirják & Enyedi 2002) and anesthetics (Patel et al. 1999); none of these compounds are selective for TASK channels. TASK channels are stimulated by halothane at the C-terminal in the regions described like Halothane Response Element (HRE). 0.1 – 1.0 mM of halothane increases more than 60% TASK-1 channel activity and 1.0 mM of halothane increases 66% TASK-3 channel activity (Patel et al. 1999; Meadows & Randall 2001). Regarding the study of the K_{2p} channels blockage, several authors have been studying the effect of local anesthetics such as bupivacaine in K_{2p} channels like TASK, TREK and TALK channels (Coburn et al. 2012; Chokshi et al. 2015; Nayak et al. 2009; Kindler et al. 1999; Kindler et al. 2003; Goldstein et al. 2001; Kim 2005); this compound is a voltage-dependent blocker inhibiting TASK1 ($IC_{50} = 41 - 68 \mu M$) and TASK-3 ($IC_{50} \approx 100 \mu M$) channels (Lotshaw 2007). Bupivacaine presumably binds TASK-1 channels at the side-fenestrations (data not published) making it a perfect candidate for the study of the role of the fenestrations in the modulation of TASK.

There are other molecules capable to bind TASK channels at the EIP such as Zn^{2+} and Red Ruthenium (RR). Zn^{2+} blocks selectively TASK-3 under physiological conditions, by binding the residues H98 and E70 (Clarke et al., 2008). Our group showed that inhibition of TASK-3 by Zn^{2+} , just as pH_o gating, is cooperative and strongly impeded by increasing extracellular K^+ concentration. MDs experiments suggest that two Zn^{2+} ions might plausibly bind at sites defined by neutral H98 side chains flipped upwards into the

EIP at both sides of the SF entrance. Blockade of TASK-3 by Zn^{2+} and RR are K^+ -dependent and show virtual voltage independence, as expected from an interaction with superficial sites at the selectivity filter. Both E70 and H98 are proposed to form the blocker-binding site. It is also possible that E70 side chain additionally favors the interaction of the blockers by increasing their local concentration electrostatically (González et al. 2013).

It has recently been reported that organic compounds such as A293 (Putzke et al. 2007) and A1899 (Streit et al. 2011); ML308 (Miller et al. 2013) and pyrido[4,3-d]pyrimidine derivatives (Coburn et al. 2012) are selective inhibitors for TASK-1 and TASK-3 channels, respectively. Recently, Noriega-Navarro et al. (Noriega-Navarro et al. 2014) reported the application of dihydropyrrolo[2,1-a]isoquinoline derivatives (DPIs) as novel TASK inhibitors. Doxapram, in the other hand, blocks TASK-1 with $IC_{50} = 0.4 \mu M$ (Cotten et al. 2006) and TASK-3 with $IC_{50} = 23 \mu M$ (Cotten 2013b; Chokshi et al. 2015) Bruner et al. described several compounds presenting inhibitory activity against TASK-3, such as: Loratadine ($IC_{50} = 63.4 \mu M$), mibefradil ($IC_{50} = 24.6 \mu M$), oligomycin A ($IC_{50} = 47.7 \mu M$), octoclothepein ($IC_{50} = 73.8 \mu M$), L-703,606 oxalate ($IC_{50} = 45.5 \mu M$), mevastatin ($IC_{50} = 159 \mu M$), dihydro-beta-erythroidine ($IC_{50} = 73.8 \mu M$) and GW2974 ($IC_{50} = 50.1 \mu M$) (Bruner et al. 2014).

Previous studies done altogether by Decher's and González's Labs have shown that some known aromatic Kv1.5 blockers studied by the pharmaceutical industry (Sanofi-Aventis GmbH - Patent WO2007/124849) are more effective on TASK-1 than on Kv1.5 channel. The drug binding to TASK-1 and Kv1.5 is caused by binding lipophilic residues which are facing the central cavity. Despite the physicochemical and sterical similarities in the two drug binding sites, there are clear differences in their geometry, primarily arising from the dimeric structure of TASK-1 versus the 4-fold symmetry of Kv1.5 channel (see chapter I) (Kiper et al. 2015). The most efficient aromatic Kv1.5 blocker in TASK-1 is A1899; it is 68-fold times more effective on TASK-1 than on Kv1.5 (Kiper et al. 2015), blocking TASK-1 channel expressed in CHO cells with an $IC_{50} = 7 \text{ nM}$; while A1899 blocks TASK-3 channel with an $IC_{50} = 70 \text{ nM}$. The binding site of A1899 in TASK channels has been already identified: the unique difference between TASK-1 and TASK-3 is a Met247 residue, TASK-3 has a Leu in this position (Streit et al. 2011). A1899 binds in

the inner cavity and presumably other aromatic molecules such as THPP compounds are also intracellular blockers of TASK channels. THPP analogues are TASK-3 channel antagonists described in 2012 by Coburn et al. (Coburn et al., 2012). They are based on 5,6,7,8- TetraHydroPyrido [4,3-d] Pyrimidine (THPP) and the best compound (PK-THPP) present an $IC_{50} = 35$ nM against TASK-3. In this sense, the use of fused heterocyclic-compounds has attracted the attention as new TASK blockers. Therefore, it is necessary the development of simpler theoretical/experimental methodologies to find new heterocyclic derivatives with potential applications as TASK modulators.

3. HYPOTHESIS

According to the state of art presented for TASK channels, their topology, structure, physiology as well as their pharmacology and the reported blockers, the present research work is focus on the following hypothesis:

“Through a theoretical and experimental approach, it is possible to describe the molecular basis of the intracellular blockage of the two-pore domain potassium channels TASK, identifying novel modulators and obtaining potential therapeutic inhibitors”

4.1. Main Objective:

To understand the molecular basis of the intracellular blockage of the two-pore domain potassium channels TASK through a theoretical and experimental approach.

4.2. Specific Objectives:

- 4.2.1. To understand why potassium voltage-gated channel (Kv1.5) blockers preferentially inhibit TASK-1 channels (Chapter I).
- 4.2.2. To study the role of the fenestrations (side-openings facing the membrane) in the binding of A1899 to TASK-1 potassium channel (Chapter II).
- 4.2.3. To discover structure-based novel TASK-3 modulators (Chapter III).

Kv1.5 blockers preferentially inhibit TASK-1 channels: TASK-1 as a target against atrial fibrillation and obstructive apnea

5.1. Introduction

Atrial fibrillation and obstructive sleep apnea are among the most prominent diseases in the elderly and responsible for significant morbidity, health care costs, and mortality in the industrialized world (Tarasiuk & Reuveni 2013; Wolf et al. 1998). Drugs currently available for the treatment of these two diseases lack effectiveness and/or specificity. Accordingly, there is a high medical need for novel drugs targeting atrial fibrillation or obstructive sleep apnea. For both diseases, Kv1.5 channels have emerged as promising drug targets.

To avoid ventricular side effects, complicating the therapy of atrial fibrillation, current drug design focuses on atrial specific targets, including the atrial sodium channel (Burashnikov et al. 2012), G protein-gated potassium channel (Dobrev et al. 2005), and voltage-gated potassium channel Kv1.5 (Decher et al. 2006; Decher et al. 2004). Kv1.5 channels are highly expressed in human atria, but not ventricle, and are the major constituents of the delayed rectifier sustained outward current ($I_{K_{sus}}$) that contributes to action potential repolarization of human atrial myocytes (Fedida et al. 1993; Wang et al. 1993). The two-pore domain potassium (K_{2p}) channel TASK-1 also contributes to human atrial $I_{K_{sus}}$ albeit to a lesser extent than Kv1.5 (Limberg et al. 2011). TASK-1 was also discussed as a target for the treatment of atrial fibrillation due to its atrial specific expression (Limberg et al. 2011). In a recent study, the Kv1.5 blocker AVE0118 was reported to be highly effective against obstructive sleep apnea. Here, Wirth et al. utilized an anesthetized pig model to propose that a sensitization of upper airway mechanoreceptors by topical, nasal administration of a potassium channel blocker is a new pharmacologic

principle to treat obstructive sleep apnea (Wirth et al. 2013). The idea of using AVE0118 was to block K^+ channels in order to depolarize superficial mechanoreceptors of the upper airways and thereby modulate the negative pressure reflex; however, the molecular target for the effectiveness of AVE0118 in this apnea model is not yet known. Although TASK-1 is strongly expressed in the hypoglossal motor neurons, forming a nerve that is, when activated, involved in keeping the upper airways open (Bayliss et al. 2003), TASK-1 or Kv1.5 expression in the superficial mechanoreceptors of the upper airways or in the sensible and sensory parts of glossopharyngeal and vagus nerves has not yet been reported.

It was previously described that Kv1.5 blockers S20951 and AVE1231 are in fact highly potent TASK-1 blockers. Due to the observation that these blockers have a strong preference for TASK-1 channels and as the structures of S20951 and AVE1231 were not yet released by Sanofi-Aventis, Decher's Lab published these compound as TASK-1 blockers using the synonyms A1899 (Streit et al. 2011) for S20951 (Knobloch et al. 2002; Brendel et al. 2004) and A293 (Putzke et al. 2007) for AVE1231 (Putzke et al. 2007). Both compounds were previously described as being effective in animal models against atrial fibrillation (Knobloch et al. 2002; Brendel et al. 2004; Wirth et al. 2007), and AVE1231 (A293) had entered clinical development (phase I trial) against atrial fibrillation.

In the present work, we analyze the abovementioned preferential block of TASK-1 by the Kv1.5 blockers AVE1231 (A293) and S20951 (A1899). In addition, we asked whether AVE0118, which had entered clinical phase IIa trials for acute cardioversion of atrial fibrillation and was recently described as a putative drug for obstructive sleep apnea, is also a potent modulator of TASK-1 channels, which turned out to be the case. In addition, we found that other known antiarrhythmic Kv1.5 blockers like S9947, ICAGEN-4, and MSD-D (Bachmann et al. 2001; Strutz-Seebohm et al. 2007) are also potent TASK-1 blockers. As Kv1.5 belongs to the family of tetrameric voltage-gated potassium (Kv) channels with six transmembrane domains per subunit and TASK-1 is a member of the dimeric family of potassium (K_{2P}) channels, we additionally focused on the analysis why these structurally unrelated channels are frequently blocked by the same blockers and why those blockers preferentially inhibit TASK-1.

5.2. Materials and Methods

Oocyte preparation, cRNS synthesis, and injection. *Xenopus laevis* oocytes were isolated as previously described (Streit et al. 2011) and incubated in OR2 solution containing the following in millimolar: NaCl 82.5, KCl 2, MgCl₂ 1, and HEPES 5 (pH 7.5) substituted with 2 mg/ml collagenase II (Sigma) to remove residual connective tissue. Subsequently, oocytes were stored at 18 °C in ND96 solution supplemented with 50 mg/l gentamicin, 274 mg/l sodium pyruvate, and 88 mg/l theophylline. Human TASK-1 complementary DNA (cDNA) was subcloned into pSGEM or pBF1 vectors and linearized with NheI or MluI, respectively. Kv1.5 cDNA was subcloned into pSGEM vector, and the construct was linearized with NheI. Complementary RNA (cRNA) was synthesized with mMESSAGE mMACHINE Kit (Ambion). The quality of cRNA was tested using agarose gel electrophoresis. Oocytes were injected with 50 nl of cRNA.

TEVC recordings. All two-electrode voltage clamp (TEVC) recordings were performed at room temperature (20–22 °C) with a Turbo TEC-10CD (npi) amplifier and a Digidata 1200 Series (Axon Instruments) as A/D converter. Micropipettes were made from borosilicate glass capillaries GB 150TF-8P (Science Products) and pulled with a DMZ-Universal Puller (Zeitz). Recording pipettes had a resistance of 0.5–1.5 MΩ and were filled with 3 M KCl solution. Recording solution, ND96, contained the following in millimolar: NaCl 96, KCl 2, CaCl₂ 1.8, MgCl₂ 1, and HEPES 5 (pH 7.5). Block was analyzed with 1 s voltage steps to +40 mV from a holding potential of -80 mV with a sweep time interval of 10 s. The frequency dependence of peak current block was analyzed by stepping from -80 to 0 mV for 250 ms at a pulse frequency that ranged from 0.5 to 4 Hz. At 4 Hz, a pulse duration of 200 ms was used. Data were acquired with Clampex 10 (Molecular Devices) and analyzed with Clampfit 10 (Molecular Devices) and Origin 7 (OriginLab Corporation).

Drugs and IC₅₀ values. The compounds AVE1231 (A293), S20951 (A1899), and AVE0118 were synthesized by Sanofi-Aventis GmbH, Germany, and MSD-D, S9947, ICAGEN-4 were provided by Prof. G. Seeböhm (Strutz-Seeböhm et al. 2007). All drugs were dissolved in DMSO, aliquoted, stored at -20 °C, and added to the external solution (ND96) on the day of experimentation. The concentration required for 50% block of current (half-maximal inhibitory concentration (IC₅₀)) was determined from Hill plots. The

concentrations of the drugs used to describe the 12 different dose-response curves and IC_{50} values varied depending on the IC_{50} of the drug on TASK-1 or Kv1.5, but at least four concentrations were used ($n = 4 - 6$), and the number of experiments ranged from three to 12 experiments per concentration ($n = 3 - 12$). For all drugs using the lowest stimulation frequency of 0.5 Hz, we applied concentrations to achieve a block of at least 90%; however, higher concentrations to reach a full inhibition were not applied. For all the TASK-1 channel blockers, a dose-response curve with a Hill factor near 1 was observed. Final DMSO concentration did not exceed 0.1%. All fitting procedures were based on the simplex algorithm.

Molecular modeling. Modeller 9v5 (Šali & Blundell 1993) was used to create the different pore homology models. The TASK-1 homology model was based on the crystal structure of TWIK-1 (Protein Data Bank (PDB) code 3UKM) [22]. The open-state Kv1.5 homology model was based on Kv1.2/Kv2.1 chimera (PDB code 2R9R), and the corresponding closed-state model was based on the computational closed-state model of the Shaker channel by Pathak et al. (Pathak et al. 2007). All models were compared to the original crystal structure template to verify that the modeling step had not altered backbone and side-chain conformations.

5.3. Results

Kv1.5 blockers preferentially inhibit TASK-1 channels. In our current study, we describe and carefully analyze the preference of known Kv1.5 blockers for TASK-1 channels. In order to confirm our theory that the effectiveness of known Kv1.5 blockers is biased by an additional or even preferential TASK-1 inhibition, we tested several substances targeting Kv1.5 for their TASK-1 affinity. For this purpose, Kv1.5 or TASK-1 channels were expressed in *Xenopus* oocytes, and IC_{50} values of the substances were determined. First, we probed the inhibition of Kv1.5 and TASK-1 channels by the biphenyl derivatives AVE0118, S20951 (A1899), and S9947 (Fig. 4A–C). All these drugs inhibited TASK-1 in a nanomolar range and were more effective on TASK-1 than on Kv1.5 (Fig. 4A–C). The IC_{50} values on TASK-1 were 603 nM for AVE0118, 35 nM for S20951 (A1899), and 200 nM for S9947, respectively. Strikingly, S20951 (A1899) was about 68-

fold more effective on TASK-1 than on Kv1.5 (Fig. 4B). Here, it is of particular interest that AVE0118 which entered clinical trials against atrial fibrillation and is very effective in a disease model against obstructive sleep apnea is about 10-fold more affine for TASK-1.

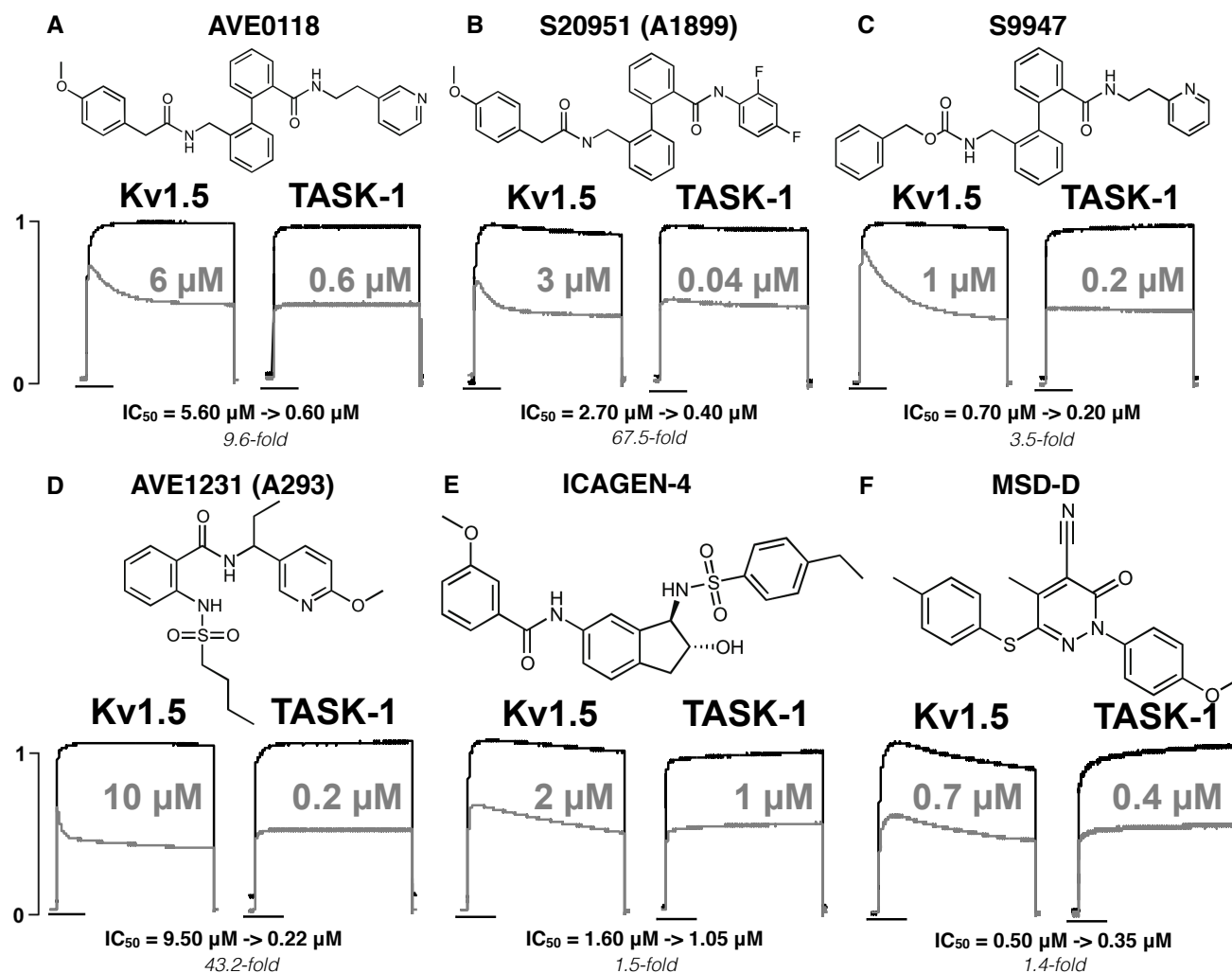


Figure 4. Chemical structures of Kv1.5 blockers and their affinity for Kv1.5 and TASK-1. Chemical structures for the biphenyl derivatives. **A.** AVE0118, **B.** S20951 (A1899), and **C.** S9947. Chemical structures for **D.** AVE1231 (A293), **E.** ICAGEN-4, and **F.** MSD-D. **A–F** Normalized currents of Kv1.5 or TASK-1 recorded in *Xenopus* oocytes by voltage steps to 0 mV before (*black*) and after (*gray*) half-maximal inhibition by different blockers are illustrated. The drug concentrations used in the recordings are indicated in *gray letters*. The IC_{50} values for Kv1.5 and TASK-1 are depicted under the current traces, and the fold decrease in IC_{50} for TASK-1 compared to Kv1.5 is indicated at the *bottom*. *Scale bars at the left* indicate the normalized Kv1.5 or TASK-1 current amplitudes, and the *scale bars of the x-axis* indicate 250 ms.

Next, we also tested Kv1.5 blockers with different chemical structures and/or from different pharmaceutical companies. Similar as described for the biphenyl compounds, the anthranilic acid derivative AVE1231 (A293) had an IC₅₀ on TASK-1, which was in the nanomolar range. The IC₅₀ was 222 nM (Putzke et al. 2007), and the drug was about 43-fold more effective on TASK-1 (Fig. 4D). The IC₅₀ of ICAGEN-4 on TASK-1 expressed in oocytes was 1.05 μM (versus 1.6 μM on Kv1.5) and 350 nM for MSD-D (versus 505 nM on Kv1.5). Thus, also for these compounds, we found a TASK-1 inhibition, which was more pronounced for TASK-1 than for Kv1.5 channels (Fig. 4E, F).

Similarities in the drug binding site of Kv1.5 and TASK-1. Next, we tried to understand the molecular reason for the similarities in the pharmacology of Kv1.5 and TASK-1 channels and why TASK-1 channels are blocked with similar or even much higher affinity. This conservation of drug affinities between the two unrelated channels is somewhat surprising, as Kv1.5 belongs to the family of Kv channels with six transmembrane domains and TASK-1 to the K_{2p} family with four transmembrane domains per subunit. Drug binding of potassium channel blockers occurs at the selectivity filter and at the inner pore-forming helices, meaning the S6 segment in Kv1.5 (Decher et al. 2004) or the M2 and M4 segments in K_{2p} channels (Streit et al. 2011). Next, we made a protein alignment of the S6 segment of Kv1.5 with the M2 and M4 domains of TASK-1 (Fig. 5A), using a glycine residue (discussed as “gating hinge”), which is conserved in most potassium channels (Jiang et al. 2002). Fig. 5A illustrates the most important residues of the previously identified drug binding site in TASK-1 (Streit et al. 2011) and Kv1.5 channels (Decher et al. 2004) highlighted in bold and color. Not unexpected, the S6 segment of Kv1.5 and the M2 or M4 segment of TASK-1 are almost entirely different in their sequence, and on first glance, one cannot identify any putative conservation of drug binding sites between these two channels (Fig. 5A). However, at a closer look, considering the dimeric nature of K_{2p} channels, the drug binding sites are conserved and in both channels formed by threonine residues of the signature sequence and by isoleucine and valine/leucine residues of the inner pore-forming helix (Streit et al. 2011; Strutz-Seebohm et al. 2007) (Fig. 5B, C). Therefore, the binding sites might be more similar than expected from the visual inspection of the S6, M2, and M4 segments. The cartoons in Fig. 5B, C show that the drug binding sites are conserved, as they include in a similar way four

threonine residues of the pore signature sequence (4× T480 in Kv1.5 and 2× T93 plus 2× T199 in TASK-1), and at the inner helices, the binding sites are formed by a “ring” of four isoleucine residues (4× I508 in Kv1.5 and 2× I118 plus 2× I235 in TASK-1). However, closer to the cytosol, the residues involved in drug binding are not identical, and while Kv1.5 has valine moieties (4× V512) facing to the central cavity, TASK-1 has larger and more aliphatic leucine residues contributing to drug binding (2× L122 plus 2× L239).

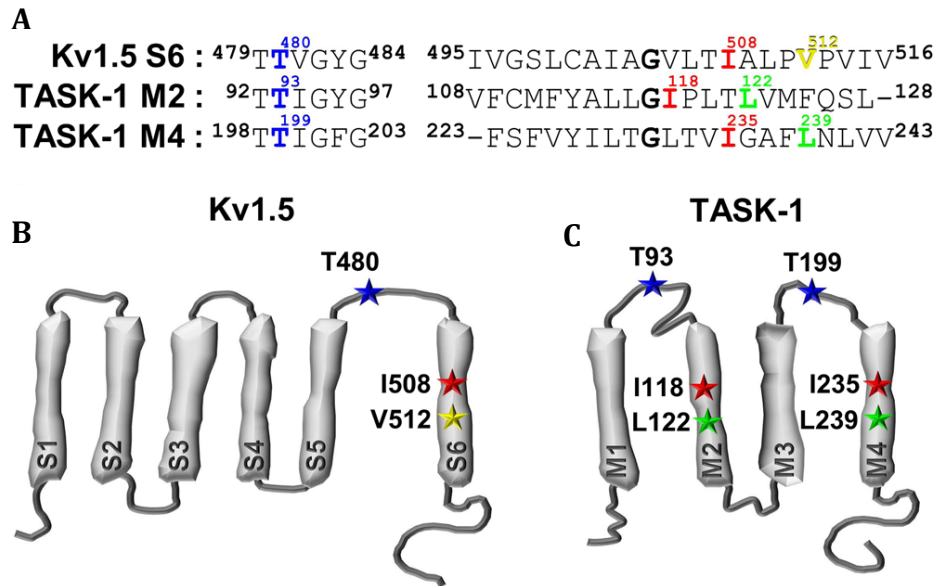


Figure 5. Sequence alignment and cartoon illustrating the drug binding site of Kv1.5 and TASK-1. A. Sequence alignment of the S6 segment of Kv1.5 and the transmembrane domains M2 and M4 of TASK-1. The glycine residue (putative “gating hinge”) conserved in most potassium channels is highlighted in *bold*.

Residues of the previously described drug binding sites in TASK-1 and Kv1.5 are labeled and also highlighted in *bold* and *colored letters*. Cartoon of a **B.** Kv1.5 and **C.** TASK-1 subunit illustrating that Kv1.5 and TASK-1 share similar residues at their drug binding sites and a similar pattern of residues that interact with drugs in the central cavity. Threonine (*blue*), isoleucine (*red*), and valine (*yellow*)/leucine (*green*).

Structural comparison of the lipophilic TASK-1 and Kv1.5 binding site. Drug binding to TASK-1 and Kv1.5 is caused by binding to threonine residues of the signature sequence and to lipophilic residues facing the central cavity. Next, we generated pore homology models to more closely compare the structures of the two previously described binding sites (Decher et al. 2004; Streit et al. 2011). The pore homology model of Kv1.5 was based on the open pore structure of the rat Kv1.2 channel (Long et al. 2005), and the TASK-1 pore model was based on the TWIK-1 crystal structure (Miller & Long 2012)

(Fig. 6). We displayed the side view of these homology models and highlighted the residues previously described as drug binding sites in the central cavity (Limberg et al. 2011) (Fig. 6A–D). The drug binding sites in the central cavities of both channels consist of a ring of threonine residues and layers of isoleucine and valine/leucine residues underneath the selectivity filter (zoomed box in Fig. 6A, C), confirming the conserved lipophilic nature of the two binding sites.

Despite these physicochemical and sterical similarities in the two drug binding sites, there are clear differences in their geometry, primarily arising from the dimeric structure and the lack of a 4-fold symmetry in K_{2p} channels. The rings of the four threonine residues (T480 versus T93/T199) are highly similar for the Kv1.5 and TASK-1 drug binding sites and do not differ in geometry (Fig. 6B, D). Considering the drug binding site V505 in Kv1.5, the channel has three rings of lipophilic residues, forming a binding site with a 4-fold rotational symmetry (4× V505, 4× I508, and 4× V512). In contrast to the expectations derived from the cartoon in Fig. 5C, the TASK-1 drug binding site is not formed by a ring of four isoleucine residues (2× I118 plus 2× I235) plus a ring of four leucine residues (2× L122 plus 2× L239), as previously proposed using a KvAP-based TASK-1 pore homology model with a 4-fold symmetry (Streit et al. 2011). Here, using a K_{2p} channel (TWIK-1)-based TASK-1 pore homology model with a rhombic 2-fold symmetry, it becomes evident that there are three layers of drug binding residues similar as in Kv1.5 (Fig. 6B, D). However, due to the dimeric nature of the channel, the uppermost, first lipophilic layer of drug binding residues is not formed by a ring, but by only two isoleucine residues (I118) of the M2 segments. Similarly, the lowermost, third layer of drug binding residues is formed by only two leucine residues (L239) of the M4 segments. Only in the middle, second layer of drug binding residues, the binding site is formed by a ring of four lipophilic residues, albeit it is a “mixed ring” containing two leucine residues of M2 (L122) and two isoleucine residues of M4 (I235). In addition, this second “layer” does not have a rotational symmetry, reflecting the rhombic structure of the dimeric K_{2p} channel also in the middle of the cavity (Fig. 6D).

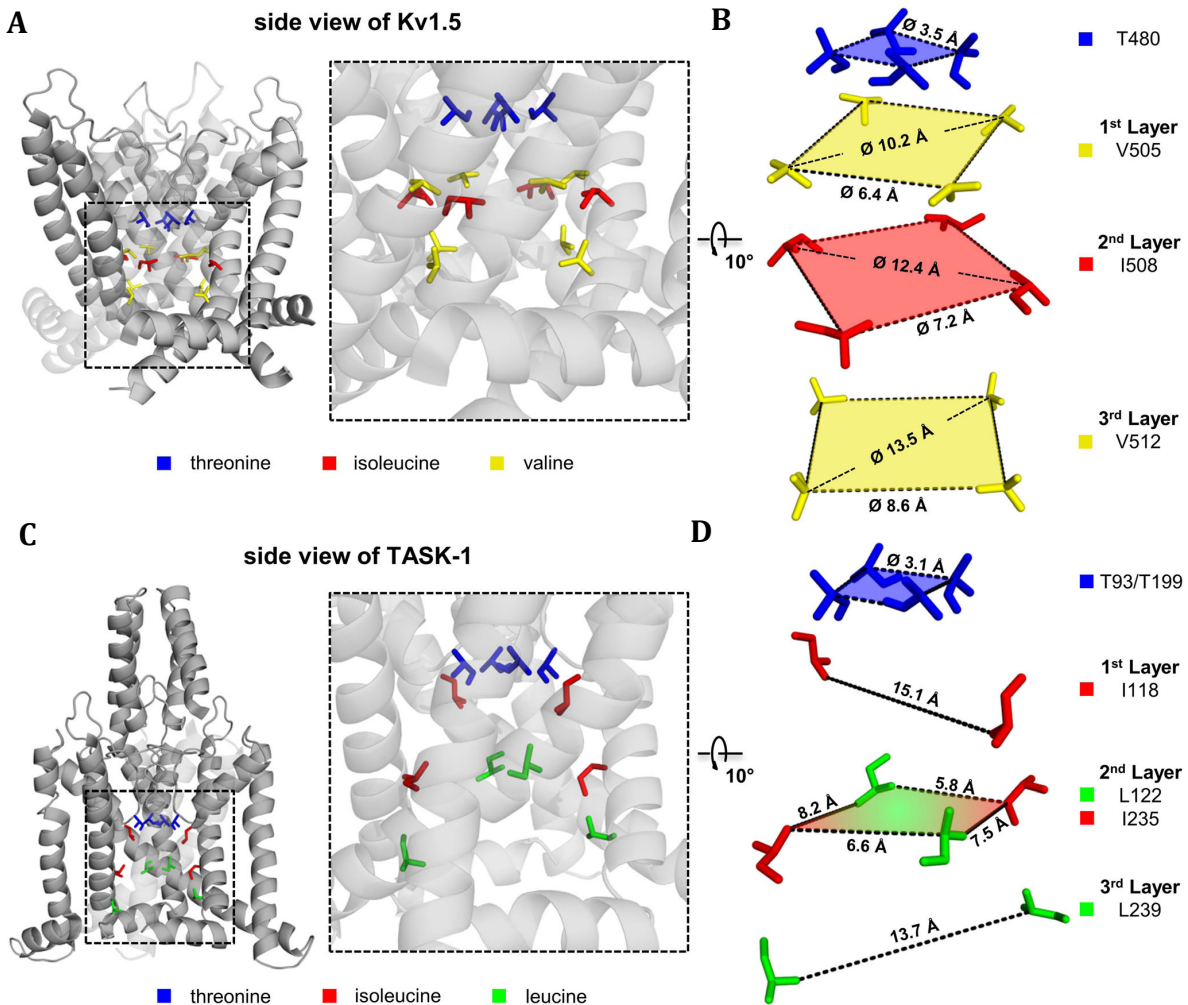


Figure 6. The drug binding sites of Kv1.5 and TASK-1 illustrated in pore homology models. Side view of the pore homology models for **A.** Kv1.5 based on the open-state Kv1.2 crystal structure and **C.** TASK-1 based on the TWIK-1 crystal structure. Residues previously described as drug binding sites (Decher et al. 2004; Streit et al. 2011) are highlighted. **B, D.** Layers or “rings” formed by lipophilic residues of the drug binding site. Shortest distances between the residues are indicated.

Thus, despite the strong similarities in the lipophilic drug binding sites between TASK-1 and Kv1.5, there are differences in the shape and symmetry of the residues that can complex drugs in the central cavity. For instance, in TASK-1, the first layer of drug binding residues seems to be wider and the second “mixed layer” is narrower than those in Kv1.5 (Fig. 6B, D). Two major differences might account to the fact that some lipophilic drugs prefer TASK-1 channels: (1) the different symmetry of the pore and the binding site and (2) the presence of a mix of lipophilic leucine and isoleucine residues at the lower two

layers of the drug binding site. In contrast, in Kv1.5 channels, the lowermost third layer is formed by a ring of smaller and less lipophilic valine residues (V512). In this context, it is noteworthy that even such a small change at a lipophilic residue of the Kv1 drug binding site can have profound effects on the drug affinity (Decher et al. 2010). For instance, an isoleucine to valine exchange in Kv1.1, at the site corresponding to I508 in Kv1.5, reduced the affinity of S20951 (A1899), AVE0118, and Psora-4 by 4- to 70-fold (Decher et al. 2010). In addition, this third layer only gains a diameter of about 13 Å, when the channel is in the open state, while the pore of TASK-1 is constitutively open, “presenting” the lipophilic isoleucine and leucine residues of the second and third layers for drug binding.

Increased accessibility to the constitutively open TASK-1 channel pore might contribute to the increased affinity of Kv1.5 blockers to TASK-1. Using a pore homology model of Kv1.5 in the open state, the size of the entrance to the central cavity is very similar for TASK-1 and Kv1.5 (Figs. 6B, D and 7A, B). However, using a closed-state model of Kv1.5, the entry pathway to the central cavity is largely diminished, as expected (Fig. 7B, C). This phenomenon is the molecular reason for the use dependence observed for Kv1.5 open-channel blockers (Decher et al. 2004; Strutz-Seebohm et al. 2007). Applying S20951 (A1899) or AVE0118 at their respective IC₅₀ concentrations and after achieving half-maximal inhibition, increasing the pulsing frequency (ranging from 0.5 to 4 Hz) caused an additional, frequency-dependent block of Kv1.5 channels (Fig. 7D, E). In contrast, no additional or use-dependent inhibition of TASK-1 was observed for S20951 (A1899) or AVE0118 at all frequencies tested (Fig. 7D, E).

This additional, use-dependent inhibition of Kv1.5 channels by open-channel blockers is caused by an increased accessibility of the blockers to the open pore. As TASK-1 channels are expected to be constitutively open at the inner gate (Piechotta et al. 2011; Rapedius et al. 2012), the relative increase in affinity of some blockers for TASK-1 compared to Kv1.5 might be caused by a facilitated accessibility of the blockers to the more lipophilic binding site at the lower end of the central cavity.

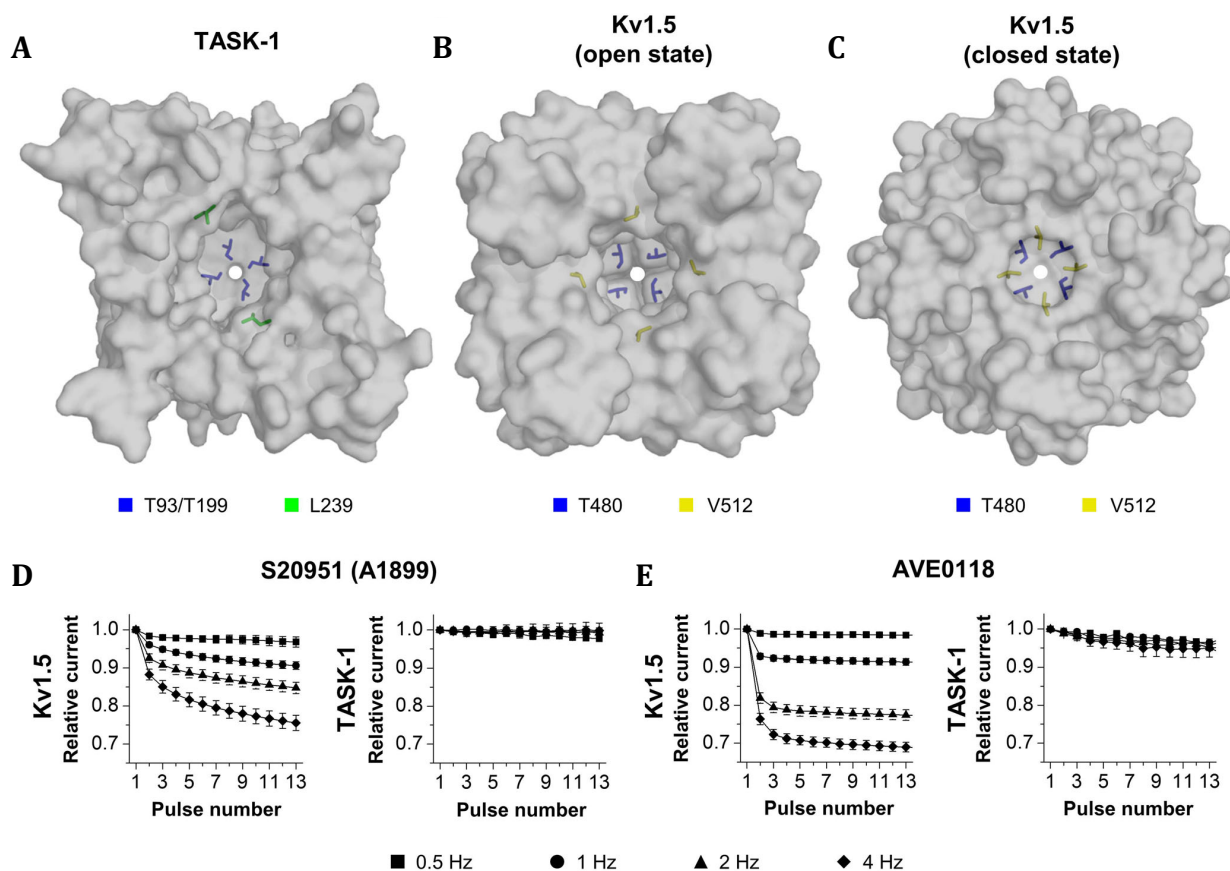


Figure 7. Diameter of the cytosolic opening to the central cavity and analysis of the frequency-dependent inhibition of Kv1.5 and TASK-1. *Bottom view* of the entry to the central cavity of **A.** TASK-1 based on the TWIK-1 crystal structure, **B.** Kv1.5 in the open state based on the Kv1.2 crystal structure, and **C.** Kv1.5 based on a closed-state model of Pathak et al. (Pathak et al. 2007). The diameter of the cytosolic entry to the central cavity is similar for the open state of Kv1.5 and the constitutively open TASK-1 channels. **D-E.** Analysis of the frequency-dependent inhibition of Kv1.5 and TASK-1. After half-maximal inhibition of Kv1.5 or TASK-1, the currents were normalized to 1 and the additional inhibition by pulsing with 0.5, 1, 2, and 4 Hz was analyzed. Frequency-dependent inhibition of Kv1.5 and TASK-1 was analyzed for **D.** S20951 (A1899) or **E.** AVE0118. Note that only for Kv1.5 inhibition, an additional use-dependent inhibition was observed.

A common pharmacophore model for the TASK-1 blockers AVE0118, S20951 (A1899), S9947, AVE1231 (A293) and MSD-D. With respect to future drug design based on the common blockers of Kv1.5 and TASK-1 channels, it is an important first to map a shared pharmacophore between these six structures. The pharmacophore could be used then as query for designing molecules with specific desired attributes (lead optimization) for each channel. Using e-Pharmacophore (Campagna-Slater et al. 2010), three common features were identified within five of the six structures: two hydrogen bond acceptor atoms

(“A”) and one aromatic ring (“R”) (Fig. 8). The A atoms could bind to the ring of threonine residues at the signature sequence of the selectivity filter as it was observed for A1 atom of S20951 (A1899), a carbonyl oxygen interacting with T93/T199 residues of TASK-1 channel (Streit et al. 2011). Meanwhile, the R part of the structures could establish hydrophobic contacts with the second layer of the drug binding site (Fig. 6). Such an interaction was also observed between R of S20951 (A1899) and I118 of TASK-1 through molecular docking (Streit et al. 2011). The compound ICAGEN-4 was not within the structures that share this common pharmacophore, although it presents the A atoms and R ring (Fig. 8A). Presumably, ICAGEN-4 was not included within the structures sharing the detected pharmacophore, as the A atoms and R ring were not in the common distances and angles shown in Fig. 8B.

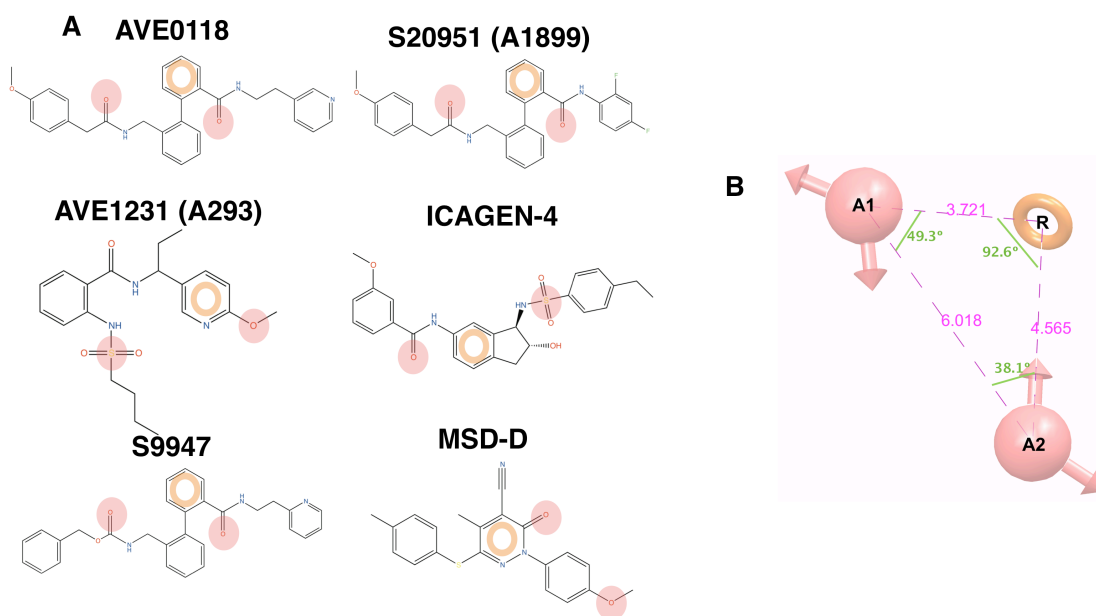


Figure 8. Common pharmacophore for the TASK-1 blockers AVE0118, S20951 (A1899), S9947, AVE1231 (A293), and MSD-D. **A.** Chemical structures of TASK-1 blockers. Circles indicate the two hydrogen bond acceptor atoms (*red*) determined for the pharmacophore model by e-Pharmacophore, and “R” indicates the aromatic ring (*orange*) of the pharmacophore model. *Dotted lines* used for the *blue circles* of ICAGEN-4 indicate that the drug has the two necessary hydrogen bond acceptor atoms, but not in the right distances and angles. **B.** Pharmacophore model in which the two hydrogen bond acceptor groups are denoted as “A1” and “A2” and the aromatic ring as R. The average distances and angles between the groups are indicated. The *arrows* in the hydrogen bond acceptors A1 and A2 indicate the direction in which the hydrogen bond interactions occur.

From the present study, it is too early to conclude about how to modify the known common blockers of Kv1.5 and TASK-1 channels. However, the shared pharmacophore shown here could be used not only for lead optimization, but also as query for retrieving potential leads from structural databases (lead discovery).

5.4. Discussion

In order to identify more effective and safer anti-arrhythmic drugs, recent research focuses on the identification of compounds that target cardiac ion channels that are exclusively or predominantly expressed in the human atria. The major repolarizing current in human atria is the ultra-rapid activating delayed rectifier K⁺ current (I_{Kur}) carried by Kv1.5 channels which seems to play a minor role in the ventricles (Li et al. 1996; Limberg et al. 2011; Wang et al. 1993). Surprisingly, we found in our study that several Kv1.5 blockers are more effectively inhibiting TASK-1 than Kv1.5 channels. For instance, AVE1231 (A293) and S20951 (A1899) block TASK-1 43- and 68-fold more efficient than Kv1.5 channels. AVE0118 was described as an atrium-specific blocker of the early action potential repolarization, as it blocks the potassium currents I_{Kur} and I_{to} carried by Kv1.5 and Kv4.3, respectively (Decher et al. 2004; Gögelein et al. 2004) as well as I_{KACH} (Christ et al. 2008). Subsequently, Burashnikov et al. reported a SCN5A affinity for this compound (Burashnikov et al. 2012). Therefore, AVE0118 might be a low potent “multichannel blocker” which could be the key to effectiveness, acting as an “aminodarone-like” compound. However, we show that AVE0118 blocks TASK-1 channels in the submicromolar range, with an IC_{50} of 603 nM, while the IC_{50} on Kv1.5, for instance, is only 5.6 μ M. This suggests that TASK-1 is the primary molecular target of AVE0118, especially, when considering that the IC_{50} value of AVE0118 was recorded in *Xenopus* oocytes and the potency of drug block is usually underestimated, when currents are measured in intact oocytes. While relative comparisons of affinities, as we have observed here for TASK-1 and Kv1.5 with 1.4- to 68-fold changes, are very accurate using the oocyte expression system, it is well known that overall lower apparent potencies (2– 10-fold) are observed, especially for lipophilic compounds. We have observed IC_{50} values for TASK-1 inhibition of 603 nM (AVE0118), 35 nM (S20951/A1899), 200 nM (S9947), 222

nM (AVE1231/A293), 1.05 μ M (ICAGEN-4), and 350 nM (MSD-D). Accordingly, the IC_{50} values are expected to be for most of these anti-arrhythmic compounds in the two-digit or even one-digit nanomolar range, when recording from mammalian cells, which do not act as a “lipophilic sink” for drugs.

It was also our aim to elucidate how different compounds can block both, TASK-1 and Kv1.5 channels, albeit they belong to very remotely related potassium channel families. Surprisingly, our molecular modeling experiments showed a similar topology of the drug binding sites. For both channels, the drug binding sites are formed by a ring of threonine residues at the signature sequence of the selectivity filter plus three layers of lipophilic residues facing the central cavity underneath the selectivity filter. Despite the strong similarities in the drug binding sites between TASK-1 and Kv1.5, there are differences in the nature of the lipophilic residues and the symmetry of the drug binding site that might explain why we observed a preferential TASK-1 block for most of the Kv1.5 blockers. The fact that TASK-1 channels are constitutively open at the intracellular gate and have more lipophilic isoleucine residues at the entry of the pore (versus a ring of valine in Kv1.5), might in part explain the relative preference of many of the Kv1.5 blockers for TASK-1 channels. These unexpected pharmacological similarities, but also the differences in the molecular architecture of the drug binding sites, should be considered in future drug design of specific TASK-1 or Kv1.5 blockers. Another question arising is whether these Kv1.5 blockers also cause an inhibition of TASK-3, the closest relative of TASK-1. Although we did not investigate the affinity for TASK-3, it is very likely that these channels have a similar affinity, since the drug binding site, which was previously determined using S20951 (A1899), only differs by a single residue in the M4 segment (Streit et al. 2011). This residue in the halothane response element of M4, M247, of TASK-1 is at the homologue position of TASK-3 replaced by a leucine. On the other hand, as it was previously shown that a M247L mutation in TASK-1 can cause an about 3.3-fold change in the IC_{50} for S20951 (A1899) (Streit et al. 2011), it is also possible that the conservation of drug affinities does only comprise Kv1.5 and TASK-1 channels.

In the past years, the preference of Kv1.5 blockers for TASK-1 channels was not known, and thus, the data obtained using those compounds and the conclusions may need to be revisited. For example, Kun et al. used AVE0118 to propose that blocking of neuronal

Kv1.5-type potassium channels in the medio-adventitial layer of rat small mesenteric artery (Kun et al. 2014) mediates a vascular contraction. Expression of TASK-1 channels has been also shown in rat mesenteric artery (Gardener et al. 2004), and therefore, TASK-1 may participate in this effect. Wirth et al. used AVE0118 and found that topical, nasal administration of AVE0118 to the upper airway sensitized and amplified the negative pressure reflex, suggesting that this is a promising pharmacologic approach for the treatment of obstructive sleep apnea (Wirth et al. 2013). Although the idea of using AVE0118 was to block K⁺ channels in order to depolarize superficial mechanoreceptors of the upper airways and thereby modulate the negative pressure reflex, the molecular target for the effectiveness of AVE0118 in this apnea model is not yet known. Interestingly, in the hypoglossal motor neurons, forming a nerve that is, when activated, involved in keeping the upper airways open, TASK-1 is strongly expressed (Bayliss et al. 2003). In addition, TASK-1 plays an important role in motoneuron excitability (Talley et al. 2000) and thus is a major candidate to mediate the observed effects. However, TASK-1 expression in the superficial mechanoreceptors of the upper airways or in the sensible and sensory parts of glossopharyngeal and vagus nerves has not yet been reported. Although we have obtained preliminary results detecting TASK-1 in the ganglia of these nerves (data not shown), the analyses of the TASK-1 expression, especially in the mechanoreceptors and the nerves of the upper airways, are clearly hindered by the lack of specific TASK-1 antibodies. As there are currently no reliable tools to detect TASK-1 in these tissue or mechanoreceptors, the use of highly specific TASK-1 blockers in the recently described obstructive sleep apnea model might be the most reliable experiment to show that some or even most of the anti apnea effects are mediated by TASK-1 inhibition. Currently, it seems most reasonable to assume that TASK-1 inhibition in the mechanoreceptors of the upper airways or the glossopharyngeal and vagus nerves might result in a membrane depolarization which modulates the negative pressure reflex. In this context, it is noteworthy that the drug doxapram which is used to treat drug-induced ventilator depression, chronic obstructive pulmonary disease, and apnea in premature infants was shown to be a very potent TASK-1 channel blocker (Cotten et al. 2006). Taken together, it appears very likely that TASK-1 is a promising target for sleep disorders, especially obstructive sleep apnea.

Due to the atrium-specific expression of TASK-1 in the human heart, TASK-1 channels were previously proposed as drug targets against atrial fibrillation (Limberg et al. 2011). This becomes more likely, taking our data into account, that Kv1.5 blockers effective in animal models against atrial fibrillation are in fact more potent TASK-1 blockers. It is noteworthy that in mice, after repeated atrial and ventricular burst stimulation with different cycle lengths, a fraction of wild-type mice develops atrial fibrillation whereas in TASK-1 knock-out animals, it appears that they are protected against provoked atrial fibrillation (Petric et al. 2012). Also, these data suggest that TASK-1 may indeed be a drug target against atrial fibrillation. Future studies would do well in examining what is the best atrium-specific channel to target for the prevention or conversion of atrial fibrillation. Subject of future research might be, for instance, whether a specific TASK-1 inhibition is as beneficial as a specific inhibition of Kv1.5 or whether a combined inhibition of the two channels is a more superior pharmacological approach to treat or prevent atrial fibrillation. TASK-1 inhibition might be more efficient for the treatment of chronic atrial fibrillation as Kv1.5 inhibition, since patients with chronic atrial fibrillation undergo a strong electrical remodeling, including a TASK-1 upregulation, whereas Kv1.5 is downregulated (Nattel et al. 2007; Pathak et al. 2007). In contrast, an advantage of targeting Kv1.5 channels is the positive use dependence of open-channel blockers (Decher et al. 2006; Decher et al. 2004; Strutz-Seebohm et al. 2007) which we did not observe for TASK-1 channel inhibition, as K_{2p} channels are constitutively in the open state (Piechotta et al. 2011; Rapedius et al. 2012). Thus, Kv1.5 blockers become more efficient/potent under atrial fibrillation, which is an excellent prerequisite for the development of drugs for the prevention of atrial fibrillation, as under “attacks” of atrial fibrillation, Kv1.5 channels are more efficiently blocked as under “normal” conditions. In addition, while the close correlation between the reduction in $I_{K_{sus}}$ current density and the reduction in Kv1.5 expression in atrial fibrillation supports the hypothesis that the Kv1.5 α -subunit is the major component of $I_{K_{sus}}$ current in human atria (Fedida et al. 1993; Van Wagoner et al. 1997), we found that I_{TASK-1} contributes only about 15% to the sustained potassium current in right human auricular cardiomyocytes (Limberg et al. 2011).

To identify whether the inhibition of TASK-1 or Kv1.5 channels or the combined block is the most superior principle of action it requires the development of novel and more

selective blockers and the subsequent testing in disease models of atrial fibrillation or chronic sleep apnea. However, the fact that most of the Kv1.5 blockers that we have analyzed are very potent TASK-1 blockers already indicates that TASK-1 channel block contributes to the effectiveness of these drugs against atrial fibrillation or obstructive sleep apnea.

5.5. Future work

Different questions have emerged about why Kv1.5 blockers preferentially inhibit TASK-1 channels? And also what are the differences in the binding mode of those blockers? To answer this and other remarkable questions we consider that the analysis of the structure-activity relationship (SAR) between the blockers and the target must be explored using computational tools as well as wet lab validation. The relationship between the 3D structure of the studied blockers and its biological activity enables the determination of the chemical groups responsible for evoking a potassium channel biological effect against atrial fibrillation and obstructive sleep apnea. This SAR analysis followed by long MDs and point mutations (according to the initial theoretical findings) will allow us to get valuable knowledge to design novel and potent modulators of Kv1.5 and TASK-1 channels.

5.6. Scientific Production

Pflugers Arch - Eur J Physiol (2015) 467:1081–1090
DOI 10.1007/s00424-014-1665-1

ION CHANNELS, RECEPTORS AND TRANSPORTERS

Kv1.5 blockers preferentially inhibit TASK-1 channels: TASK-1 as a target against atrial fibrillation and obstructive sleep apnea?

Aytug K. Kiper · Susanne Rinné · Caroline Rolfes ·
David Ramírez · Guiscard Seeböhm · Michael F. Netter ·
Wendy González · Niels Decher

Received: 8 October 2014 / Revised: 14 November 2014 / Accepted: 28 November 2014 / Published online: 17 December 2014
© Springer-Verlag Berlin Heidelberg 2014

Abstract Atrial fibrillation and obstructive sleep apnea are responsible for significant morbidity and mortality in the industrialized world. There is a high medical need for novel drugs against both diseases, and here, Kv1.5 channels have emerged as promising drug targets. In humans, TASK-1 has an atrium-specific expression and TASK-1 is also abundantly expressed in the hypoglossal motor nucleus. We asked whether known Kv1.5 channel blockers, effective against atrial fibrillation and/or obstructive sleep apnea, modulate TASK-1 channels. Therefore, we tested Kv1.5 blockers with different chemical structures for their TASK-1 affinity, utilizing two-electrode voltage clamp (TEVC) recordings in *Xenopus* oocytes. Despite the low structural conservation of Kv1.5 and TASK-1 channels, we found all Kv1.5 blockers analyzed to be even more effective on TASK-1 than on Kv1.5. For instance, the half-maximal inhibitory concentration (IC₅₀) values of AVE0118 and AVE1231 (A293) were 10- and 43-fold lower on TASK-1. Also for MSD-D, ICAGEN-4, S20951 (A1899),

and S9947, the IC₅₀ values were 1.4- to 70-fold lower than for Kv1.5. To describe this phenomenon on a molecular level, we used in silico models and identified unexpected structural similarities between the two drug binding sites. Kv1.5 blockers, like AVE0118 and AVE1231, which are promising drugs against atrial fibrillation or obstructive sleep apnea, are in fact potent TASK-1 blockers. Accordingly, block of TASK-1 channels by these compounds might contribute to the clinical effectiveness of these drugs. The higher affinity of these blockers for TASK-1 channels suggests that TASK-1 might be an unrecognized molecular target of Kv1.5 blockers effective in atrial fibrillation or obstructive sleep apnea.

Keywords Atrial fibrillation · K_{2P} channel · Kv1.5 · Two-pore domain potassium channel · TASK-1 · Obstructive sleep apnea

Aytug K. Kiper, Susanne Rinné, and Caroline Rolfes contributed equally.

This article is published as part of the Special Issue on K_{2P} channels.

A. K. Kiper · S. Rinné · M. F. Netter · N. Decher (✉)
Institute for Physiology and Pathophysiology, Vegetative Physiology,
Philipps-University of Marburg, Deutschhausstraße 2,
Marburg 35037, Germany
e-mail: decher@staff.uni-marburg.de

C. Rolfes
Klinik für Anästhesie und Intensivtherapie, Philipps-University of
Marburg, Marburg, Germany

G. Seeböhm
Institut für Genetik von Herzerkrankungen (IfGH),
Universitätsklinikum Münster, Münster, Germany

D. Ramírez · W. González
Center for Bioinformatics and Molecular Simulations, University of
Talca, Talca, Chile

Introduction

Atrial fibrillation and obstructive sleep apnea are among the most prominent diseases in the elderly and responsible for significant morbidity, health care costs, and mortality in the industrialized world [33, 38]. Drugs currently available for the treatment of these two diseases lack effectiveness and/or specificity. Accordingly, there is a high medical need for novel drugs targeting atrial fibrillation or obstructive sleep apnea. For both diseases, Kv1.5 channels have emerged as promising drug targets.

To avoid ventricular side effects, complicating the therapy of atrial fibrillation, current drug design focuses on atrial specific targets, including the atrial sodium channel [3], G protein-gated potassium channel [11], and voltage-gated potassium channel Kv1.5 [8, 9]. Kv1.5 channels are highly expressed in human atria, but not ventricle, and are the major

Side fenestration provide an ‘anchor’ for a stable binding of A1899 to the pore of TASK-1 potassium channels.

6.1. Introduction

Two-pore domain potassium (K_{2p}) channels are widely expressed, with highest expression levels in the central nervous system, cardiovascular, genitourinary and gastrointestinal system (Goldstein et al. 2001). The mammalian K_{2p} channel family consists of 15 family members divided into six subfamilies based on sequence similarity and their functional hallmarks (Enyedi & Czirják 2010). They are crucial for setting the resting membrane potential, regulation of excitability, ion transport, sensory transduction, metabolic regulation and neuroprotection, just to name some (patho)physiological processes and therapeutical potentials (Lotshaw 2007).

The TASK (tandem of pore domains in a weak inwardly rectifying K^+ channel [TWIK]-related acid-sensitive K^+ channel) subgroup, includes five members. The closest relatives of TASK-1 (Talley et al. 2000) are TASK-3 (Rajan et al. 2000) and TASK-5 (Kim & Gnatenco 2001). Functional K_{2p} channels form dimers and each subunit has two pore-forming loops (P1, P2), four transmembrane domains (M1-M4) and an extended extracellular loop between M1 and P1. Amino (N-) and carboxyl (C-) terminal domains of the channels are exposed to the cytoplasm (Lesage & Lazdunski 2000). Both pore regions (P1, P2) have the conserved ‘TXGXG’ motif, known as the selectivity filter, a structure characteristic of all selective potassium channels (O’Connell et al. 2002), where X denotes a hydrophobic amino acid. The crystallized structures of K_{2p} channels TWIK-1 (Miller & Long 2012), TRAAK (Brohawn et al. 2012)(Brohawn et al. 2013), TREK-1 –PDB: 4TWK–, and TREK-2 (Dong et al. 2015); reveal differences that give insights into distinctive gating and ion permeation properties. Near to the center of the membrane, the M2 transmembrane segment is kinked by approximately 20°: This twist generates in each

subunit a fenestration –open lateral passages connecting the pore with the lipid bilayer inner leaflet– (Aryal et al. 2014). Recently it has been hypothesized that the opening or closing of the fenestrations in response to bilayer inner leaflet deformation determines the gating of TRAAK channel by allowing lipids to penetrate into the inner cavity thus interfering with ion permeation. The conductive and non-conductive conformations of TRAAK channels would therefore be associated with the closed and open fenestration state respectively (Brohawn, Campbell, et al. 2014). However, one should mention that this view of the mechanism of TRAAK gating is not shared by a contemporary structural study (Lolicato et al. 2014), or by experimental work that points to a selectivity filter opening and closing as the sole mechanism of K_{2P} channel gating (Niemeyer et al. 2016; Piechotta et al. 2011; Schewe et al. 2016). Nevertheless, the intramembrane fenestrations appear to be important in the interaction of lipids and hydrophobic molecules with K_{2P} channels. This is supported by the work of Dong et al. which described how lipids and other hydrophobic molecules such as Prozac interact in the fenestrations of TREK-2 (Dong et al. 2015). These side cavities of K_{2P} channels are therefore potentially mechanistic ‘active sites’ and/or pathways that can warrant blockers access to their binding sites.

K_{2P} channels have been associated with several human pathophysiological processes or they provide therapeutic options: for instance TASK-1 is an important modulator of multiple sclerosis (Bittner et al. 2010) and modulates T cell effector function (Meuth et al. 2008) and TASK-3 promotes tumorigenesis when overexpressed (Mu et al. 2003). Thus, from a medical point of view TASK channels represent an important molecular target to study. These channels are blocked by a variety of compounds and molecules, such as bupivacaine (Kindler et al. 1999), Zn^{2+} (Czirják & Enyedi 2006), doxapram (Cotten 2013b), loratadine, mevastatin, mibefradil and octoclothepein (Bruner et al. 2014); and also by congeneric series such as THPP-derived compounds (Coburn et al. 2012) and bis-amide derived compounds (Flaherty et al. 2014). The highly potent TASK-1 blocker A1899, originally designed as a Kv1.5 channel blocker with a strong preference for TASK-1 channels (Kiper et al. 2015), blocks TASK-1 in the low nanomolar range (Streit et al. 2011). The blockade is selective for TASK-1 as the closely related TASK-3 channel is inhibited with only a tenth of the potency. It was previously reported that A1899 acts as an open-channel blocker and binds to residues at P1, P2 regions, M2, M4 segments and the

halothane response element (Streit et al. 2011). The presence of side-fenestrations within the crystallized structures of K_{2p} channels might redefine the drug binding site of TASK channels, initially proposed at the wall of the central cavity. In the same way side-fenestrations might represent a route for A1899 to access its binding site. In this study, we describe the binding mechanism of A1899 to TASK-1, using several computational techniques such as homology modeling, molecular dynamics simulations, molecular docking and binding free energy calculations as well as experimental electrophysiological measurements. Our results show that A1899 binds to the central cavity to cause a physical pore occlusion. Strikingly, most of the residues relevant for the TASK-1 inhibition also face into the side fenestrations and binding of A1899 to these fenestrations is a major requirement for an efficient binding to the central cavity. Moreover, we show that A1899 cannot travel from the membrane through the fenestrations to reach the binding site in the central cavity and side fenestrations.

6.2. Material and Methods

TASK-1 Homology Modeling. Since the structure of TASK-1 has not been solved, we built four homology models for TASK-1 using as template the crystal structures of TRAAK (PDBs: 4I9W, 3UM7), TREK-2 (PDB: 4BW5) and TWIK-1 (PDB: 3UKM); according to the multiple sequence alignment published by Brohawn et al. (Brohawn et al. 2012). The rationale for using multiple structures as templates for the TASK-1 homology models was to study the interactions between A1899 and the fenestrations in open and closed conformations. The four homology models were named according to the template and the fenestration state of the structures used (Table 1). The models are named: T1treCC (*TASK-1 from TREK-2 in Closed-Closed fenestration state*); T1twiOO (*TASK-1 from TWIK-1 in Open-Open fenestration state*); T1trCO (*TASK-1 from TRAAK in Open-Closed fenestration state*) and T1trOO (*TASK-1 from TRAAK in Open-Open fenestration state*). TASK-1 homology models were built and optimized using ICM software (Abagyan & Totrov 1994). Models were built as monomers and assembled as dimers using the STAMP algorithm (Russell & Barton 1992) implemented in VMD program (Humphrey et al. 1996). The homology models were validated using PROCHECK (Laskowski et al. 1993). Two K^+

ions were associated to the models in positions S2 and S4 of the selectivity filter and two water molecules at sites S1 and S3. Schrödinger Master version 9.2 software (Schrödinger 2011) interface was used to add hydrogen atoms by assigning the bonds and charges to the homology models.

The models were embedded into a pre-equilibrated phosphatidyl oleoyl phosphatidylcholine (POPC) bilayer in a periodic boundary condition box with pre-equilibrated Simple Point Charge (SPC) water molecules. Each system was subjected to a conjugate gradient energy minimization and 10 ns Molecular Dynamic simulation (MDs) in Desmond v3.0 program (Bowers et al. 2006; Schrödinger 2011). A restriction was applied to the backbone atoms of the protein and to the K^+ ions at the selectivity filter using a spring constant force of $0.5 \text{ kcal} \times \text{mol}^{-1} \times \text{Å}^{-2}$.

Table 1. Nomenclature of the TASK-1 homology models

Template	TASK-1 Homology model name
TREK-2 (PDB: 4BW5)	T1treCC
TWIK-1 (PDB: 3UMK)	T1twiOO
TRAAK (PDB: 4I9W)	T1trCO
TRAAK (PDB: 3UM7)	T1trOO

HOLE Radius Profiles. To determine the dimensions of the fenestrations and the pore the algorithm HOLE was used (Smart et al. 1996). For each MDs, one snapshot each 0.5 ns was taken, in total 80 structures (20 per model) were collected from the TASK-1 homology models MDs to perform HOLE and further analyses.

A1899 modelling. The TASK-1 blocker A1899 (Section 12.3 – Fig. 4) was sketched with the GaussView software (Dennington et al. 2009) and optimized with the Gaussian09 software (Frisch et al. 2009) by using the hf/3-21g *ab initio* calculations (Pan et al. 2002) to obtain the equilibrium geometry, the geometrical parameters and the potential energies surfaces. Later, A1899 was processed using LigPrep (Schrödinger 2011) with the force field OPLS_2005 (Shelke et al. 2011).

Molecular Docking. To find the best A1899 pose interacting with TASK-1 models taking into account the flexibility of the receptor we performed several molecular

docking in the structures collected from the MDs of all homology models using the software Glide v5.7 (Halgren et al. 2004; Schrödinger 2011) and the standard precision (SP) scoring function, obtaining 10 poses per docking simulation. Incorporating conformational rearrangements of the receptor binding pocket into predictions of the ligand binding pose is critical for improving docking results (Totrov & Abagyan 2008; Feixas et al. 2015). The ligand-binding site was defined by the residues forming the experimentally determined binding site of A1899 in TASK-1 (Streit et al. 2011). The center of the grid box was focused into the residues T92 and T198 at the bottom of the selectivity filter. The molecular docking simulations were carried out with the outer box edge of the grid setting as 30 Å. The generated grid information for each receptor is given in Appendix B – Supplemental Table S1 and Supplemental Fig. S1. We obtained a total of 200 poses (10 poses for each frame, 20 frames for each model) per model.

Binding Free Energy Calculations. The Molecular Mechanics-Generalized Born Surface Area (MM/GBSA) method that combines molecular mechanics energy and implicit solvation models (Hou et al. 2012) was employed using Prime (Schrödinger 2011) after the docking process to rescore and to analyze the 200 A1899 poses per model. In MM/GBSA, the binding free energy between the ligand (A1899) and the receptor (TASK-1 channel) to form a complex is calculated as (Eq. 1):

$$\Delta G_{bind} = \Delta H - T\Delta S \approx \Delta E_{MM} + \Delta G_{sol} - T\Delta S$$

$$\Delta E_{MM} = \Delta E_{internal} + \Delta E_{electrostatic} + \Delta E_{vdw} \quad ; \quad \Delta G_{sol} = \Delta G_{PB/GB} + \Delta G_{SA}$$

Where ΔE_{MM} , ΔG_{sol} and $T\Delta S$ are the changes in the Molecular Mechanics energy, the solvation free energy and the conformational entropy upon binding at a certain temperature T , respectively. ΔE_{MM} includes $\Delta E_{internal}$ (bond, angle and dihedral energies), electrostatic and van der Waals energies, and the term is the difference in energy between the complex structure and the sum of the energies of the ligand and the receptor alone. ΔG_{sol} is the sum of electrostatic solvation energy $\Delta G_{PB/GB}$ (polar contribution), and non-electrostatic solvation component ΔG_{SA} (non-polar contribution); this term correspond to the difference in the GBSA solvation energy of the complex and the sum of the solvation energies for the ligand and the unliganded receptor. The polar contribution is calculated using the Generalized Born model, while the non-polar energy is calculated by solvent

accessible surface area (SASA) (Adasme-Carreño et al. 2014; Rastelli et al. 2010). Corrections for entropic changes were not applied because we use the same ligand (A1899) in all calculations. It has been previously reported that the lack of an evaluation of the entropy is not critical for calculating the MM/GBSA free energies for similar systems (Wang & Kollman 2001; Massova & Kollman 2000; Hou & Yu 2007; Mena-Ulecia et al. 2015).

Experimental Interaction Scoring. According to the Alanine Mutagenesis Screening (AMS) results previously reported (Streit et al. 2011) we assigned a score for each interaction between A1899 and the residues of the binding site for each A1899 conformation. The experimental interaction score (EIS) represents the sum of the contribution to the inhibition obtained by AMS for each amino acid when the block by 400 nM A1899 was analyzed. EIS was normalized in a way that residues contribution to the binding site sum 100 (T92: 5.671; T93: 9.845; I118: 12.386; L122: 7.277; T198: 7.370; T199: 8.507; I235: 7.531; G236: 6.835; L239: 11.811; N240: 8.106; V243: 7.544 and M247: 7.116). Accordingly, we analyzed the interactions of all A1899 poses from docking; for instance, the pose 1 (Appendix B – Supplemental Table S2) interacts with T92 (5.671); T93 (9.845); I118 (12.386); L122 (7.277); T198 (7.370); T199 (8.507); G236 (6.835); L239 (11.811); N240 (8.106) and V243 (7.544), therefore the EIS is 85.3.

Clustering of Conformers. We obtained a total of 800 poses (10 poses for each frame, 20 frame for each model, 4 different TASK-1 models). To process and to organize the 800 poses we use the Conformer Cluster script (available in www.schrodinger.com/scripcenter/). The script builds a matrix (Lorenzen & Zhang 2007) using a measure of pairwise distance between conformations. This measure was the root mean square displacement (RMSD) between pairs of corresponding atoms following optimal rigid-body superposition (Shenkin & McDonald 1994). The atomic RMSD was calculated considering the atoms from A1899 numbered in Appendix B – Supplemental Fig. S2, and the linkage average method was used to cluster the A1899 poses.

Molecular Dynamics Simulations. The eight complexes A1899 - TASK-1 with the best ΔG_{bind} and EIS were subjected to a conjugate gradient energy minimization and MDs in Desmond v3.0 using OPLS-2005 (Jorgensen et al. 1996; Kaminski et al. 2001)

force field. The receptor-ligand complexes were embedded into a POPC lipid bilayer and were solvated by an orthorhombic box of SPC water model, covering the whole surface of each system. Cl⁻ were used as counter ions in order to neutralize the systems and a 0.096 M concentration of KCl was added to match the concentration used in electrophysiological measurements of A1899 on TASK-1 (Streit et al. 2011). The temperature was maintained at 300 K, while pressure was kept at 1 atm, employing the Nose-Hoover thermostat method with a relaxation time of 1 ps using the MTK algorithm (Martyna et al. 1994). Data were collected every 5 ps during the MDs for further analysis. We performed two MDs for each A1899 – TASK-1 complex. In the first one 40 ns were done applying a restraint spring constant of $0.5 \text{ kcal} \times \text{mol}^{-1} \times \text{\AA}^{-2}$ to the secondary structure of the receptor, then, the last frame was taken and a second non-restricted 100ns–MDs was performed. For the TASK-1 homology model T1trOO two MDs using the same protocol described above were performed.

Oocyte Preparation, cRNA Synthesis and Injection. Oocytes were obtained from anesthetized *Xenopus laevis* frogs and incubated in OR2 solution containing in mM: NaCl 82.5, KCl 2, MgCl₂ 1, HEPES 5 (pH 7.5) supplemented with 2 mg/ml collagenase II (Sigma) to remove residual connective tissue. Subsequently, oocytes were stored at 18 °C in ND96 solution containing in mM: NaCl 96, KCl 2, CaCl₂ 1.8, MgCl₂ 1, HEPES 5 (pH 7.5), supplemented with 33.6 μM gentamycine, 2.5 mM sodium pyruvate and 0.5 mM theophylline. Human TASK-1 (*KCNK3*, NM_002246) was subcloned into the oocyte expression vector pSGEM. Mutations were introduced with the QuickChange Site Directed Mutagenesis Kit (Stratagene) according to the instructions of the manufacturer. Subsequently, cDNA was linearized and cRNA was synthesized with the mMACHINE mMESSAGE mMACHINE-Kit (Ambion). The quality of cRNA was tested using agarose gel electrophoresis. cRNA was quantified using a UV-Vis spectrophotometer (NanoDrop 2000). Oocytes were each injected with 50 nl (5ng) of cRNA.

Electrophysiology. Two electrode voltage clamp (TEVC) recordings were performed 48 h after cRNA injection at room temperature (20-22 °C) with a TurboTEC 10CD (npi) amplifier and a Digidata 1200 Series (Axon Instruments) as A/D converter. Micropipettes were made from borosilicate glass capillaries GB 150TF-8P (Science Products) and pulled with a DMZ-Universal Puller (Zeitz). Recording pipettes had a

resistance of 0.5-1.5 M Ω and were filled with 3 M KCl solution. As recording solution ND96 was used. Inhibition by 400 nM A1899 was analyzed with voltage steps from a holding potential of -80 mV. A first test pulse to 0 mV of 1 s duration was followed by a repolarizing step to -80 mV for 1 s, directly followed by another 1 s test pulse to +40 mV. The sweep time interval was 10 s. Wash in was studied at +40 mV. For current-voltage (IV) curves, voltage was ramped from -120 to +45 mV within 3.5 s from a holding potential of -80 mV.

6.3. Results

Characterization of the side fenestrations in TASK-1 models. To simulate the behavior of TASK-1 within a lipid membrane, and considering the different conformation and fenestration states of the crystallized K_{2P} channels, we built four-homology models: T1treCC, T1twiOO, T1trOO and T1trCO (See section 13.2 and Table 1). All models were subjected to 10ns-MDs. The RMSDs of the position for all backbone atoms of the TASK-1 models from their initial configuration as a function of simulation time are illustrated in Appendix B – Supplemental Fig. S3. All models were equilibrated after 1 ns of MDs. The RMSD values remain within 0.65 Å for all TASK-1 models, demonstrating the conformational stabilities of the receptor structures.

For each MDs, 20 structures (0.5 ns frames each) were taken. In total we collect 80 structures from the TASK-1 homology models MDs. All structures were analyzed with the HOLE algorithm to gain insights for the putative relevance of the fenestrations for the interaction of A1899 with the TASK-1 channel. The fenestrations (F1, F2) formed at the interface between the subunits A (yellow) and B (red) are illustrated in Fig. 9A. HOLE radius profile analysis (along the 10ns-MDs) showed different diameter between the three models that exhibit open fenestrations: T1trCO, T1trOO and T1twOO (Fig. 9B). T1trCO presents F1 (left) open with a bottleneck diameter (BD) of 4.25 ± 0.91 Å in contrast to F2 (right) that is closed and has a BD of 1.79 ± 1.07 Å. In T1trOO the fenestrations showed a BD of 2.44 ± 0.71 Å in F1 and 2.57 ± 0.98 Å in F2. In the case of T1twOO its fenestrations exhibited the largest BD compared to the other two models mentioned above, 4.82 ± 0.71 Å in F1 and 4.36 ± 0.99 Å in F2.

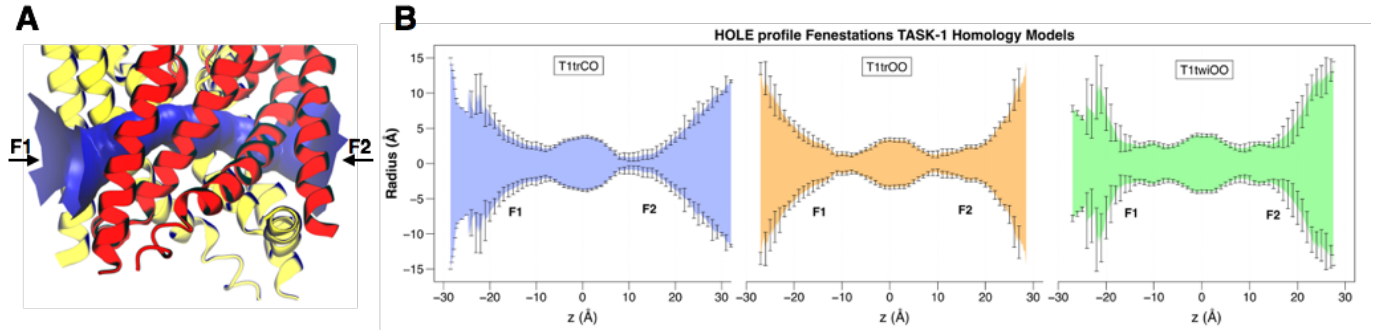


Figure 9. Characterization of the side fenestrations in TASK-1 models. HOLE profiles of the fenestrations for the TASK-1 models derived from 10 ns MDs. **A.** Representation of the fenestrations (blue solid surface) in the T1twOO model. Subunit A (yellow) and B (red) are shown in cartoon representation. **B.** Graphic shows the diameter of the fenestrations in T1trCO (blue), T1trOO (orange) and T1twOO (green) models. F1 left, F2 right. The bottleneck diameters are at the following positions in the z-Axis in each model T1trCO: F1 z-Axis = -8\AA and F2 z-Axis = 10\AA ; T1trOO: F1 z-Axis = -8\AA and F2 z-Axis = 10\AA ; T1twOO: F1 z-Axis = -7\AA and F2 z-Axis = 8\AA .

Next we analyzed the position of the residues of the previously described A1899 binding site (Streit et al. 2011) in more detail, studying T92, T93 in the P1 region, T198, T199 in the P2 region; I118, L122 in the M2 segment; L232, I235, G236, L239 and N240 in the M4 segment; and V243 and M247 in the Halothane Response Element (HRE). We examined for each model the relative presence of these amino acids during the MDs in the central cavity and/or fenestrations. Table 2 summarizes whether the residues of the A1899 binding site face into the fenestration and/or the pore. Unexpected from the initial description of the A1899 binding site using a KvAP open state model of TASK-1, only the residues T93, N240 and M247 are exclusively present in the central cavity of the channel during the MDs. Residues L122, T199 and L239 are present both in the pore and the fenestrations. In addition, different from our previous study having no K_{2p} crystal structure as a modeling template available (Streit et al. 2011), we observed that the residues I188, T198, L232, I235 and G236 were exclusively oriented towards the fenestrations and did not protrude into the central cavity.

Table 2. TASK-1 residues in the fenestration (F) and the Pore during the MDs – HOLE results. Above 50% of the MD time is considered that the residue forms part of a cavity (NP: No presence)

Residue	T1treCC	T1trCO	T1trOO	T1twOO
T92	NP	NP	NP	NP
T93	Pore	Pore	Pore	Pore
I118	NP	F	F	F
L122	Pore	Pore & F	Pore & F	Pore & F
T198	NP	F	F	F
T199	Pore	Pore & F	Pore & F	Pore & F
L232	NP	NP	F	F
I235	NP	F	F	F
G236	NP	F	F	F
L239	NP	F	F	Pore & F
N240	Pore	NP	Pore	Pore
V243	NP	NP	NP	NP
M247	Pore	Pore	NP	NP

The results for T1trCO model falls in the open fenestration.

In a model with a closed fenestration state (T1treCC) the residues of the experimentally determined binding site are only in 38.5 % present in the central cavity, whereas the other residues are hidden inside the protein. Also in models with open fenestrations, the majority of the residues of the binding site are not facing the central cavity, but point into the lateral openings: 53.8 % of the residues in T1trCO, and 61.5 % in both T1trOO and T1twOO models. Only 30.8 % of the residues of the binding site are present in the pore at both T1trCO and T1trOO models, and their presence in the pore is 38.5 % in T1twOO (Table 2).

Ordering of A1899 docking solutions in TASK-1 by cluster analyses. To study the interaction of A1899 with TASK-1 in the four different TASK-1 homology models we took the flexibility of the residues of the channels into account, especially for those of the binding site. To this end we performed docking assays in the 80 frames obtained from the four TASK-1 homology models during the 10ns-MDs. The structures were prepared for molecular docking simulations retaining the structural and energetic properties from the MDs. The top-10 poses for each docking were saved. With this protocol we collected 200 poses of A1899 for each of the four TASK-1 models (800 in total). All poses were clustered using a RMSD matrix (see Materials and Methods). Fig. 10A shows the RMSD matrices before and after grouping into clusters by conformational similarities. Significant

conformational clusters, for which the populations depart by more than 2σ from the mean cluster population (Bottegoni et al. 2006) are summarized in Table 3. Fig. 10A illustrates the significant clusters and their size as blue squares, visible on the diagonal lines. The significant clusters within the different TASK-1 models, located in the central cavity and/or fenestrations, are depicted in different colors (Fig. 10B). From the clustering process it can be seen that A1899 poses docked in T1twiOO exhibit a lower RMSD, than in other models (Fig. 10A). For T1twiOO less diversity was observed, but two very large clusters. The most populated clusters of A1899 in T1twiOO model (Table 3) Cluster-17 (black) and Cluster-18 (blue) are located within the fenestrations (Fig. 10B zoom). Also the cluster No. 57 (Table 3) of the T1trCO model, which has with 93 conformations the highest population of all the clusters we identified, is oriented inside the open fenestration F1 (Fig. 10B zoom). These open hydrophobic fenestrations allow the ligand (LogP value = 4.738) to anchor inside. Accordingly, the T1trCO and T1twiOO structures which have side fenestrations with a larger diameter (Fig. 9B) have increased populations within their clusters.

Table 3. Significant clusters in TASK-1 models.

Model	No. Cluster	Population	Average Docking Energy (kcal * mol ⁻¹)
T1treCC	1	37	-48.392
	2	31	-51.927
	3	23	-47.410
	4	23	-50.966
T1twiOO	17	67	-48.712
	18	45	-49.873
T1trOO	36	26	-49.706
	37	26	-47.979
	38	20	-49.878
	39	18	-48.945
	40	17	-49.347
T1trCO	57	93	-51.124

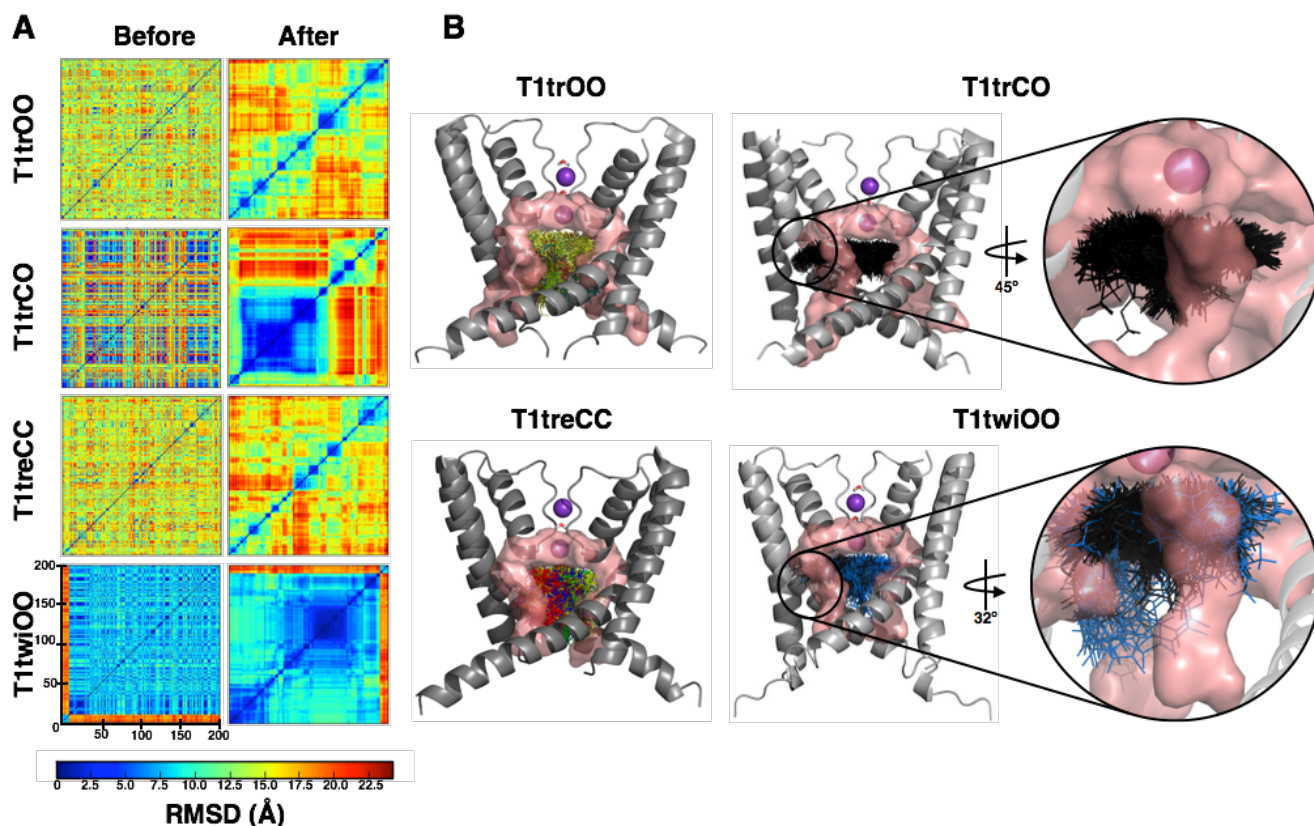


Figure 10. Ordering of A1899 docking solutions in TASK-1 by cluster analyses. Clustering of A1899 poses was performed by atomic RMSD comparison. **A.** The symmetrical distance matrix illustrates atomic RMSD comparison of the 200 poses of A1899 found by molecular docking *per model*. On the diagonal line the RMSD is zero because the poses are compared with itself. Left: Matrix of A1899 poses organized by number before clustering. Right: Matrix of A1899 poses after clustering. The poses are organized by atomic RMSD comparison between them and conformational similarity. The input order is kept on the diagonal; accordingly, the significant clusters are now visible as squares on the line. The inferior bar is the RMSD atomic distance scale in Å. Appendix B – Supplemental Table S3 shows all the clusters of A1899 poses *per model*, the mean cluster population and the associated standard deviation (σ). **B.** Significant clusters are represented by colored lines. K^+ ions are shown in sphere representation and TASK-1 models in cartoon representation. For better display only the segments P1, M1 and M2 are shown. The binding site is represented in red surface representation. Clusters No. 17 (black) and No. 18 (blue) interacting with T1twiOO and cluster No. 57 (black) interacting with T1trCO are zoomed for a better visualization.

Ordering A1899 poses of significant clusters by their free binding energy.

Next, only the A1899 poses from the significant clusters were further analyzed and scored by their free binding energy, ΔG_{Bind} ($\text{kcal} \times \text{mol}^{-1}$) which was calculated with the MM/GBSA method. In Fig. 11A we plotted for all A1899 poses within significant clusters the experimental interaction score (EIS) against the ΔG_{Bind} . The framed poses in the top left

corner represent the best docking solutions according to their lower ΔG_{Bind} value (between -120 and -100 kcal \times mol $^{-1}$) and their higher EIS (between 65 and 95). The best A1899 poses are found for models in which both fenestrations are in the open state, for instance, 224 and 387 are from the T1twiOO, and the poses 479, 562, 565, 567, 569 and 570 are from the T1trOO model (Fig. 11A-B).

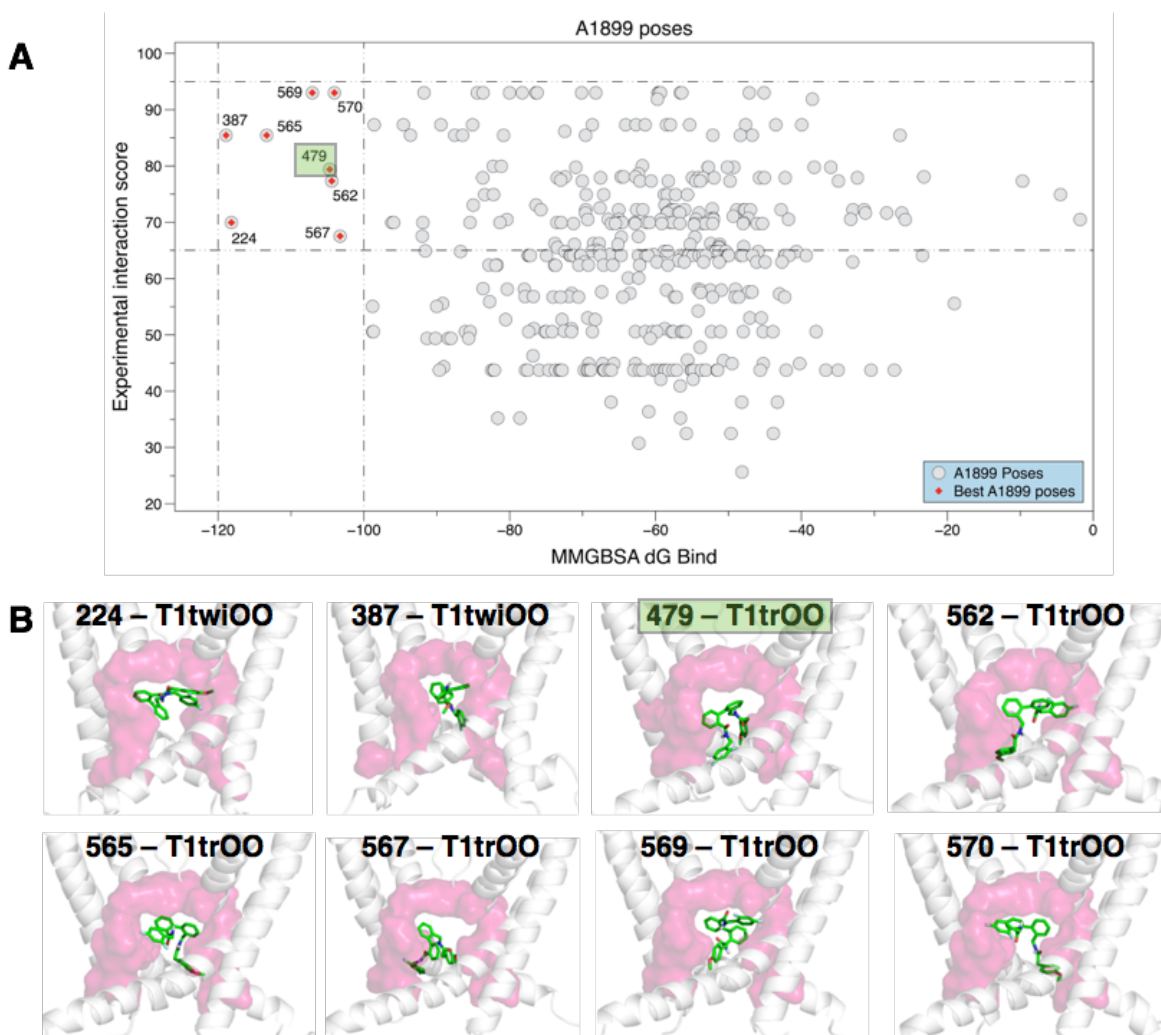


Figure 11. Ordering A1899 poses of significant clusters by their free binding energy. **A.** ΔG_{Bind} energy vs Experimental interaction score plot of the A1899 poses of significant clusters represented in gray dots. The best A1899 poses are represented in red dots. In Appendix B – Supplemental Table S2 the ΔG_{Bind} for each pose in the significant clusters is given. The best pose selected for further experiments, as it reflects all the functional data from a previous mutagenesis study (Streit et al. 2011), is highlighted with a green square (pose 479). **B.** A1899 best poses in stick representation interacting with TASK-1 models (cartoon representation), only the segments P1, M1 and M2 are shown. The binding site is represented in pink surface representation.

Analyzing all A1899 poses from the significant clusters (gray dots in Fig. 11A) reveals that the drug is mostly oriented perpendicular to the pore, consistent with a direct blockage of the ion flux through the channel. This becomes also evident from the best docking solutions illustrated in Fig. 11B. We found that the residues T93 and T199 located at the base of the selectivity filter are relevant for these interactions. 95.1 % and the 98.8 % of the poses interact with the residues T93 and T199, respectively. Probably, they interact with A1899 through H-bonds. Analyzing all complexes with the four different models, a total of 56 H-Bonds are present in the interaction of A1899 with T93 and a total of 26 H-Bonds are present in the interaction with T199. Note, that the T1treCC model, the only one with a closed-closed fenestration state, presents only one pose (pose 161) with a H-Bond to T93 (Appendix B – Supplemental Table S2). This phenomenon can indicate that the fenestrations may strengthen the interactions between A1899 and TASK-1.

To study how A1899 interacts with the residues of the binding site, the complexes of A1899 with TASK-1, having the lowest ΔG_{Bind} energy and the highest EIS (poses 224, 387, 479, 562, 565, 567, 569 and 570. Fig. 11A), were selected and subjected to MDs. The atomistic systems were equilibrated and relaxed for 40 ns. Then, the relaxed complexes were subjected to 100 ns unrestrained MDs. In all MDs the TASK-1 structure remained stable (Appendix B – Supplemental Fig. S4A), even for the A1899-TASK-1 complex (pose 387). The A1899 poses were stable during the MDs and the structures showed only minor deviations from their initial docking positions (Supplemental Fig. S4B).

Contacts of A1899 with residues of the TASK-1 binding site and the nature of the chemical interactions. Next, we analyzed how frequently during the 100 ns MDs A1899 interacts with the residues of the binding site. Therefore, the contact frequencies of A1899 were calculated looking at the residues within less than 4 Å distance to the ligand. From these eight 100 ns MDs only the A1899 pose # 479 interacted with all the residues of the binding site including M247, which could previously not be predicted by docking (Streit et al. 2011) (Fig. 12A).

To characterize changes in the A1899 heavy atoms position along the 100 ns unrestrained MDs of our final model (pose 479 from the *T1trOO* model), the RMSF (Root Mean Square Fluctuation) was calculated. RMSF shows the stability of the ligand in the

binding site along the MDs due to the established interactions with the residues of the binding site. The low RMSF values indicate that A1899 remains in the binding site during the whole MDs (Appendix B – Supplemental Fig. S5A-B). This is in agreement with the stable time dependence of RMSD for A1899 in our model (Appendix B – Supplemental Fig. S4A) and indicates that A1899 has not undergone a major rearrangement of its conformation during the MDs (Appendix B – Supplemental Fig. S4B).

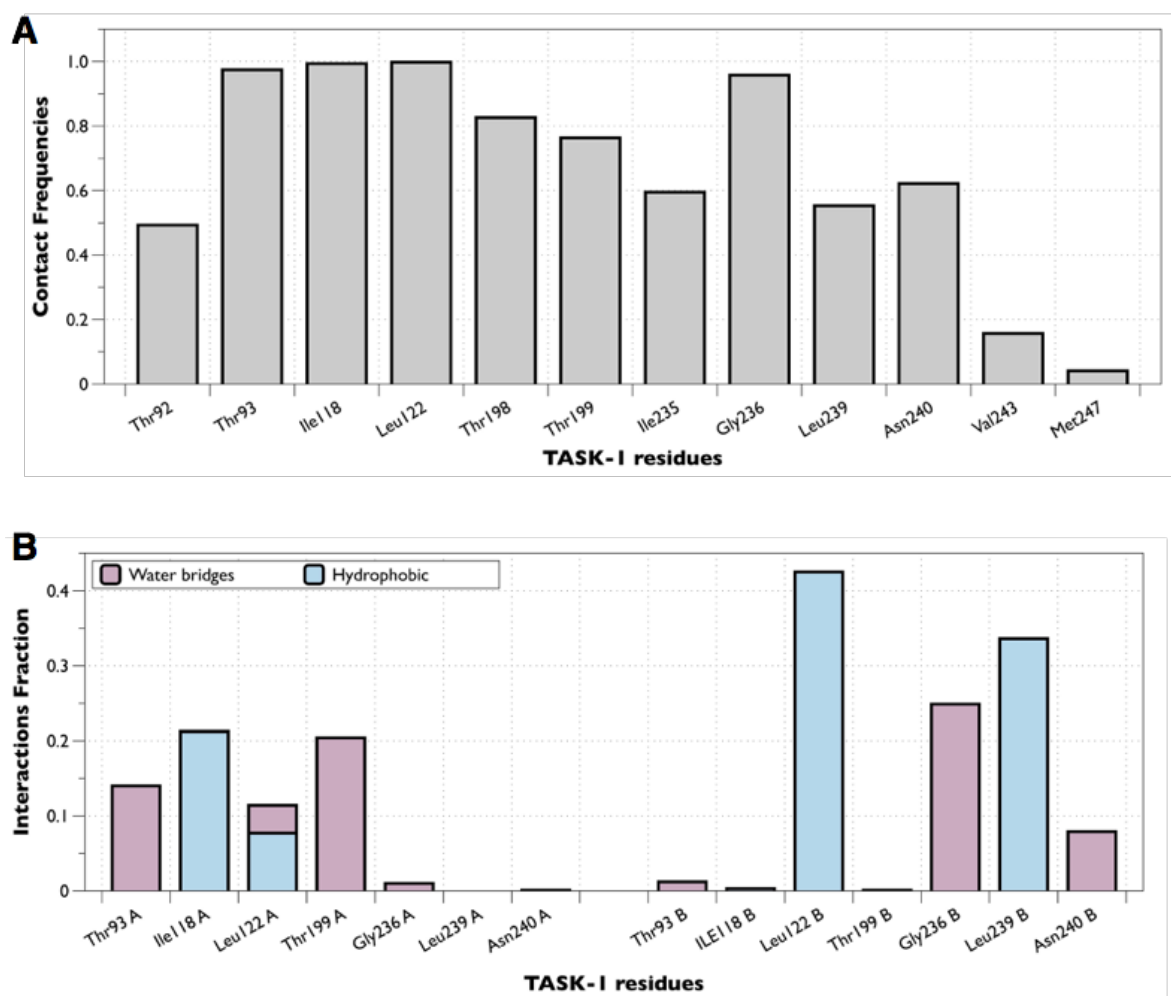


Figure 12. Contacts of A1899 with residues of the TASK-1 binding site and the nature of the chemical interactions. **A.** A1899 pose 479 is at 4 Å of all the residues of the binding site. Contact frequencies of A1899 with T1trOO residues at 4 Å. Bars indicate the contacts frequency along the 100ns-MDs. **B.** Effective interactions between the residues of T1trOO and A1899-pose 479 are categorized into two types: Hydrophobic and Water bridges. The stacked bar charts are normalized over the course of the unrestrained MDs.

Next we analyzed the chemical nature of the A1899 interaction with TASK-1, over the time period of the unrestricted MDs. The data were categorized and summarized into two types: hydrophobic and water bridges (Fig. 12B). The stacked bar charts were normalized over the course of the trajectory. It can be seen that although pose 479 is within 4 Å from all the residues of the binding site, not all of them chemically interact with A1899. Only T93, L122 and T199 from subunit A and G236 and N240 from subunit B form water bridges with the drug through H-bonds. The residues I188, L122 from subunit A and L122 and L239 from subunit B interact with A1899 via hydrophobic contacts (Fig. 12B). This network of hydrophobic and water bridges interactions allows A1899 to block the K⁺ flux due to its conformational location at the bottom of the SF (Fig. 13).

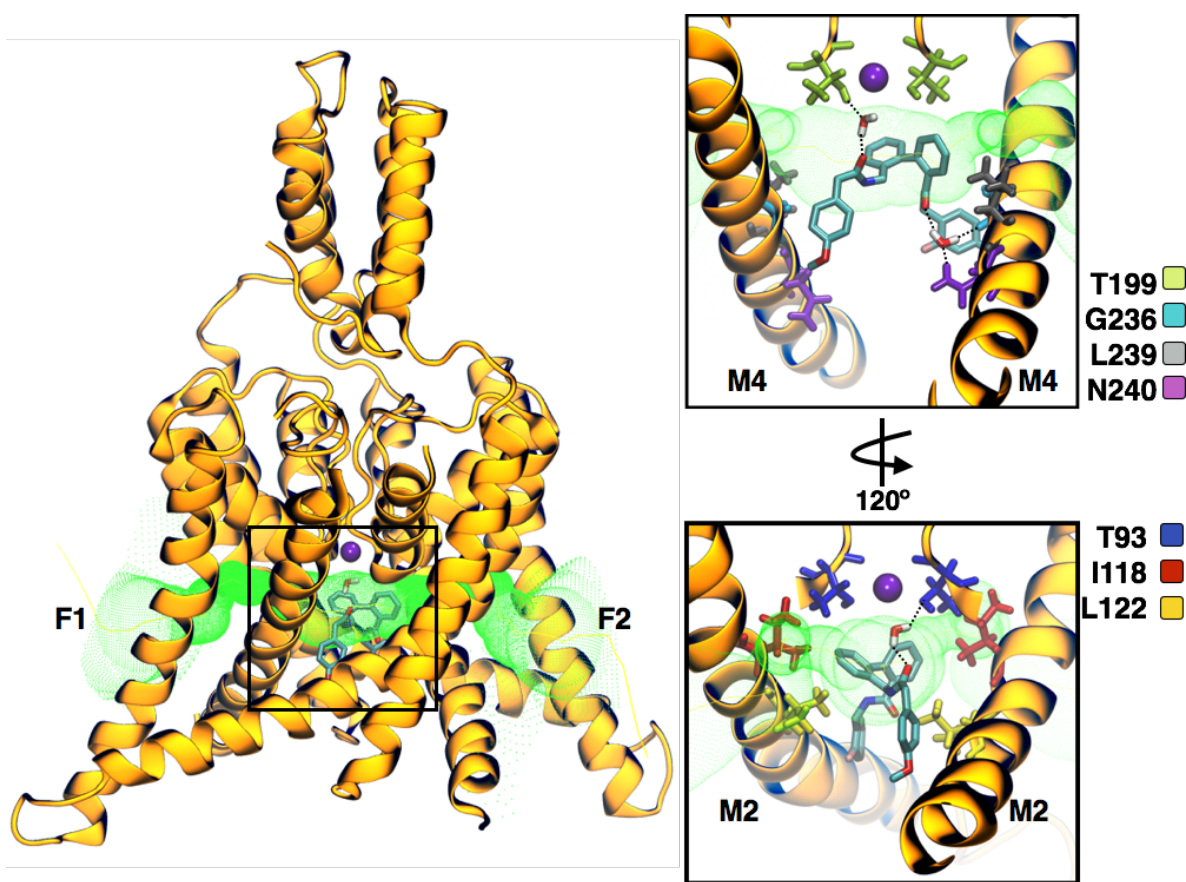


Figure 13. Redefined binding mode of A1899 in TASK-1 includes residues that contribute to the side fenestrations. Residues T93 (blue) from P1 and N240 (magenta) from M4 segment are exclusively in the pore. Residues L122 (yellow) from M2 and T199 (green) from P2 are facing the pore and the fenestrations; G236 (cyan), L239 (gray) from M4 segment and I188 (red) from M2 are exclusively in the fenestrations (Table 2). All the amino acids as well as the water molecules are shown in stick representation. The H-Bond interaction between A1899-T93, A1899-T199, A1899-G236 and A1899-N240 through water bridges are showed as black dotted lines. Fenestrations (F1 and F2) are showed as green dotted surface.

A1899 stabilizes the open fenestrations of TASK-1. HOLE radius profiles were determined for the T1trOO model and the A1899-T1trOO complex after 0 and 100 ns of the unrestricted MDs, to study how the fenestrations change over time due to the presence of A1899. A1899 is located in the inner cavity protruding to the fenestration F2. At the beginning of MDs (0 ns – green) both fenestrations are open. With A1899 the F1 fenestration remains unchanged but F2 changed and opened by an additional 4 Å (after 100 ns, blue) indicating that the ligand despite being located in the inner cavity favors the fenestration open-state. This phenomenon can be appreciated at 16.2 Å in the Z-axis (Fig. 14).

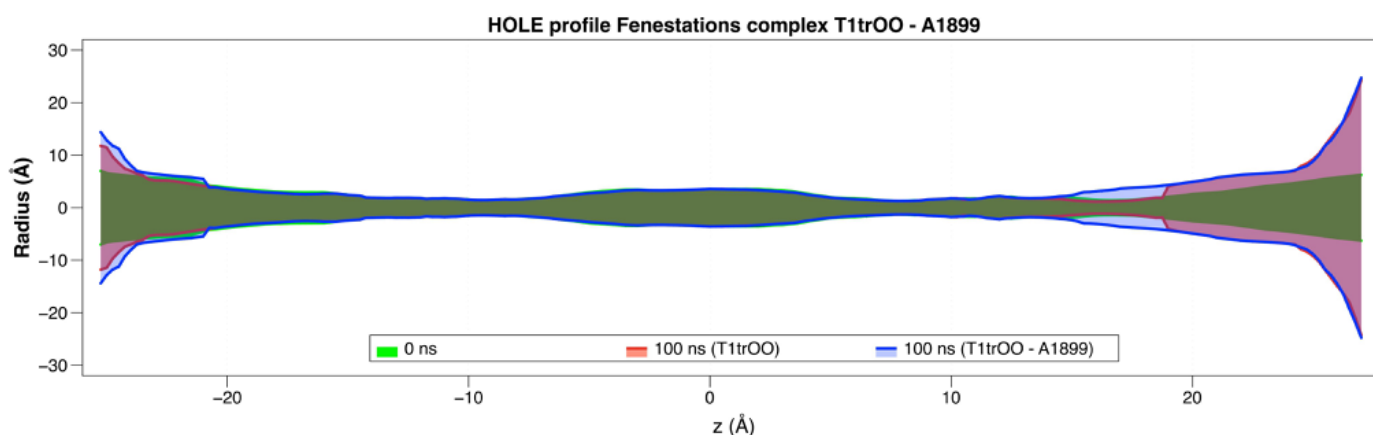


Figure 14. A1899 stabilizes the open fenestrations of TASK-1. A1899 pose 479 protrudes into the side fenestration F2. HOLE radius profile of the T1trOO fenestrations at the start of the MDs (0ns - green) and after 100 ns with (blue) and without (red) A1899. The bottleneck diameter at F2 are T1trOO 0ns: BD=2.29 Å z-Axis → 16.7 Å; T1trOO 100ns: BD= 2.29 Å z-Axis → 16.2 Å; T1trOO + A1899 100ns: BD= 6.34 Å z-Axis → 16.2 Å.

A1899 does not pass the side fenestrations to reach the binding site. To determine if A1899 can go from the membrane through the fenestrations to its binding site, we experimentally blocked the fenestrations by individually mutating the residues L115 and F238 to tryptophan, as these moieties will project into the lateral openings of the fenestrations of the channels. Both mutants L115W and F238W are likely to close the fenestrations (Fig. 15A). This effect can be visualized by analyzing the HOLE radius profiles of the mutants models in comparison with wild-type channel model mainly at

position 16.25 Å of the Z axis where the fenestration diameter in WT = 6.34 Å, L115W = 4.18 Å and F238W = 2.76 (Fig. 15B). In voltage clamp recordings, the mutants are inhibited as efficiently as wild-type TASK-1 by 400 nM A1899 (Fig. 17C-D), which is not unexpected, as these residues do not directly contribute to the A1899 binding site. Most importantly, these mutations do not alter the kinetics for the onset of inhibition, meaning that they are not occluding the access of the drug to the central cavity via the fenestrations (Fig. 15E).

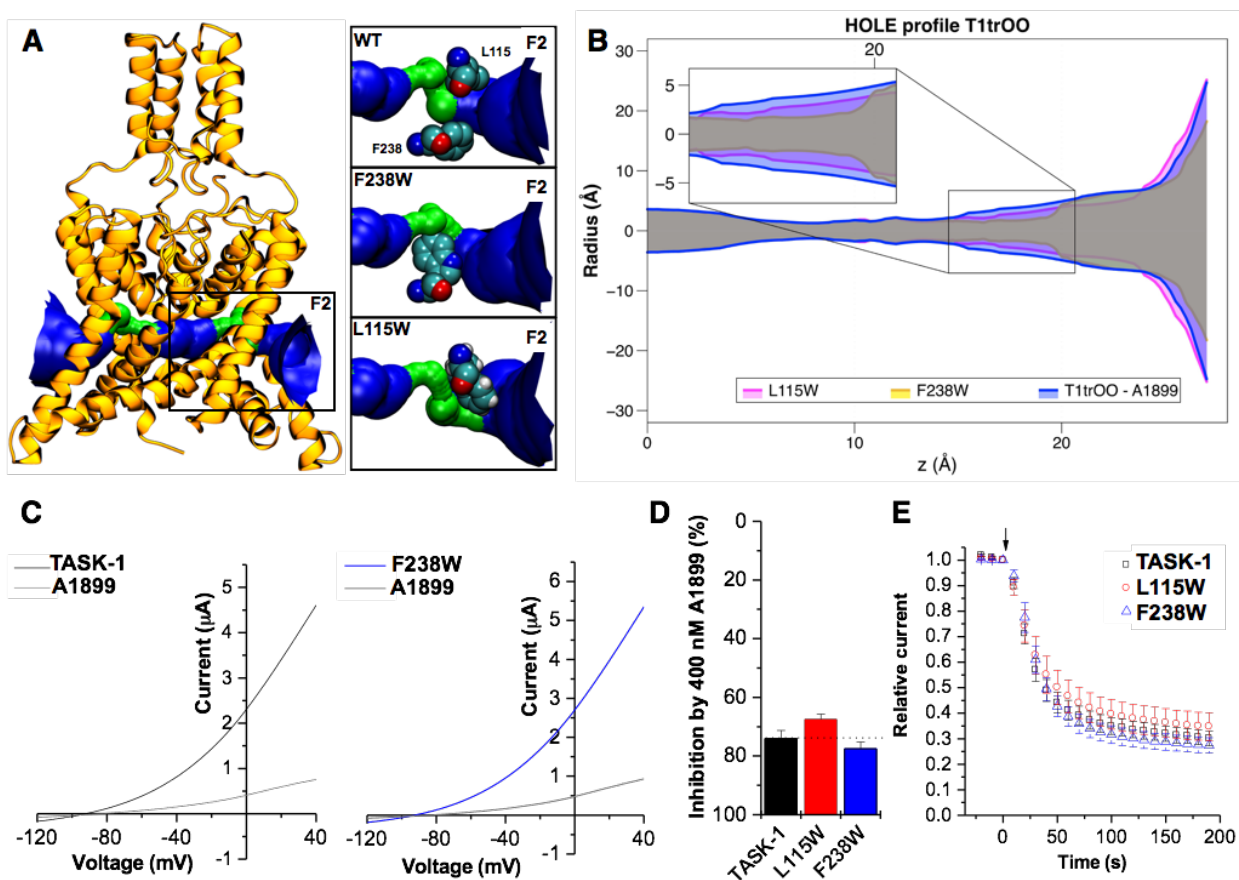


Figure 15. A1899 does not pass the side fenestrations to reach the binding site. Replacement of L115 and F238 by tryptophan reduces fenestration radii. **A.** Surface representation of the fenestrations of T1trOO-WT (corresponds to T1trOO – A1899 after 100ns of MDs), L115W and F238W residues are showed in sphere representation. The *in silico* mutations were done at the structure of T1trOO – A1899 after 100ns of MDs. Fenestration radii > 2.30 Å (Blue), fenestration radii < 2.30 Å (green). **B.** HOLE radius profile of T1trOO-A1899-L115W (pink), T1trOO-A1899-F238W (yellow) and T1trOO-A1899 (blue); only fenestration F2 is represented. **C.** TEVC recordings of TASK-1 (black) and TASK-1 F238W (blue) before and after application of 400 nM A1899 (gray). **D.** Percentage of block by 400 nM A1899 of TASK-1 wildtype (black) or the mutants L115W (red) and F238W (blue) analyzed at +40 mV. **E.** Wash in kinetics of A1899 of TASK-1 wildtype (black) and the mutants L115W (red) and F238W (blue).

6.4. Discussion

A key feature of K_{2p} channels is the presence of intramembrane side fenestrations located just underneath the selectivity filter that -according to the recent literature- could be 'drugable' (Jorgensen et al. 2016). In our study we probed whether the TASK-1 specific blocker A1899 is utilizing these fenestrations to cause a channel inhibition. To study the interaction of A1899 with TASK-1 in four different TASK-1 homology models with different fenestration states we were taking the flexibility of the residues of the binding site into account, and we collected 200 poses of A1899 for each of the models (800 in total). Then we faced the problem of choosing a single binding mode from a burden of several different docking conformations to reflect the previous experimental results of our group (Streit et al. 2011). Often, docking scoring functions might not help with the choice. To tackle this issue, it was proposed to utilize a clustering approach (Bottegoni et al. 2006). The pose 479 selected belongs to cluster #40 with a population of 17 conformations docked into the T1trOO model (Table 3 and Supplemental Table S2). As expected from our previous work A1899-pose 479 blocks the K^+ flux due to its conformational location underneath the selectivity filter (Fig. 13). However, the ligand, despite being located in the central cavity, favors a binding to open fenestrations (Fig. 14).

Almost all the poses of A1899 are located underneath the selectivity filter, rather remote from the distal part of the M4 segment, including the residue M247 of the TASK-1 binding site (Streit et al. 2011). Streit *et al.*, 2011 (Streit et al. 2011) could not explain the interaction of A1899 with the remote M247 and therefore suggested that this residue might be only relevant as it is located in the pathway to the central cavity. But here, as we explored eight-hundred A1899 conformations, we found a pose (479) within 4 Å from all the residues of the binding site including M247 (Fig. 12A). Therefore, our final binding model of A1899 could be also a starting point to study the structural differences in the drug affinities of TASK-1 and TASK-3 channels, as M247 is the only amino acid of the A1899 binding site which is not conserved between these two channels.

As discussed above it was previously suggested that M247 might influence drug sensitivity because it regulates the accessibility of A1899 to the pore. As A1899 was able to tightly bind to TASK-1 models with open fenestrations and these lateral cavities can

potentially work as drug access pathways (Jorgensen et al. 2016) we wondered whether M247 regulates accessibility of the pore for A1899 or whether the compound travels a completely different way entering the central cavity via the side fenestrations. When the residues L115 and F238 that are exposed to the lateral cavities in the homology models are replaced by voluminous residues, the respective mutants are inhibited just as efficiently and with the same kinetics as wildtype TASK-1 (Fig. 15). These data suggest that A1899 does not travel in a lateral manner from the lipid face through the side fenestrations to reach the binding site.

The lateral fenestrations in K_{2p} channels are only present in what has been called the 'down state' which refers to the position of the M4 segment that extends intracellularly in a rather straight way. In the 'up state', the fenestrations are closed by the upward movement and rotation of M4 (Dong et al. 2015). All of our TASK-1 homology models exhibit different fenestration shapes; in fact, these structural differences appear to play a major role in the interaction of A1899 with TASK-1. In the model with closed fenestration states (T1treCC) the sole option of A1899 to interact is underneath the selectivity filter. The open fenestrations in T1trCO and T1twiOO, on the other hand, allow A1899 hydrophobic moieties to be oriented towards the interior of the fenestrations (Fig. 10B – zoom view). The T1trOO fenestrations are not sufficiently large to permit the complete entry of A1899 into the fenestrations (Fig. 9B). We observed A1899 average poses of the five significant clusters in T1trOO (Table 3) and all of them are placed in the central cavity (Supplemental Fig. S6) but anchored by the residues of the binding site placed in T1trOO at the fenestrations (Table 2). The mechanism that blockers located in the central cavity requires also side wards interactions (anchor) with residues in the side fenestrations might be conserved among K_{2p} channels, as the relevant residues forming the fenestrations share high sequence similarities within the K_{2p} channel family (Brohawn et al. 2012; Jorgensen et al. 2016)

This relevance of the structural differences in the fenestrations for the interaction of A1899 with TASK-1 is also supported by the number of binding site residues that become available in the open fenestrations. Whereas in a model with a closed fenestration state (T1treCC) A1899 would be able to only interact with 38.5% of the binding site residues, since they are exclusively present in the central cavity. In contrast, in models with

lateral fenestrations interactions with binding site residues located within these structures become possible: these reflect 53.8% of the TASK-1 binding site residues in T1trCO, and 61.5% in both T1trOO and the T1twOO models (Table 2).

Streit *et al.* previously reported that A1899 acts as an open-channel blocker and binds to residues of the P1, P2 regions, M2, M4 segments and the halothane response element (HRE) in TASK-1 channel (Streit *et al.* 2011). The mode of A1899 binding was modeled using an open state KvAP crystal structure as a template. This TASK-1 homology model had however, due to the lack of K_{2P} crystal structures available at that time, a fourfold symmetry and it lacked the side fenestrations. Although A1899 can bind to structures with closed fenestrations such as T1treCC, our data suggests a redefinition of the A1899 binding mode, in which the blocker additionally binds tightly to structures within the open fenestrations. TASK-1 open probability increases with depolarization (Duprat *et al.* 1997), suggesting that there are more channels in the up-state with closed fenestrations. However, A1899 is not a state-dependent blocker, because there was no voltage-dependence of inhibition (Streit *et al.* 2011). In fact no reduced block was observed during depolarization which one would expect for a preferential binding to the down-state with open fenestrations. On the other hand our data suggests that once A1899 has bound and blocked TASK-1 the closed state of the channel with open fenestrations is more favorable. This becomes evident (1) as in open fenestrations all the residues of the binding site can participate in drug binding and (2) as we found in MDs in the presence of A1899 an opening of the fenestrations (Fig. 14). This stabilization of the closed state might be directly mediated by residues of the drug binding site in or near the fenestrations, i.e. I235 and L239, as the homologous residues in TWIK-1 (M260 and L264) were reported to be crucial for the equilibrium between open and closed fenestration states (Jorgensen *et al.* 2016). Taken together these data suggest that A1899 can bind to both the open and the closed fenestration states and that the drug will stabilize the closed state after pore block.

In summary we demonstrate that the TASK-1 specific blocker A1899 requires a binding to residues that are located in the side fenestrations. Unexpectedly, the majority of residues previously described to interfere with TASK-1 block by A1899 project their side chains towards the fenestration lumina, underlining the relevance of these structures for drug binding in K_{2P} channels. Despite its hydrophobicity, A1899 does not seem to use the

fenestrations to gain access to the central cavity from the lipid bilayer. In contrast binding of A1899 to residues of the side fenestrations might provide a physical ‘anchor’, reflecting an energetically favorable binding mode that after pore occlusion stabilizes the closed state of the channels.

6.5. Future work

The selective TASK-1 blocker A1899 described here is a powerful tool for studying the structural role of the fenestration in the blockage mechanism of TASK-1 channel. We took advantage of the blocker to probe the direct interaction with amino acids located at the inner pore as well as the side-fenestration. However, the experimental evidence reveals an understanding role of the amino acid M247, which, together with N240 and V243, are responsible for the binding of A1899 to the HRE. Although, our theoretical findings of A1899 to the TASK-1 homology models predicts interactions of the HRE N240 and V243 with the drug, M247 seems to be too remote from the final binding site. For these reason it is worth to explore the role of M247 in the binding of A1899, to figure out if the residue is part of the binding site indeed, or if somehow plays a carrier-role driven A1899 to the final binding site.

Here, using a K_{2P} channel-based TASK-1 homology models we describe the role describe the role of the fenestration for the d of A1899 to TASK-1, nevertheless the role of the fenestration in the gated/blockage modulation mechanisms of K_{2P} channels remains unknown. Recently, strong voltage-dependence activation has been observed in some K_{2P} channels (Schewe et al. 2016), an a non-canonical voltage-sensing mechanism mediated by the selectivity filter was proposed to control gating in K_{2P} channels. However, we consider that the recently release K_{2P} crystal structures, along with the evidence from electrophysiology measurements as well as molecular simulation will allow to propose a more general gating/blockage mechanism mediates by the fenestrations-SF system.

6.6. Scientific Production

Ramirez, D., Arévalo, B., Martínez, G., Rinné, S., Sepúlveda, F., Decher, N. & González, W. “*Side fenestration provide and ‘anchor’ for stable binding of A1899 to the pore of TASK-1 potassium channel*”. Submitted to *Molecular Pharmacology* (2016).

Abstract. A1899 is a potent and selective antagonist of the two-pore domain potassium (K_{2p}) channel TASK-1. It was previously reported that A1899 acts as an open-channel blocker and binds to residues of the P1, P2 regions, the M2, M4 segments and the halothane response element. The recently described crystal structures of K_{2p} channels together with the newly identified side-fenestrations indicate that residues that are relevant for TASK-1 inhibition, are not as initially proposed purely facing the central cavity. Accordingly, the TASK-1 binding site and the mechanism of inhibition might need a re-evaluation. We have used TASK-1 homology models based on recently crystalized K_{2p} channels and molecular dynamics simulation to demonstrate that the highly potent TASK-1 blocker A1899 requires a binding to residues that are located in the side fenestrations. Unexpectedly, the majority of residues previously described to interfere with TASK-1 block by A1899 project their side chains towards the fenestration lumina, underlining the relevance of these structures for drug binding in K_{2p} channels. Despite its hydrophobicity, A1899 does not seem to use the fenestrations to gain access to the central cavity from the lipid bilayer. In contrast binding of A1899 to residues of the side fenestrations might provide a physical ‘anchor’, reflecting an energetically favorable binding mode that after pore occlusion stabilizes the closed state of the channels.

Structure-based discovery of potential two-pore domain potassium channels TASK-3 modulators

7.1. Introduction

Two-pore domain potassium (K_{2p}) channels have been widely studied since the KCNK gene family – those that codify for K_{2p} channels- was discovered (Goldstein et al. 2001), providing important advances in the understanding of their physiological roles. K_{2p} subunits contain two pore-forming loops creating dimeric channels (Bayliss & Barrett 2009). The TASK subfamily includes three members (TASK-1, -3 and -5) (Cotten 2013b). The closest relatives of the TASK-3 ($K_{2p}9.1$) channel (Rajan et al. 2000) is TASK-1 ($K_{2p}3.1$) (Talley et al. 2000). TASK-3 plays an important role under physiological conditions and is very sensitive to extracellular pH changes in the range of 6 to 7 (Rajan et al. 2000; González et al. 2013; Zúñiga et al. 2011).

The tertiary structure of K_{2p} is different in relation with other potassium channels. The crystallized structures of K_{2p} channels TWIK-1 (PDB: 3UKM (Miller & Long 2012)), TRAAK (PDBs: 3UM7 (Brohawn et al. 2012), and 4I9W (Brohawn et al. 2013)), TREK-1 (PDB: 4TWK), and TREK-2 (PDBs: 4BW5, 4XDJ, 4XDK and 4DKL (Dong et al. 2015)); reveal differences that give insights into distinctive gating and ion permeation properties. Near to the center of the membrane, the M2 transmembrane segment is kinked by approximately 20°, the kinks generate two fenestrations, one on each side of the dimer that expose the central cavity to the hydrophobic core of the lipids membrane (Aryal et al. 2014). These fenestrations are potentials sites for the interaction of lipids and other hydrophobic molecules, as well as a pathway that can guide blockers into the binding site (Jorgensen et al. 2016).

Some studies have demonstrated that TASK channels participate in the chemical control of breathing due to their intrinsic pH and O_2 sensitivity (Bayliss et al. 2001; Bayliss

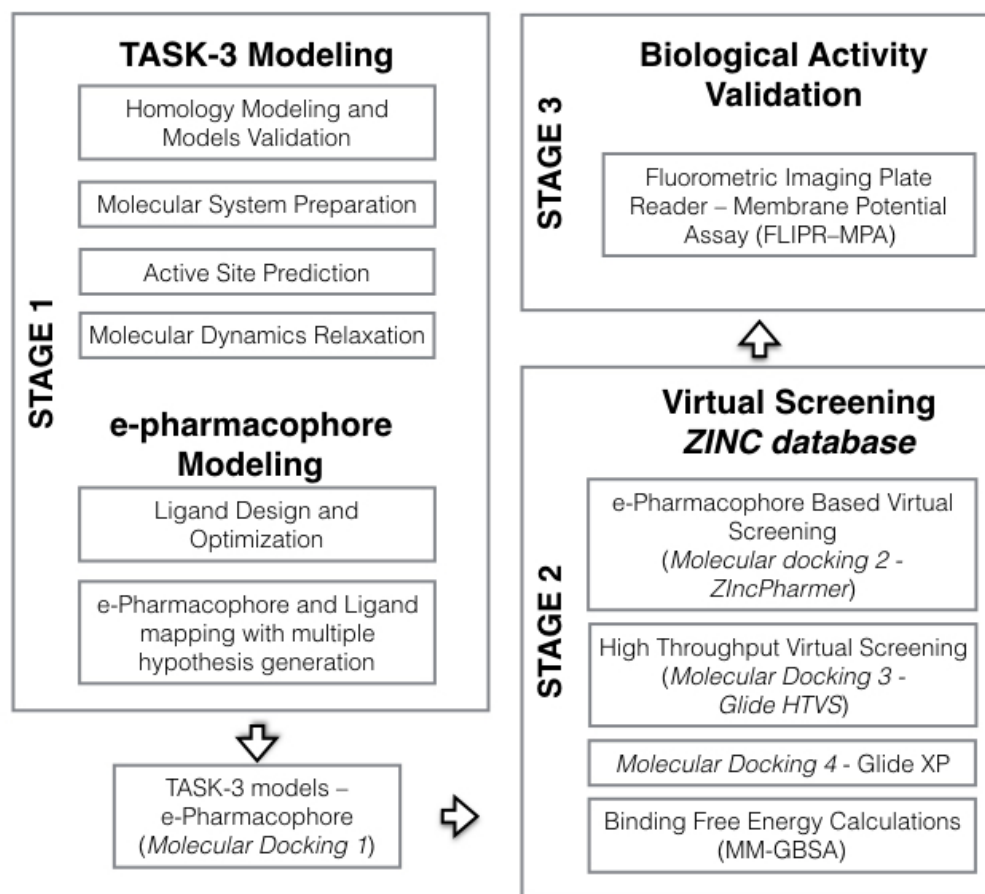
et al. 2003; Talley et al. 2003). These channels are expressed in the nervous, cardiovascular, genitourinary and gastrointestinal systems (Goldstein et al. 2001). Besides to be evolve in chemosensation (Trapp et al. 2008) they also have a role in the regulation of the immune system (Meuth et al. 2008). TASK channels contribute to immobilizing effects of volatile anesthetics due to background K^+ currents activated by these anesthetics causing decreased excitability by membrane hyperpolarization (Lazarenko et al. 2010). For this reason, TASK-1 and TASK-3 are potential molecular targets for these anesthetics, activating neuronal background K^+ currents.

TASK-3 is abundant in the hippocampus, cerebellum and cortex (Talley et al. 2001), some previous studies have described the regulate neurotransmitter function as well as the mediating effect of the neurotransmitter activation function (Meuth et al. 2003). The development of new selective TASK-3 modulators could influence the pharmacological treatment of several neurological conditions such as sleep disorders, neurodegeneration, cognitive impairment, Huntington's disease, Parkinson's disease or major depressive disorder (Gotter et al. 2011).

Not many promising inhibitory TASK-3 modulators have been reported in the scientific literature. One of the few works in this context was made by Coburn et al. (Coburn et al. 2012); they reported the use of aminopyrimidine derivatives as potent TASK-3 blockers. Recently, Noriega-Navarro et al. (Noriega-Navarro et al. 2014) reported the application of dihydropyrrolo[2,1-a]isoquinoline derivatives (DPIs) as novel TASK inhibitors. In this sense, the use of fused heterocyclic-compounds has attracted the attention as new TASK modulators. Therefore, it is necessary the development of simple theoretical/experimental methodologies to find new heterocyclic derivatives with potential applications as TASK-3 modulators.

In this study, we developed a protocol to search novel TASK-3 modulators that includes a pharmacophore based virtual screening, docking based high throughput virtual screening (HTVS), molecular docking to refine binding-poses, and the prediction of free energy ligand-binding affinities through Molecular Mechanics/Generalized Born Surface Area calculations (MM/GBSA). Initially, an energy-based pharmacophore (e-pharmacophore) model was built based upon known TASK-3 modulators. The e-

pharmacophore hypothesis was screened against the commercial ZINC database (Koes & Camacho 2012) identifying 5000 compounds that fulfill the e-pharmacophore parameters. Molecular docking inside TASK-3 structural models was used to identify the compounds that fit with our pharmacophore model. In order to decrease the library of compounds from ZINC database the molecules were filtered and selected using several molecular docking simulations and the docking energy scoring was corrected using MM/GBSA binding free energy calculation (Adasme-Carreño et al. 2014; Rastelli et al. 2010). Finally, all hits compounds were screened against hTASK-3 by Fluorometric imaging plate reader – Membrane potential assay (FLIPR–MPA) (Whiteaker et al. 2001; Baxter et al. 2002) obtained two lead ligands: DR6 ($IC_{50} = 40.6 \pm 1.9 \mu M$) and DR17 ($IC_{50} = 43.1 \pm 6.6 \mu M$). The flowchart of the whole study is represented in the Scheme 1.



Scheme 1. Systematic representation of the workflow to identify TASK-3 modulators.

7.2. Material and Methods

TASK-3 modeling. Since the structure of TASK-3 has not been solved, four homology models were developed using the following crystal structures as templates: TRAAK (PDBs: 4I9W and 3UM7), TREK-2 (PDB: 4BW5), and TWIK-1 (PDB: 3UKM). These structures have differences in the fenestration states (they could be open or closed); therefore, the different TASK-3 models were used to study the interactions between the lead ligands and TASK-3 with diverse fenestrations characteristics. The steps of the TASK-3 modeling are represented in the stage 1 of the general flowchart in Scheme 1. The TASK-3 homology models were built and optimized using ICM software (Abagyan & Totrov 1994) using the multiple alignment reported by Brohawn et al. (Brohawn et al. 2012). The four models were named according to the template and the fenestration state (Table 4). In this sense, the model names are: T3treCC (TASK-3 built from TREK-2 in Close-Close fenestration state); T3twiOO (TASK-3 built from TWIK-1 in Open-Open fenestration state); T3trCO (TASK-3 built from TRAAK in Close-Open fenestration state), and T3trOO (TASK-3 built from TRAAK in Open-Open fenestration state).

Table 4. Nomenclature of the TASK-3 homology models

Template	TASK-3 Homology model name
TREK-2 (PDB: 4BW5)	T3treCC
TWIK-1 (PDB: 3UMK)	T3twiOO
TRAAK (PDB: 4I9W)	T3trCO
TRAAK (PDB: 3UM7)	T3trOO

Maestro software version 9.2 (Schrödinger Release, 2011) was used for adding hydrogen atoms, to assign the bonds order and partial charges to the homology models. Then, they were embedded into a pre-equilibrated phosphatidyl oleoyl phosphatidylcholine (POPC) bilayer in a periodic boundary condition box ($15 \times 15 \times 15 \text{ \AA}^3$) with pre-equilibrated single point charge (SPC) water molecules. Two K^+ ions were associated to the models at positions S2 and S4, and two water molecules at sites S1 and S3 of the selectivity filter. The systems were neutralized by adding K^+ counter ions to balance the net charge and KCl at a concentration of 0.096 M was added to simulate physiological conditions of the

channel. An excluded region for counter ions was set at 5 Å from the selectivity filter of the models.

The constructed models were subjected to a conjugate gradient energy minimization and then subjected to molecular dynamics simulation (MDs) to reduce any close contacts resulting from the inclusion of new residues. All the MDs calculations were performed using the OPLS-AA force field (Kaminski et al. 2001) within the Desmond package v2.0 contained in Maestro 9.2 suite. The simulation was set in 10 ns at an isothermal-isobaric ensemble, with temperature (300 K), pressure (1 atm) and number of atoms constant using the Nosé-Hoover method with a relaxation time of 1 ps applying the MTK algorithm. The SHAKE algorithm (Kräutler et al. 2001) was employed for every hydrogen atom and the cutoff for van der Waals forces was set at 9 Å and the long-range electrostatic forces were modeled using the particle mesh Ewald method. A restriction was applied on the backbone atoms of the protein and atoms in the selectivity filter with a constant force of $0.5 \text{ kcal} \times \text{mol}^{-1} \times \text{Å}^{-2}$. Data were collected every 4ps during the MDs. The stability of the models during the MDs was validated by calculating the Root Mean Squared Deviation (RMSD). The last frames of each MDs were taken and the binding sites of the models were identified by using the SiteMap software (Tubert-Brohman et al. 2013). To test the quality of the models (after MDs), they were validated using PROCHECK (Laskowski et al. 1993).

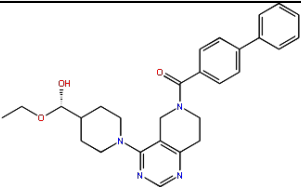
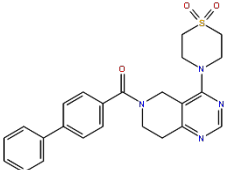
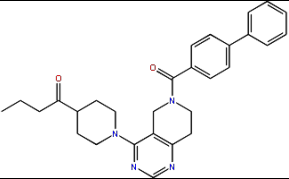
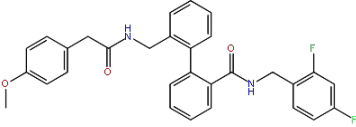
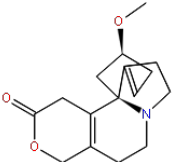
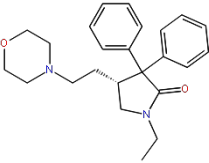
Pharmacophore modeling. Twelve TASK-3 modulators presented in Table 5 were taken for hypothesis generation using energy-optimized pharmacophore (e-pharmacophore). The structures were sketched using GaussView software (Dennington et al. 2009). Then, they were processed using LigPrep with the force field OPLS-2005 (Shelke et al. 2011); possible states of ionization at $\text{pH } 7.0 \pm 2.0$ were generated with Epik. Finally, they were optimized using the hf/3-21g *ab initio* calculations (Pan et al. 2002) contained in Gaussian09 software (Frisch et al. 2009).

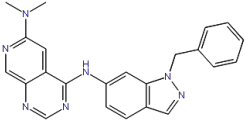
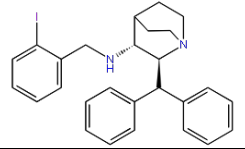
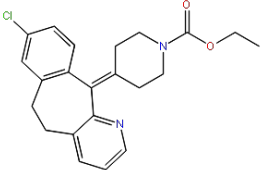
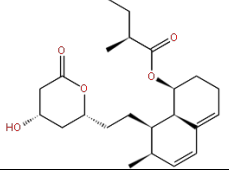
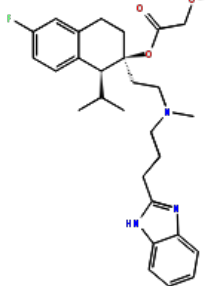
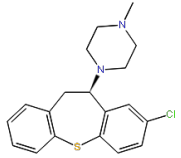
e-Pharmacophore is a novel approach to generate structure-based pharmacophores (Campagna-Slater et al. 2010). This method utilizes a scoring function to accurately characterize protein-ligand interactions, resulting in improved database screening.

Pharmacophore and ligand mapping were generated from TASK-3 modulators selected for the present study (Table 5) with the software Phase (Dixon et al. 2006), using

six pharmacophore features: Hydrogen bond acceptor (A), hydrogen bond donor (D), hydrophobic group (H), negatively charged group (N), positively charged group (P) and aromatic ring (R). Each feature is defined by a set of SMARTS patterns (with the exception of H and R feature); then, the active and inactive ligands were defined to develop the pharmacophore model. Stereochemical properties as the isomerism were preserved according with the data reported in the literature (Table 5).

Table 5. Reported TASK-3 modulators. Modulators with chemical characteristics used for the generation of the energy-optimized pharmacophore.

Blocker	ID	IC ₅₀ (μM)	Reference
	12f	0.074	(Coburn et al. 2012)
	17e	0.57	(Coburn et al. 2012)
	PK-THPP	0.035	(Coburn et al. 2012; Cotten 2013a)
	A1899	1.6	(Streit et al. 2011; Cotten 2013a)
	Dihydro-Beta-erythroidine	73.8	(Bruner et al. 2014)
	Doxapram	23.1	(Cotten 2013a)

	GW2974	50.1	(Bruner et al. 2014)
	L-703,606	45.5	(Bruner et al. 2014)
	Loratadine	63.4	(Bruner et al. 2014)
	Mevastatin	159	(Bruner et al. 2014)
	Mibefradil	24.6	(Bruner et al. 2014)
	OctoclothePIN	73.8	(Bruner et al. 2014)

In the scoring hypotheses process, all common pharmacophores were examined. From the data set we choose as active ligands (12f, 17e, 23, A1899, Doxapram, GW2974, L-703,606, Loratadine, and Mibefradil) those that have the IC_{50} value under 70 μ M and these ligands were aligned to the hypotheses and Phase calculates the score for the actives. Keeping that in mind, the model was subjected to a scoring and rescoring of the inactive ligands (Dihydro-beta-erythrodine, Mevastatin and OctoclothePIN). Finally, several generated hypotheses were clustered with the average linkage method (Kelly & Mancera 2004) producing clusters when the distance between them is greater than the average distance between all pairs of objects in the two clusters.

Finally, the e-pharmacophore features were mapped into TASK-3 modulators, and a molecular docking using Glide software (Friesner et al. 2004) was done in each TASK-3 model to localize the conserved e-pharmacophore into the inner cavity, where blockers like A1899 interact with TASK-3 (Streit et al. 2011), obtaining four complexes (Scheme 1. Molecular docking 1).

Virtual screening. The hypothesis generated in e-pharmacophore mapping step, docked into each TASK-3 model, was used as a query for screening within the ZINCPharmer pharmacophore search software (Koes & Camacho 2012). This software searches a database of conformations calculated from the purchasable compounds of the ZINC database (Irwin & Shoichet 2005). In the e-pharmacophore based virtual screening (e-PBVS) about 215'407.196 conformations from more than 22 millions of compounds were subjected to a docking process using ZINCPharmer (Scheme 1. Molecular docking 2). Hits were filtered by setting 1 as the maximum limit of hits per conformation, 1 as a maximum hits per molecule, 1 as the number of varied orientations of different conformations returned for each molecule, and just the best 5000 hits were considered. The hits also were filtered by setting 1 as the maximum root mean standard deviation (RMSD) to restrict the hits to those that have the best overall geometric match to the e-pharmacophore hypothesis (Koes & Camacho 2011). The e-PBVS was performed for each model (the four models described above) resulting in 5000 hits for each TASK-3 model, with a total of 20000 hits derived from the e-PBVS.

The 5000 hits were rescreening by massive docking (Scheme 1. Molecular docking 3) using the virtual screening workflow implemented in Maestro version 9.2. All molecules were prepared using LigPrep. The pre-filtering process was done by Lipinski's Rule (Walters 2012) and the filtering process was done using QikProp (Jorgensen 2006). The four constructed models of TASK-3 were employed as receptors of docking steps. The grid box was center in the inner cavity under the selectivity filter; the dimensions in each model were $(30 \times 30 \times 30) \text{ \AA}^3$ to cover the inner cavity and the fenestrations like grid boxes used in molecular docking of Chapter II (Appendix B – Supplemental Fig. S1). The high-throughput virtual screening (HTVS) was done with Glide (Friesner et al. 2004) using the HTVS scoring function to estimate protein-ligand docking affinities. The results of the HTVS were filtered according to the Glide energy and docking score, post-docking

minimization was done with OPLS-2005 force field to optimize the ligands geometries. A total of 2000 hits were obtained with this protocol, 500 hits for each TASK-3 model.

The 2000 hits corresponding to 500 hits for each TASK-3 model were then subjected to re-docking process (Scheme 1. Molecular docking 4) with Glide XP (extra-precision algorithm) (Friesner et al. 2004). A total of 400 hits were obtained with the re-docking protocol, 100 hits for each TASK-3 model.

Binding Free Energy calculations. The computational method Molecular Mechanics-Generalized Born Surface Area (MM/GBSA) that combines molecular mechanics energy and implicit solvation models (Hou et al. 2012) was employed using Prime (Schrödinger 2011) after the re-docking process to rescore and analyze the 100 hits from ZINC database corresponding to each TASK-3 model. In MM/GBSA, binding free energy between ligands and the receptors (TASK-3 models) to generate a complex was calculated as Eq 1. (See Section 13.2).

The variable dielectric surface generalized Born VSGB solvation model (Li et al. 2011) and OPLS-2005 force field were employed to accomplish the calculations. Residues located at 5 Å from the ligands were included in the flexible region, and all other protein atoms were kept frozen.

ADME prediction. The absorption, distribution, metabolism and excretions (ADME) properties of the identified lead ligands were predicted by using the program QikProp (Caporuscio et al. 2011; Jorgensen 2006). With this software, some physical significant descriptors and pharmaceutical properties were also predicted. The program was processed with the default parameters, and predicted 44 properties for each lead ligand, such as H-Bond donors, H-Bond acceptors, molecular weight, calculated LogP (octanol/water), among others. With the calculated descriptors the program also evaluated the acceptability of the compounds based on Lipinski's rule of five, that predicts that poor absorption or permeation is more likely when there are more than 5 H-Bond donors, 10 H-Bond acceptors, the molecular weight is greater than 500 and the calculated Log P is greater than 5 (Lipinski et al. 2012).

Experimental activity verification. The reported blocker PK-THPP was acquired from Aberjona Laboratories, Inc. (Massachusetts, United States). The hits compounds for

the experimental activity verification identified from ZINC database were acquired from the following suppliers: AKos Consulting & Solutions Deutschland GmbH (Steinen, Germany): DR1 to DR10; Ambinter c/o Greenpharma (Orléans, France): DR11 and DR12; EnamineStore Ltd. (Kyiv, Ukraine): DR13 to DR15 and Vitas-M Limited (Hong Kong, China): DR16 to DR18. All compounds were solubilized in DMSO (10 mM stock).

Fluorometric Imaging Plate Reader – Membrane Potential Assay (FLIPR–MPA). The reported blocker PK-THPP as a positive control (Coburn et al. 2012) and the hits ligands were screening by FLIPR–MPA (Whiteaker et al. 2001). This technique detect ion channels modulation by increasing or decreasing the fluorescent signal as cellular membrane potential changes (Baxter et al. 2002; Whiteaker et al. 2001). CHO–K1 cells, stably expressing hTASK-3 potassium channels, were loaded with the membrane potential sensitive fluorescent dye and incubated at 37°C to ensure dye distribution across the cell membrane. After recording baseline fluorescence signal (for 10 s) compounds were added and fluorescence signal was detected for 120 s. Subsequently the external potassium concentration was increased (from 2 mM to 40 mM) and the fluorescence signal was detected for another 120 s. The effect of hits ligands was determined indirectly. Inhibition of TASK-3 leads to intracellular retention of potassium ions and influx of the fluorescent dye, resulting in decreased fluorescence signal.

7.3. Results

TASK-3 modeling. TASK-3 sequence shares 31% identity with TREK-2, 31% with TWIK-1, and 31% with TRAAK (Brohawn et al. 2012); therefore, they are acceptable as templates to build homology models. The protein models inserted in their biological media were subjected to 10 ns MDs to stabilize them. RMSDs of the backbone atoms as a function of the simulation time for the four TASK-3 models, using their initial configuration as reference are shown in Fig. 16, the dependences of the RMSD values were tested to check whether the equilibrated MDs trajectories were stable. RMSD values show that the models were stabilized before 5 ns. The models were examined and it was confirmed that the state of the fenestrations (close or open) were maintained for all the models.

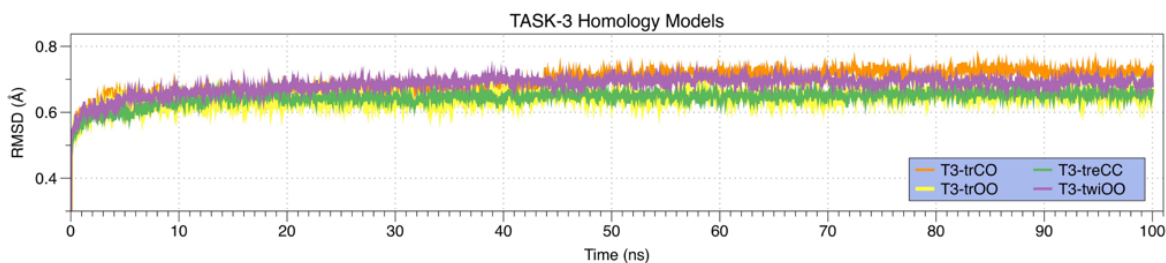


Figure 16. RMSD for backbones of TASK-3 models during MD simulations. Time dependence of the RMSD for backbone atoms from starting TASK-3 homology models during the equilibration process. RMSD is represented in yellow, orange green and violet for models of T3trOO, T3trCO, T3treCC and T3twiOO respectively.

The prediction of the TASK-3 binding site was performed by SiteMap software with the default parameters, and the potential binding sites of the reported blockers (Table 5) were identified for all models. Taking into account that the binding site identified by Streit et al. (Streit et al. 2011) for A1899 in TASK-1 is composed by T93 at the first pore loop (P1), T199 at the second pore loop (P2), I118 and L122 at the M2 segment, I235, G236, L239 and N240 at the M4 segment, and V243 and L247 at the Halotane Response Element (HRE), the only difference in the binding site of A1899 between TASK-1 and TASK-3 is due to the residue 247 (that is Met for TASK-1 and Leu for TASK-3) (Streit et al. 2011). The predicted binding sites of TASK-3 models are shown in the Appendix C – Supplemental Fig. S7. The surface maps of the predictions are shown in mesh-magenta with the specifications of each prediction shown in the right side of Appendix C – Supplemental Fig. S7, where the red-mesh surface represents the H-Bond acceptor area, the blue-mesh surface represents the H-Bond donor area and the yellow-mesh surface is the hydrophobic pocket. The residues described by Streit et al. (Streit et al. 2011) involved in the A1899 binding site (shown in green sticks) are within the potential binding sites predicted by SiteMap. This means that the predicted binding sites for each TASK-3 model are in agreement with the binding sites previously reported for drugs (Streit et al. 2011; Chokshi et al. 2015).

The different fenestration states were further analyzed in T3trCO model because it has the close-open fenestration state. In the Fig. 17 the residues identified

by Streit et al. (Streit et al. 2011) in the binding site are shown. Residues are surrounded by a white surface to detail the closed (Fig. 17 – left) and opened (Fig. 17 – right) fenestrations. The M4 segment of the chain A is farther to the M2 segment of the chain B resulting in the opening of the fenestration as described by Aryal et al. (Aryal et al. 2014). In Fig. 17 we can see how the hydrophobic side chain of L239 (yellow) at M4 segment is oriented to the hydrophobic fenestration cavity interacting with L197 (green) at M2 segment. I235 (purple) at M4 segment and V115 (white) of the inner helix 1 are also establishing non-bonding interactions. . It can be seen how L239 is closing the fenestrations in TASK-3 models contributing to the opening-closing mechanism of TASK-3 fenestration like the homologous residue L320 in TREK-2 reported by Dong (Dong et al. 2015).

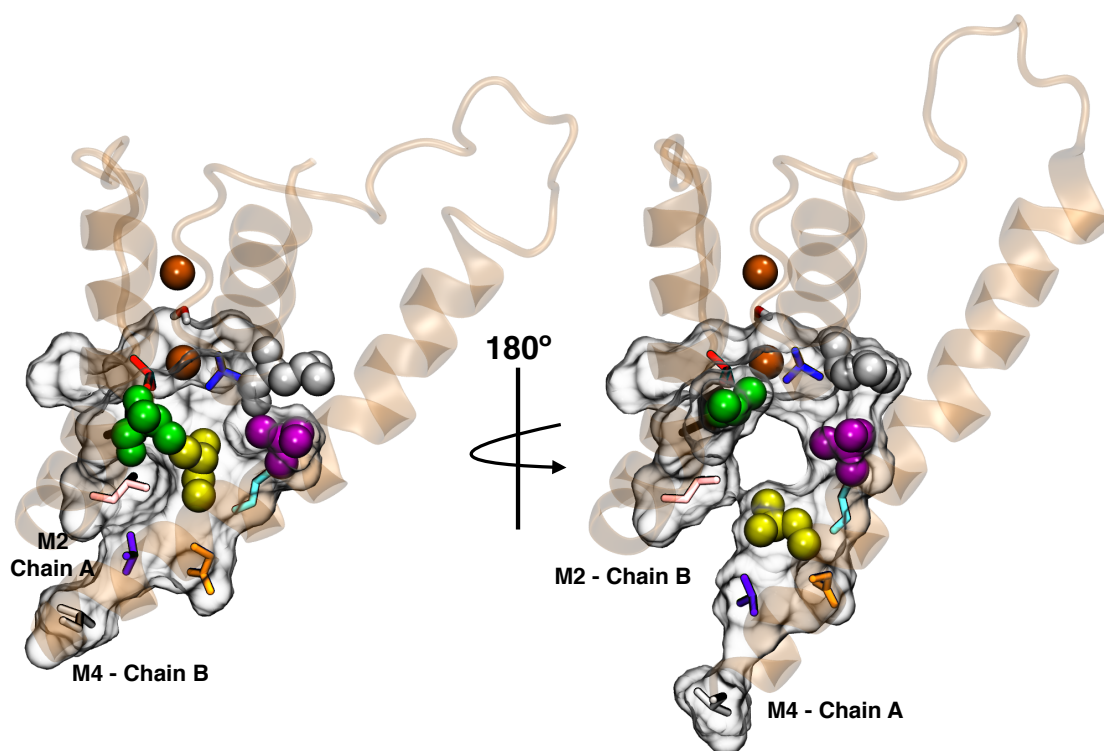


Figure 17. Fenestration states in T3trCO. Fenestration states representation in T3trCO model. **A.** Close fenestration state. **B.** Open fenestration state. Residues T93 (red) of the first pore loop (P1), T199 (blue) of the second pore loop (P2), I118 (black) and L122 (pink) of the M2 segment, G236 (cyan), N240 (orange), V243 (violet) and L247 (silver) of the M4 segment are shown in sticks representation. V115, (green), L197 (white), I235 (magenta) and L239 (yellow) are showed in van der Waals representation. T3trCO (orange) is showed in cartoon representation. For better display of fenestration state, the T3trCO model is shown in two orientations (rotated by 180°). K⁺ ions located in S₂ and S₄ positions are showed in van der Waals representation. Waters located in S₃ position is showed in sticks representation.

Pharmacophore modeling. The 12 TASK-3 blockers selected for the energy-optimized pharmacophore (e-pharmacophore) modeling had IC_{50} range of 0.035 μ M – 160 μ M (Table 5). Three pharmacophore features were identified: hydrogen bond acceptor (*A*), hydrophobic group (*H*), and aromatic ring (*R*). Then, the e-pharmacophore hypotheses were scored according with the site scoring function giving as a result four e-pharmacophore hypotheses (Table 6). The top score pharmacophore hypothesis was the No. 1 with two hydrogen bond acceptors (*A*) and one aromatic ring (*R*) that exhibits a site score of 0.71. This score measures how well the vectors for pharmacophore features are aligned in the structures that contribute to this hypothesis. A value of 0.870 of selectivity was calculated for pharmacophore hypothesis No. 1. This value estimates the rarity of the hypothesis, based on the World Drug Index, this term is the negative logarithm of the fraction of molecules in the Index that matches the hypothesis. A selectivity of 2 means that 1 of 100 molecules match; high selectivity means that the hypothesis is more likely to be unique to the TASK-3 reported modulators. In Fig. 18 the 3D representation of the pharmacophore hypothesis No. 1 (upper-right panel) is shown fitting the TASK-3 blockers: PK-THPP, A1899, Doxapram, Lortadine and L-703,606. The rest of the reported blockers (Table 5) also fit with the e-pharmacophore (data not shown). The geometry of the hypothesis No. 1 is conserved in the blockers. For compounds 12f, 17e, and PK-THPP the *A1* feature is the carbonyl oxygen, *A2* is the N3 of the 5,6,7,8-tetrahydropyrido[4,3-*d*]pyrimidine, and *R* is the phenyl bound to the carbonyl group. For A1899, *A1* and *A2* correspond to carbonyl oxygens and *R* is the phenyl group of methoxyphenyl substituent. For GW2974, *R* is the phenyl of the 1*H*-indazole and *A1* and *A2* correspond to N3 and N7 of the pyrido[3,4-*d*]pyrimidine group. For loratadine *A1* is the nitrogen of the pyridine, *A2* is the ether oxygen of the carboxylate group and *R* is the chlorophenyl group. We analyzed the local charges of atoms that occupy *A1* and *A2* and we observed that they have high Mulliken atomic charges. For instance, Mulliken atomic charges of the atoms of compound 23 that are at *A1* and *A2* are -0.72 au and -0.62 au respectively; this implies that these atoms have a high electronic density, and can accept H-Bonds.

Table 6. e-Pharmacophore hypotheses. Identified by e-pharmacophore modeling.

e-Pharmacophore Hypotheses		Site score	Selectivity
ID	Pharmacophore features		
1	AAR	0.71	0.870
2	AHR	0.65	0.985
3	AHR	0.55	0.973
4	AAR	0.44	0.878

Hydrogen bond acceptor (A), hydrophobic group (H), and aromatic ring (R)

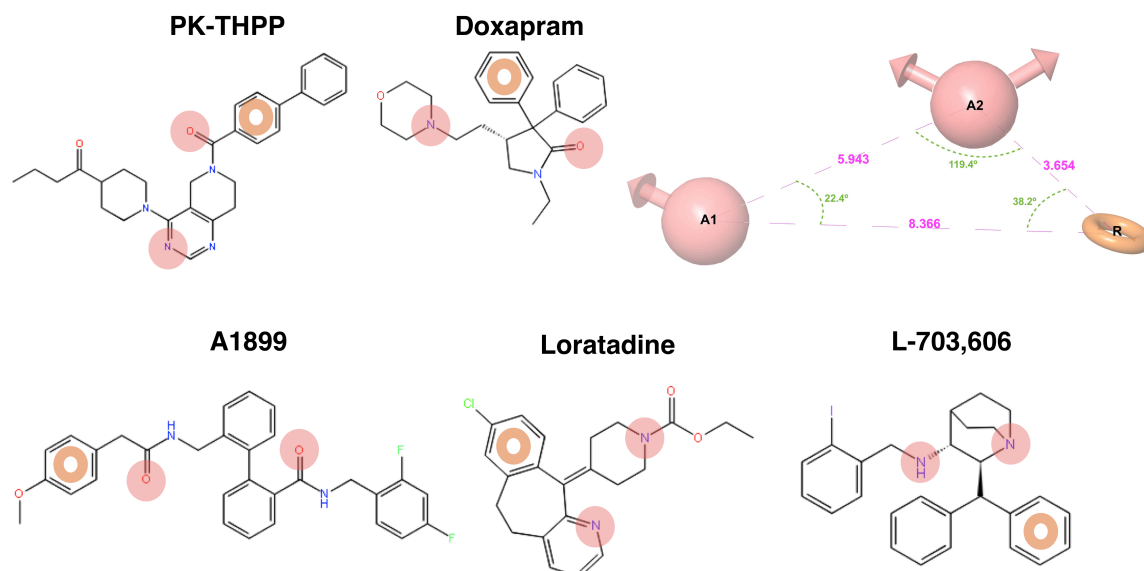


Figure 18. Common e-Pharmacophore for the TASK-3 reported blockers PH-THPP, A1899, Doxapram, Loratadine and L-703,606. Common pharmacophore hypothesis No. 1 based on the pharmacophore generation. *A1* and *A2* correspond to the hydrogen bond acceptor feature and *R* represents the aromatic ring.

Virtual screening. The e-pharmacophore hypothesis in conjunction with the four TASK-3 models was used as input for e-PBVS using ZINCPharmer pharmacophore search software (Koes & Camacho 2012). The search explored 215'407.196 conformations from 22'723.923 compound of the ZINC (purchasable) database (Irwin & Shoichet 2005). Database hits were ranked according to RMSD resulting in 5000 hits for each TASK-3 model, with a total of 20000 hits.

After the re-docking process (Scheme 1. Molecular docking 4) with Glide XP and the implementation of the stage 2 of the protocol represented in Scheme 1, the predicted hit ligands from ZINC database were identified. In the Table 7 the 18 ligands (DR1 to DR18) with the lower MM/GBSA binding free energy are listed. The hits ligands interact with at least two of the four TASK-3 models, with different ΔG_{Bind} energies. These hits share several chemical features among them (Appendix C – Supplemental Fig. S8) and also with the TASK-3 blockers reported in the literature.

Table 7. Ligands hits interacting with TASK-3 homology models.

ID	ZINC ID	T3treCC	T3trOO	T3twiOO	T3trCO
		ΔG_{Bind}	ΔG_{Bind}	ΔG_{Bind}	ΔG_{Bind}
DR1	ZINC03556155	-59.55	-58.78		
DR2	ZINC09367111		-64.27	-55.03	
DR3	ZINC10950931	-59.94	-48.84	-51.23	
DR4	ZINC11147234		-68.54	-54.96	
DR5	ZINC16278437	-67.62	-95.92		
DR6	ZINC17053289	-54.66	-70.88		
DR7	ZINC68916649		-66.25	-67.73	
DR8	ZINC72040642	-49.75			-52.58
DR9	ZINC78792039	-50.67	-78.33		
DR10	ZINC94819975		-50.77		-70.57
DR11	ZINC00246887		-57.27	-53.86	
DR12	ZINC05269754	-52.79		-53.97	
DR13	ZINC32460999	-69.21		-54.29	
DR14	ZINC70728711		-64.84	-57.97	
DR15	ZINC09315946		-55.17	-51.02	
DR16	ZINC00183531	-47.41		-53.68	
DR17	ZINC02943852	-65.75		-53.41	-76.95
DR18	ZINC71279984	-38.27	-53.06		

ΔG_{Bind} : MM/GBSA ΔG_{Bind} term in kcal * mol⁻¹

Biological activity validation. The reported blocker PK-THPP and the 18 hits were screening against TASK-3 using the FLIPR-MPA and the compounds DR6 and DR17 were identified as lead ligands with IC₅₀ of 40.6 ± 1.9 μM and 43.1 ± 6.6 μM respectively; the positive control PK-THPP exhibited an IC₅₀ = 48.5 ± 6.3 nM. In the Fig. 19A it can be seen

the Δ Fluorescence in hTASK-3–transfected CHO-K1 cells in response to KCl depolarization. After baseline fluorescence for 10 s, compounds were added and fluorescence signal was detected for 120 s, then the external potassium concentration was increased (from 2 mM to 40 mM) to induce a change in the membrane potential and the employed dye as a result of depolarizing or hyperpolarizing stimuli in cells cause changes in fluorescence (signal was detected for another 120 s). The dose-response curves (Fig. 19B) show the IC_{50} for the lead ligands and the positive control PK-THPP.

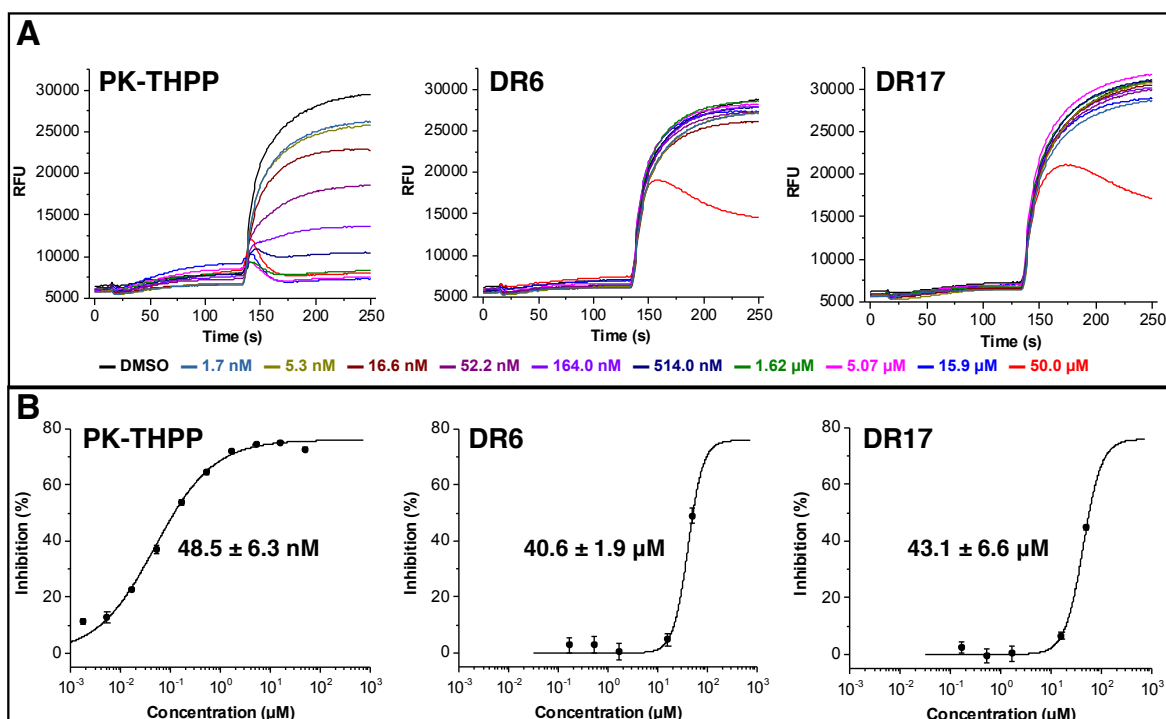


Figure 19. Biological activity validation. Biological activity of the reported blocker PK-THPP and lead ligands DR6 and DR17 by Fluorometric Imaging Plate Reader – Membrane Potential Assay (FLIPR–MPA).

A. Changes in fluorescence responses as RFU (relative fluorescence units) of the dye in FLIPR-MPA in response to KCl depolarization. K^+ concentration was increased from 2 mM to 40 mM after 130 s. **B.** Dose – response curves evoked by TASK-3 modulators PK-THPP, DR6 and DR17. The values are the average of four assays.

The binding modes of the lead ligands DR6 and DR17 in the TASK-3 channels with different fenestration states predicted by our protocol are shown in Fig. 20 and Fig. 21 (respectively). It is noticeable that different orientations were predicted for each compound in different models due to the large space of the inner cavity, at the bottom of the SF.

However, in general it is possible to see that compounds are located at the bottom of the selectivity filter, blocking the flux of K⁺ ions through the K_{2p} channel. To study the residues involved in the binding site of DR6 and DR17 in TASK-3 the HOLE radius profile of each model along the MDs was calculated. Table 8 summarizes whether the residues reported as responsible of A1899 binding site into TASK-1 as well as the residues predicted here by SiteMap are present in the binding site of DR6 and DR17. Only the residues P119, L197, I235 and A237 are exclusively present in the fenestration and did not protrude into the central cavity during the MDs. Residues T93, I118, L122, G236, and P238 are present both in the inner cavity and the fenestrations.

Table 8. Location of the interacting residues of DR6 and DR17 in TASK-3 models. HOLE radius profile of TASK-3 models during the 10ns-MDs. Above 50% of the MDs time is considered that the residue forms part of a cavity. The residues for T3trCO model falls in the open fenestration.

Residues	T3-treCC	T3-twiOO	T3-trOO	T3-trCO
I91	IC ^{1,2}	IC ²	IC ¹	IC ²
T92*	IC ^{1,2}	IC ²	IC ¹	IC ²
T93*	IC ^{1,2}	IC & F ²	IC & F ¹	IC & F ²
I94	IC	IC	IC	IC
I118*	IC ²	IC & F ²	IC & F ¹	IC & F ²
P119	NP ¹	F ²	F ¹	F ²
T121	IC ^{1,2}	IC ²	IC	IC ²
L122*	IC ^{1,2}	IC & F ²	IC & F ¹	IC & F ²
L197	NP	F ²	F ¹	F ²
T198*	IC ^{1,2}	IC ²	IC ¹	IC & F ²
T199*	IC ^{1,2}	IC ²	IC ¹	IC & F ²
L229	IC ¹	IC	IC	IC
L232	IC ^{1,2}	IC ²	IC	IC
T233	IC ²	IC	IC	IC
I235*	NP	F ²	F ¹	F ²
G236*	NP ²	IC & F ²	IC & F ¹	IC & F ²
A237	NP	F	F	F
P238	NP	IC & F	IC & F ¹	IC & F
L239*	IC ²	F ²	F ¹	IC & F ²
N240*	IC ²	IC	IC	IC & F
V242	IC	IC	IC	IC
V243*	IC	IC	IC	IC
L247*	IC	IC	IC	IC

* Residues from the binding site of A1899; ¹ Residues interacting with DR6; ² Residues interacting with DR17; **IC**: Inner cavity; **F**: Fenestrations; **NP**: No presence. All residues were identified by SiteMap (except NP).

The binding mode of DR6 is produced due to H-Bond interactions between the ligand–oxygen of the amide group and the side chain OH of the residue T93 (Fig. 20 – dotted magenta arrow). DR6 also present a H-Bond between the Nitrogen atom of the pyridine moiety and the side chain OH of the T121, a Cation–Pi interaction with the K⁺ located in S4 and a Pi–Pi interaction with the F125 in complex with T3-treCC (Fig. 20A); nevertheless is important to notice that F125 was reported as a putative false positive by our group because the docking pose of A1899 predicted this residue as part of the binding site but the experimental data did not fit with those results in TASK-1 (Streit et al. 2011). DR6 is surrender by polar (threonines located at the bottom of the SF) and hydrophobic residues (Fig. 20A – right panel) for both TASK-3 models, T3trOO and T3treCC.

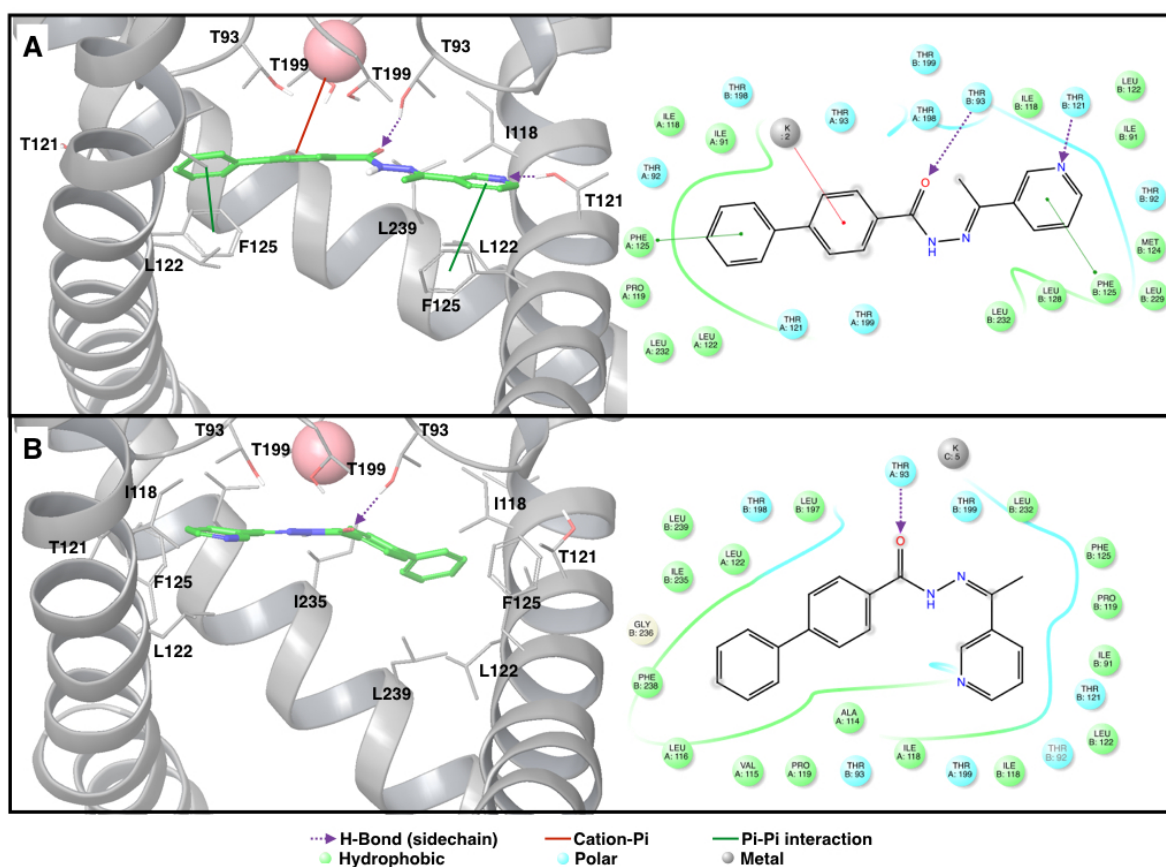


Figure 20. DR6 binding mode. Lead ligand DR6 in green stick representation complexes with TASK-3 homology models in cartoon representation. The bonding interaction H-Bonds (magenta dotted arrow) and non-bonding interactions Cation-Pi (red line), Pi-Pi (green line), Hydrophobic (green circle) and polar (cyan circle) interactions are displayed. **Left panel:** Fenestrations are perpendicular to the plane. The figure represent two M2 helix (parallel), one M4 helix (diagonal), and some highlight interacting residues are showed in stick representation. Potassium ion is located in the S4 position in the selectivity filter. **Right**

panel: 2D-diagram showing the lead ligand and the surrender residues at (5 Å). **A.** T3treCC – DR6 complex,
B. T3-trOO – DR6 complex.

It can be seen in the complex T3-trOO – DR6 how the hydrophobic aromatic moiety of the ligand is oriented inside the fenestration interacting with the residues I118, P119, L197 (Fig. 20B – right panel), I235 and L239 (Fig. 20B – left panel) located in the fenestrations (Appendix C – Supplemental Table S5). Basically, the interactions that govern the binding of DR6 in TASK-3 are mostly hydrophobic with the pore-forming residues located in both the pore and the fenestrations (Table 8) and an H-Bond with the threonine from the selectivity filter. These different binding modes of DR6 in two different models of TASK-3 with the fenestration in closed state (T3treCC) and open state (T3trOO) allow us to postulate that the hydrophobic moieties could interact with the fenestration hydrophobic residues when TASK-3 has the fenestrations in open state.

DR17 presents two H-Bond interactions with T93 and T199 (Fig. 21 – magenta dotted arrow) and always is located in the bottom of the SF and not in the fenestrations, as DR6 (Fig. 20). In the models with open fenestration state, no relevant interactions were found with the residues inside the fenestration, nevertheless, the 2D diagram (Fig. 21 – right panel) shows how DR17 is always surrendered (like DR6) by polar (threonines in the bottom of the SF) and hydrophobic residues (located in the wall of the inner cavity). According to the binding free energies predicted by MM/GBSA (Table 4), the complex T3trCO – DR17 exhibits the best ΔG Bind energies due to the bonding interactions present, two H-Bond between the carbonyl oxygens and the side chains OH of T93 and T199 as well as several non-bonding interactions such as a Cation-Pi between the pyridine moiety and F125 (Fig. 21B – left panel) and several polar interactions present between the Nitrogen of the pyridine ring and T92 and T121 of the subunit A, the Nitrogen of the amide group and T93 of the subunit A, and the Oxygen of the ester and T92 and T199 of the subunit B (Fig. 21B – left panel). However, the range of the predicted ΔG Bind energies for the lead ligands is not significantly different (Table 7) and neither is the experimentally determined activity (Fig. 19) allowing us to conclude that the lead ligands have a very similar binding mode due to they share the same pharmacophore (Fig. 18) that the reported modulators (Table 5).

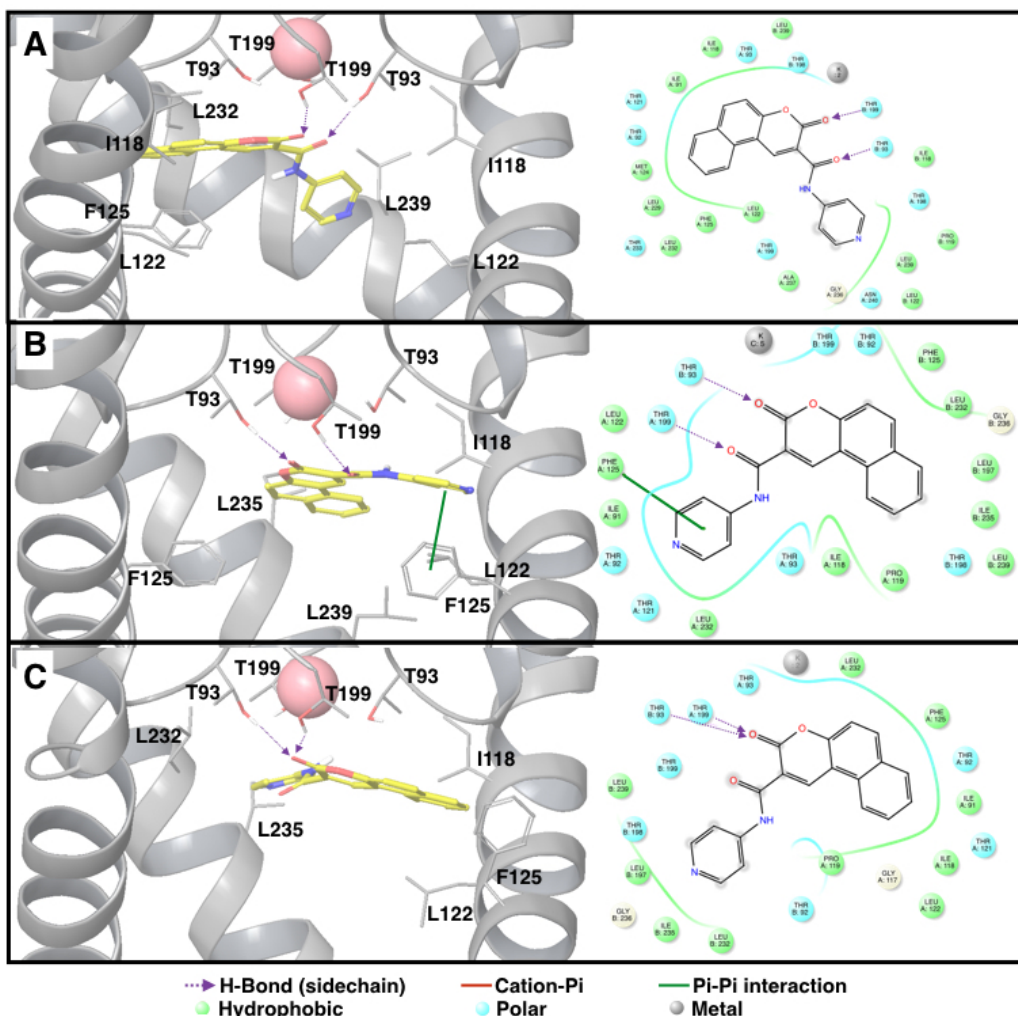


Figure 21. DR17 binding mode. Lead ligand DR17 in yellow stick representation complexes with TASK-3 homology models in cartoon representation. The bonding interaction H-Bonds (magenta dotted arrow) and non-bonding interactions Cation-Pi (red line), Pi-Pi (green line), Hydrophobic (green circle) and polar (cyan circle) interactions are displayed. *Left panel:* Fenestrations are perpendicular to the plane. The figure represents two M2 helix (parallel), one M4 helix (diagonal), and some highlight interacting residues are showed in stick representation. Potassium ion is located in the S4 position in the selectivity filter. *Right panel:* 2D-diagram showing the lead ligand and the surrender residues at (5 Å). **A.** T3treCC – DR17 complex, **B.** T3trCO - DR17 complex, **C.** T2twiOO – DR17 complex.

The binding mode of DR6 and DR17 with TASK-3 is very similar between them, always a threonine from the selectivity filter (T93 or T199) located within both the pore and the fenestration (in models with open fenestration states) is interacting through a H-Bond with the H-Bond acceptor moiety of the compounds, and several hydrophobic interactions with the pore-forming residues (some times located also in the fenestrations)

are presents, This results are in concordance with those reports previously for TASK-1/3 modulators (Streit et al. 2011; Coburn et al. 2012; Chokshi et al. 2015), were the main interactions are present with the residues described in the present work.

ADME prediction. Physicochemical descriptors were analyzed for DR6 and DR17 ligands, including molecular weight (MW), total number of H-Bonds donors (HB-D), total number of H-Bonds acceptors (HB-A), rotatable bonds, total solvent accessible surface area (SASA), total solvent-accessible volume (MV) and van der Waals surface area of polar nitrogen and oxygen atoms (PSA) (Table 9). Both ligands have the MW in the optimal range for a potential drug (< 500 g/mol) according to the Lipinski's rule. All the physicochemical descriptors are in the acceptable range defined for potential drugs. Pharmacokinetics properties were also analyzed for the lead ligands such as LogP (octanol/water), HERG K⁺ channel blockage, logKp for skin permeability, % human oral absorption in gastrointestinal system and their violations according to Lipinski's rule of five (Lipinski et al. 2012; Walters 2012). The predicted properties are listed in Table 10. The compliance of Lipinski's rules indicates that the ligand with a certain pharmacological or biological activity has properties that would likely make it orally appropriate for humans. However, Lipinski's rule does not predict whether a compound is pharmacologically active (Singh et al. 2012).

Table 9. Physicochemical descriptor calculated by QikProp simulation

Lead Ligands	MW (g/mol) ^a	HB-D ^b	HB-A ^c	Rotatable bonds	Total SASA ^d	MV (Å ³) ^e	PSA ^f
DR6	315.374	1.00	3.50	5	641.854	1088.333	60.025
DR17	316.315	0.00	5.50	2	572.398	975.872	85.911

^a Molecular Weight. Range 95% of drugs (130.0 - 725.0).

^b Estimated number of H-Bond that would be donated by the solute to water molecules in an aqueous solutions. Values are averages takes over a number of conformations, so they can be non-integer. Range 95% of drugs (0.0 – 6.0).

^c Estimated number of H-Bond that would be accepted by the solute to water molecules in an aqueous solutions. Values are averages takes over a number of conformations, so they can be non-integer. Range 95% of drugs (2.0 – 20.0).

^d Total Solvent Accessible Surface Area (SASA). Range 95% of drugs (300.0 – 1000.0).

^e Total solvent-accessible volume in cubic Å³ using in a probe with radius of 1.4 Å. Range 95% of drugs (500.0 – 2000.0).

^f Van de Waals surface area of polar nitrogen and oxygen atoms. Range 95% of drugs (7.0 – 200.0).

All predictions are based in a data set of 1712 drugs.

Table 10. Pharmacokinetics properties predicted by QikProp simulation

Lead Ligands	QP log P (o/w) ^a	QP log S ^b	QP log Kp ^c	% HOA in GI ^d	Qual HOA model ^e	Lipinski's rule of 5 violations ^f
DR6	4.486	-5.292	-1.238	100	HIGH	0
DR17	2.582	-3.859	-2.219	91	HIGH	0

^a QP log P for octanol/water. Range 95% of drugs (-2.0 – 6.5).

^b Predicted aqueous solubility. Log S, S in dm³ is the concentration of the solute in a saturated solution that is in equilibrium with the crystalline solid. (-6.5 – -0.5).

^c QP log Kp for skin permeability. Kp in cm/h (-8.0 – -1.0)

^d % model for Human Oral Absorption in Gastro Intestinal System. < 20% is poor.

^e Quality of model for Human Oral Absorption in Gastro Intestinal System. > 80% in high.

^f Maximun is 4.

DR6 and DR17 ligands were in an optimal range of Lipinski's rule of five exhibiting 0 violations (Table 10). For the lead ligands, the partition coefficient (QP logP) and the water solubility (QP logS) are within allowed ranges; this is important when estimating drug absorption and distribution pharmacokinetics properties within the human body.

7.4. Discussion

In the current work, we proposed a novel and efficient protocol that include pharmacophore-based virtual screening, docking-based high throughput virtual screening, re-docking to refine poses, and binding free energy calculations to find new potent modulators for TASK-3 channel. We also identified the residues involved in the binding site of the studied compounds and our results contain the majority of residues of the previously identified A1899 binding site (Fig. 20-21).

TASK-3 homology models (Table 4) present different fenestrations (close or open) states according with the templates. Using the prediction of the binding site by SiteMap we identified different chemical environments in the binding site detected and A1899 binding site (Streit et al. 2011); it can be seen that the residues described by Streit et al. are included in the mapping surface for the predicted binding site, but the binding site is bigger than that for A1899 (Appendix C – Supplemental Fig. S7) because the fenestration-forming residues were identified with SiteMap. Analysis of the different fenestration states in T3trCO (Fig. 17) shows how the hydrophobic interaction between L239 (M4 segment) and L197 (M2

segment) and also between I235 (M4 segment) and V115 (inner helix 1) modulates the fenestration opening-closing mechanism. These interactions are in concordance with the results presented by Brohawn et al. (Brohawn et al. 2013) where the residues L151, L236, I279, and L283 of TRAAK are implicated in the opening-closing mechanism of the TRAAK fenestration (González et al. 2015) (TASK-3 residues V115, L197, I235, and L239 are equivalent to TRAAK residues L151, L236, Ile279, and L283 respectively). As observed for previously reported structures of K_{2p} channels, TASK-3 fenestrations are integrated by hydrophobic residues (Brohawn, Su, et al. 2014; Brohawn, Campbell, et al. 2014; Lolicato et al. 2014), allowing the hydrophobic regions of the identified ligands DR6 and DR17 to orient to the fenestrations (Fig. 20-21).

The e-pharmacophore model from the reported 12 blockers (Table 5) present two hydrogen bond acceptors (*A*) and one aromatic ring (*R*). This e-pharmacophore exhibit the possibility of interaction between the *A* and some hydrogen bond donor groups like amines or hydroxyls, and the *R* could present non-bonding interactions like Pi-Pi, Cation-Pi or other hydrophobic interactions. Our results are in concordance with those reported by our group previously (Kiper et al. 2015) since the common pharmacophore identified for TASK-1 and Kv1.5 blockers is similar to our model because both are composed by the same features, two H-Bond acceptors and one aromatic ring.

The *AAR* common pharmacophore was identified using previously reported TASK-3 blockers. Afterwards, e-pharmacophore based virtual screening (ePBVS) was performed to select which compounds of the ZINC database (> 22 millions) fitted the defined pharmacophore requirements; then a docking-based HTVS following by a re-docking process with a more precise function and binding free energy calculations (MM/GBSA) were done to obtain 18 hits ligands (DR1 to DR18 in Table 7 and Supplemental Appendix C – Supplemental Fig. S8). These hits contain at least two rigid aromatic units connected by amide or ester groups (except DR7), which have the function of linkers. They also have H-Bond acceptors groups that correspond to the identified pharmacophore, and hydrophobic groups that can interact with the hydrophobic residues of TASK-3 binding site. These common chemical features between the obtained hits and the previously reported blockers allow us to postulate that the experimental evaluation of the hits may be

interesting since they should share similar interactions with TASK-3 than previously reported blockers.

In the A1899 binding site identified here (see Chapter II), T93 is facing into the inner cavity in TASK-1, some residues are present in both, pore and fenestration (see chapter II – Table 2) and I118, T198, L232, I235 and G236 are exclusively oriented towards the fenestration and did not protrude into the pore. In TASK-3 models, HOLE (Smart et al. 1996) profiles were studied to determinate the locations of the interacting residues (Table 8) with DR6 and DR17, and, as A1899 binding site, some residues are present in both, pore and fenestration (T93, I118, L122, G236, P238), some are exclusively oriented towards the fenestration (I235) or the pore (T92, T121, L228, L232, T233, V242, V243 and L247); nevertheless the hydrophobic amino acidic environment in the binding site is conserved and the H-Bond with T93/T199 is always present.

Streit et al. observed that the affinity of A1899 for TASK-1 decreases around the 50% when the residue M247 was mutated to Ala, and when M247 was mutated to Leu the affinity of A1899 for TASK-1 decreases in a 3.3-fold (Streit et al. 2011). In our TASK-3 models L247 is located at the bottom of the inner cavity (Appendix C – Supplemental Fig. S9) and is too far to establish an interaction with the identified compounds. For this reason, we consider that this residue is not involved in ligand interactions but it could play an important role driven the ligand to the binding site.

The experimental activity evaluation using FLIPR-MPA was validated using PK-THPP as positive control, where we obtained an $IC_{50} = 48.5 \pm 6.3$ nM, value very close to the results reported in 2012 by Coburn et al. (35 ± 0.5 nM) (Coburn et al. 2012). We obtained two lead ligands: DR6 ($IC_{50} = 40.6 \pm 1.9$ μ M) and DR17 ($IC_{50} = 43.1 \pm 6.6$ μ M). The result shows that DR6 and DR17 binds TASK-3 with a 1000-fold lower affinity than PK-THPP; but also shows that the lead ligands are in the same range of IC_{50} than other reported blockers such as dihydro-Beta-erythromidine, Doxapram, GW2974, L-703,606, Loratadine, Mevastatin, Mibefradil and Octoclothebin (Table 5). Our results are in concordance with those results reported by several authors where novel modulators have been identified through VS and/or molecular docking simulations (Kumar et al. 2014; Ewing et al. 2001; Jain & Trivedi 2014; Mittal et al. 2014; Hecht et al. 1998; Kincaid et al.

2015; Coburn et al. 2012; Bressi et al. 2001; Murray et al. 1997); indicating that our protocol allow the prediction of compounds in the same biological activity range that the reported modulators used to calculated the pharmacophore.

The results presented in this work allow us to conclude that interactions of the identified compounds were established in the TASK-3 inner cavity and not in the fenestrations, like the binding site observed for Dong et al., were Norfluoxetine is located in the fenestrations of TREK-2 (Dong et al. 2015). However, the interactions of DR6 and DR17 involves residues located in the fenestrations and in the inner cavity (Fig. 20-21 and Table 8). The lead ligands presents always a hydrophobic interaction with L122 in the inner cavity, like the interaction observed by Chokshi et al., were L122 was described like a key residue in the binding site of PK-THPP in TASK-3 (Chokshi et al. 2015). In the present work we identified by computational methods the residues described by Streit et al. (Streit et al. 2011) as contributing to A1899 binding site in TASK-1, and also all residues described by Chokshi et al., as contributing to A1899, PK-THPP and Doxapram binding in TASK-3 (Chokshi et al. 2015).

The identified compounds are moderately active TASK-3 antagonist and could be used in the lead-optimization process to obtain novel series of TASK-3 modulators based on DR6/DR17 high-throughput screening lead from which a subseries of potent and selective inhibitors should be identified; these lead-optimization process have been successfully used in drug discovery targeting TASK-3 channels obtained the most potent inhibitor reported to date: PK-THPP (Coburn et al. 2012).

TASK-3 channels are expressed throughout the nervous, cardiovascular, genitourinary and gastrointestinal systems and play an important role controlling the neuronal resting membrane potential and excitability. Also are involved in chemosensation and in the regulation of the immune system. The rational drug design of TASK modulators is a field of interest and brings novel pharmacotherapeutic advances in the treatment of several medical disorders. By virtual screening, docking molecular, binding free energy calculations and using a rational drug design theoretical – experimental approach, we have identified the compounds DR6 and DR17 as novel TASK-3 modulators. The structure activity relationship around the identified modulators and the reported

blocker reveals the crucial role of the conserved pharmacophore for significant TASK-3 inhibitory activity. Furthermore, computational studies have provided relevant insights into the binding mode of this class of modulators. Although the identified ligands showed moderate potencies, the conserved pharmacophore and novel chemical characteristics of this chemical class makes them good candidates for future development into highly potent TASK-3 modulators through medical chemistry optimization.

7.5. Future work

Here we established a general protocol including virtual screening, massive docking simulations and binding free energy calculation to search from a big compound-dataset structures which are most likely to bind to a drug target, in our case, we identified the compounds DR6 and DR17, blocking TASK-3 in the micromolar range by using FLIPR-MPA, with IC_{50} of 40.6 μ M and 43.1 μ M respectably. We pretend to use TEVC as well as patch clamp to validated our results.

Furthermore, we consider that the conserved pharmacophore and novel chemical characteristics of this new TASK-3 blockers makes them good candidates for future development into highly potent TASK-3 modulators through medical chemistry optimization.

7.6. Scientific Production

Ramirez, D., Caballero, J., Zuñiga, L., Arévalo, B., Kipper, A., Decher, N. & González, W. “*Structure-based discovery of potential two-pore domain potassium channels TASK-3 modulators*”. To be submitted to *Molecular Pharmacology* (2016).

Abstract. TASK-3 is a two-pore domain potassium (K_{2p}) channel highly expressed in hippocampus, cerebellum, and cortex. TASK-3 regulates neurotransmitter functions and has been identified as an oncogenic potassium channel and it is overexpressed in different cancer types, for this reason the development of new selective TASK-3 modulators could influence the pharmacological treatment of cancer and several neurological conditions. In the present work we search for potential TASK-3 modulators using a virtual screening (VS) protocol that includes pharmacophore modeling, molecular docking, and free energy calculations (MM/GBSA). At the end, 18 hits were identified, these hits were screened against TASK-3 using Fluorometric imaging plate reader – Membrane potential assay (FLIPR–MPA), and two lead ligands showing inhibition of 40.6 μ M and 43.1 μ M were obtained as potential modulators.

Additional Studies

-
- 8.1. González, W., Valdebenito, B., Caballero, J., Riadi, G., Riedelsberger, J., Martínez, G., **Ramírez, D.**, Zúñiga, L., Sepúlveda, L., Dreyer, I., Janta, M., and Becker, D., “*K_{2P} channels in plants and animals*” *Pflugers Arch.*, vol. 467, no. 5, pp. 1091–1104, **2015**.
 - 8.2. Goldstein, M., Rinné, S., Kiper, A., **Ramírez, D.**, Netter, M., Bustos, D., Ortiz-Bonnin, B., González, W., and Decher, N. “*Functional mutagenesis screens reveal the ‘cap structure’ formation in disulfide-bridge free TASK channels*” *Sci. Rep.*, vol. 6, pp. 19492, 2016, **2016**.
 - 8.3. **Ramírez, D.** “*Computational methods applied to rational drug design*” *Open Med. Chem. J.*, vol. 10, pp. 7–20, **2016**.
 - 8.4. **Ramírez, D.**, and Caballero, J. “*Is It Reliable to Use Common Molecular Docking Methods for Comparing the Binding Affinities of Enantiomer Pairs for Their Protein Target?*” *Int. J. Mol. Sci.*, vol. 17, no. 4, pp. 525, **2016**.
 - 8.5. Rodríguez, Y., Gutiérrez, M., **Ramírez, D.**, Alzate-Morales, J., Bernal, C., Güiza F., and Romero, A. “*Novel N-allyl/propargyl tetrahydroquinolines: Synthesis via three-component cationic imino Diels-Alder reaction, binding prediction and evaluation as cholinesterase inhibitors*” *Chem. Biol. Drug Des.*, **2016**.
 - 8.6. Almeida, J., Lancellotti, M., Soares, A., Calderon, L., **Ramírez, D.**, González, W., Marangoni, S., and Da Silva, S. “*CoaTx-II, a new dimeric Lys49 phospholipase A2 from Crotalus oreganus abyssus snake venom with bactericidal potential: Insights into its structure and biological roles*” *Toxicon*, 120, pp.147–158, **2016**.
 - 8.7. Resende, L., Ramos, R., Collaço, R., Simiomni, L., **Ramírez, D.**, González, W., Soares, A., Calderon, L., Marangoni, S., Da Silva S and Almeida, J. “*Exploring and understanding the functional role, and biochemical and structural characteristics of an acidic phospholipase A2, AplTx-I, purified from Agkistrodon piscivorus leucostoma snake venom*” Submitted to *Toxicon*, **2016**.

- 8.8. Jørgensen, M., Xu, D., Crocoll, C., **Ramírez, D.**, Motawia, M., Olsen, C., Nour-Eldin, H., and Halkier, B. "Origin and evolution of a transporter substrate specificity". Submitted to eLife. **2016**.

K_{2P} channels in plants and animals

Wendy González · Braulio Valdebenito · Julio Caballero · Gonzalo Riadi ·
Janin Riedelsberger · Gonzalo Martínez · David Ramírez · Leandro Zúñiga ·
Francisco V. Sepúlveda · Ingo Dreyer · Michael Janta · Dirk Becker

Received: 30 September 2014 / Revised: 18 October 2014 / Accepted: 21 October 2014 / Published online: 6 November 2014
© Springer-Verlag Berlin Heidelberg 2014

Abstract Two-pore domain potassium (K_{2P}) channels are membrane proteins widely identified in mammals, plants, and other organisms. A functional channel is a dimer with each subunit comprising two pore-forming loops and four transmembrane domains. The genome of the model plant *Arabidopsis thaliana* harbors five genes coding for K_{2P} channels. Homologs of *Arabidopsis* K_{2P} channels have been found in all higher plants sequenced so far. As with the K_{2P} channels in mammals, plant K_{2P} channels are targets of external and internal stimuli, which fine-tune the electrical properties of the membrane for specialized transport and/or signaling tasks. Plant K_{2P} channels are modulated by signaling molecules such as intracellular H⁺ and calcium and physical factors like temperature and pressure. In this review, we ask the following:

What are the similarities and differences between K_{2P} channels in plants and animals in terms of their physiology? What is the nature of the last common ancestor (LCA) of these two groups of proteins? To answer these questions, we present physiological, structural, and phylogenetic evidence that discards the hypothesis proposing that the duplication and fusion that gave rise to the K_{2P} channels occurred in a prokaryote LCA. Conversely, we argue that the K_{2P} LCA was most likely a eukaryote organism. Consideration of plant and animal K_{2P} channels in the same study is novel and likely to stimulate further exchange of ideas between students of these fields.

Keywords K_{2P} channels · Plants · Animals

Electronic supplementary material The online version of this article (doi:10.1007/s00424-014-1638-4) contains supplementary material, which is available to authorized users.

W. González (✉) · B. Valdebenito · J. Caballero · G. Riadi ·
J. Riedelsberger · G. Martínez · D. Ramírez
Centro de Bioinformática y Simulación Molecular (CBSM),
Universidad de Talca, 2 Norte 685, Talca, Chile
e-mail: wgonzalez@utalca.cl

L. Zúñiga
Centro de Investigaciones Médicas (CIM), Escuela de Medicina,
Universidad de Talca, 2 Norte 685, Talca, Chile

F. V. Sepúlveda
Centro de Estudios Científicos (CECs), Arturo Prat 514, Valdivia,
Chile

I. Dreyer
Centro de Biotecnología y Genómica de Plantas, Universidad
Politécnica de Madrid, Madrid, Spain

M. Janta · D. Becker (✉)
Plant Molecular Biology and Biophysics, University of Wuerzburg,
Wuerzburg, Germany
e-mail: dirk.becker@uni-wuerzburg.de

Introduction

Two-pore domain potassium (K_{2P}) channels are membrane proteins that have been identified in mammals and other organisms such as *Drosophila*, *Caenorhabditis elegans*, as well as different plant species [22, 30]. The functional channel is a dimer with each subunit comprising two pore-forming loops and four transmembrane domains (4TM/2P). The genome of the model plant *Arabidopsis thaliana* harbors five such genes (TPK1-5, for tandem-pore potassium, K⁺, named in this review, AtTPKs) that code for K_{2P} channels. Orthologs of AtTPKs are found in all higher plants sequenced so far. In contrast, in algae, they have only been found in the chlorophyte *Ostreococcus* [71]. Although AtTPKs share their 4TM/2P topology with human K_{2P} channels (named in this review, hK_{2Ps}), their sequence identities and similarities are low, varying between 5.9 and 18.9 % for identity and 12.1 and 31.7 % for similarity (Online Resource 1). What did the last common ancestor (LCA) of both groups of proteins look like? Was the LCA a prokaryotic or a eukaryotic channel? What are the similarities and differences between AtTPKs and hK_{2Ps} in

SCIENTIFIC REPORTS

OPEN

Functional mutagenesis screens reveal the 'cap structure' formation in disulfide-bridge free TASK channels

Received: 08 October 2015
Accepted: 14 December 2015
Published: 22 January 2016

Matthias Goldstein^{1,*}, Susanne Rinné^{1,*}, Aytug K. Kiper^{1,*}, David Ramírez², Michael F. Netter¹, Daniel Bustos², Beatriz Ortiz-Bonin¹, Wendy González² & Niels Decher¹

Two-pore-domain potassium (K_{2p}) channels have a large extracellular cap structure formed by two M1-P1 linkers, containing a cysteine for dimerization. However, this cysteine is not present in the TASK-1/3/5 subfamily. The functional role of the cap is poorly understood and it remained unclear whether K_{2p} channels assemble in the domain-swapped orientation or not. Functional alanine-mutagenesis screens of TASK-1 and TRAAK were used to build an *in silico* model of the TASK-1 cap. According to our data the cap structure of disulfide-bridge free TASK channels is similar to that of other K_{2p} channels and is most likely assembled in the domain-swapped orientation. As the conserved cysteine is not essential for functional expression of all K_{2p} channels tested, we propose that hydrophobic residues at the inner leaflets of the cap domains can interact with each other and that this way of stabilizing the cap is most likely conserved among K_{2p} channels.

Two-pore domain potassium (K_{2p}) channels have four transmembrane domains (M1 to M4) containing two pore loops per subunit¹. The functional channels are formed by an antiparallel dimeric assembly, so that four pore loops form the selectivity filter of the channel^{2–4}. Crystallization of K_{2p} channels revealed a unique cap structure formed by the two large extracellular linkers from the M1 to the pore loop (M1-P1 linker)^{2–4}. The cap structure forms two tunnel-like side portals which serve as extracellular ion pathway (EIP) after the selectivity filter⁵. These side portals also play an important role in regulating the extracellular pH dependence of TASK channels⁵. Interestingly, following the initial crystal structure of TRAAK², a second structure with higher resolution showed a domain-swapped chain connectivity of the M1-P1 linker at the helical cap which also results in structural rearrangement of two opposing transmembrane helices³. However, whether most of the TRAAK channels or only a fraction of the functional channels are domain-swapped still remained elusive, although the recently released TREK-1 (PDB ID: 4TWK) and TREK-2⁶ structures were also crystallized in the domain-swapped orientation. Thus, a study providing information about the function of the cap and experiments providing insights towards the physiological orientation of the assembled channels would be very valuable.

In 1996 it was suggested by Lesage *et al.*, that a K_{2p} channel dimer is covalently assembled by a disulfide-bridge and that the extracellular domain as well as the cysteine residues are essential elements for the dimerization process of TWIK-1⁷. Crystallization of TWIK-1, TRAAK and TREK-2 confirmed the presence of a disulfide-bridge in homomeric K_{2p} channels^{2,4,6}. In addition, TASK-2, TASK-4, TALK-1, TREK-1, TRESK, KCNK7 and TWIK-2 share a homologous cysteine residue. However, for some K_{2p} channels there is evidence that the disulfide bond is not required for dimerization or the functional expression of homodimers^{8–10}. Accordingly, other unidentified mechanisms may exist for the functional assembly of K_{2p} channels, especially as the TASK-1/3/5 and THIK-1/2 subfamilies do not contain a homologous cysteine residue in the M1-P1 linker. Unfortunately, no 'disulfide-bridge free' K_{2p} channel could be crystallized yet. The lack of a cysteine in the M1-P1 linker, together with a very strong computational coiled-coil prediction in this domain of TASK channels, prompted us to study the role of this linker in TASK-1 channels. In the current study, using functional alanine-mutagenesis screens, we have built

¹Institute for Physiology and Pathophysiology, University of Marburg, 35037 Marburg, Germany. ²Center for Bioinformatics and Molecular Simulation, University of Talca, Talca, Chile. *These authors contributed equally to this work. Correspondence and requests for materials should be addressed to N.D. (email: decher@staff.uni-marburg.de)



The Open Medicinal Chemistry Journal

Content list available at: www.benthamopen.com/TOMCJ/

DOI: 10.2174/1874104501610010007



Computational Methods Applied to Rational Drug Design

David Ramírez*

Centro de Bioinformática y Simulación Molecular, Universidad de Talca, 2 Norte 685, Casilla, Talca, Chile

Received: October 27, 2015

Revised: January 27, 2016

Accepted: January 28, 2016

Abstract: Due to the synergic relationship between medical chemistry, bioinformatics and molecular simulation, the development of new accurate computational tools for small molecules drug design has been rising over the last years. The main result is the increased number of publications where computational techniques such as molecular docking, *de novo* design as well as virtual screening have been used to estimate the binding mode, site and energy of novel small molecules. In this work I review some tools, which enable the study of biological systems at the atomistic level, providing relevant information and thereby, enhancing the process of rational drug design.

Keywords: Bioinformatics, *de novo* design, medical chemistry, molecular docking, molecular modeling, rational drug design, virtual screening.

INTRODUCTION

Synergic relationship between experimental biochemistry sciences and computational theoretical methods has increased in recent years, providing significant benefits in different biological sciences areas, specially biochemistry and molecular biology. It has also brought advantages in medicinal chemistry for the rational design of drugs [1]. Regarding theoretical study of biochemical systems, one of its greatest profits is the molecular knowledge of the currently studied structures; these studies allow an exhaustive system analysis, and find meaningful answers to research questions that scientists face in their experimental laboratories.

Before exploring some of the computational methodologies currently used in drug design, it is important to consider that researchers have to draw from relevant information such as the three-dimensional structure of one or several substrates and molecular targets in order to start the theoretical study of certain biological systems. This information is essential, and in many cases, it determines the success or failure of the ongoing theoretical study. For instance, if a researcher wants to study the system formed by an endogenous or an exogenous inhibitor with its respective molecular target, the three-dimensional structure of the molecules involved in the interaction to be simulated has to be known.

The number of molecular targets with a well known structure is exponentially increasing due to the dramatic progress of spectroscopic techniques such as X-ray crystallography, Nuclear Magnetic Resonance (NMR) [2], and the development of the super-resolved fluorescence microscopy that shows a 3D image of a single molecule [3]. In addition, structures which have been produced from structural genomics have also become valuable tools for the study of systems whose molecular targets have not been solved yet [4, 5]. This growth has allowed a massive and constant use of computational tools in research centers worldwide. Furthermore, the developed methodologies for the production and optimization of small molecules (as most of the substrates studied in biochemistry sciences), are already registered in special databases and have provided vital information to research and find inherent characteristics which have never been described before [6, 7].

Nowadays, there are multiple computational methodologies used as bioinformatics tools for the study of biological

* Address correspondence to this author at the Centro de Bioinformática y Simulación Molecular, Universidad de Talca, 2 Norte 685, Casilla 721, Talca, Chile; Tel: +56972983600; E-mail: davramirez@utalca.cl



Article

Is It Reliable to Use Common Molecular Docking Methods for Comparing the Binding Affinities of Enantiomer Pairs for Their Protein Target?

David Ramírez and Julio Caballero *

Centro de Bioinformática y Simulación Molecular (CBSM), Universidad de Talca. 2 Norte 685, Casilla 721, Talca, Chile; damach.david@gmail.com

* Correspondence: jcaballero@utalca.cl; Tel.: +56-712-418-850

Academic Editors: Humberto González-Díaz, Roberto Todeschini and Alejandro Pazos Sierra

Received: 22 February 2016; Accepted: 1 April 2016; Published: 20 April 2016

Abstract: Molecular docking is a computational chemistry method which has become essential for the rational drug design process. In this context, it has had great impact as a successful tool for the study of ligand–receptor interaction modes, and for the exploration of large chemical datasets through virtual screening experiments. Despite their unquestionable merits, docking methods are not reliable for predicting binding energies due to the simple scoring functions they use. However, comparisons between two or three complexes using the predicted binding energies as a criterion are commonly found in the literature. In the present work we tested how wise is it to trust the docking energies when two complexes between a target protein and enantiomer pairs are compared. For this purpose, a ligand library composed by 141 enantiomeric pairs was used, including compounds with biological activities reported against seven protein targets. Docking results using the software Glide (considering extra precision (XP), standard precision (SP), and high-throughput virtual screening (HTVS) modes) and AutoDock Vina were compared with the reported biological activities using a classification scheme. Our test failed for all modes and targets, demonstrating that an accurate prediction when binding energies of enantiomers are compared using docking may be due to chance. We also compared pairs of compounds with different molecular weights and found the same results.

Keywords: molecular docking; modeling of enantiomers; prediction capability; docking accuracy; docking scoring; binding affinities

1. Introduction

Molecular docking has become a major computational method for the prediction of ligand–receptor interactions [1] and is an important and powerful tool for rational drug design [2]. Over the last few years the number of new molecular targets has increased due to the completion of the human genome project, as well as the protein and protein–ligand complex structures isolated by high-throughput protein purification [3] and solved by crystallography and nuclear magnetic resonance spectroscopy techniques [4,5]. At the same time, the improvement of computational techniques for studying interactions of ligands with the biological targets at the atomic scale have increased and developed.

In the last 25 years, the use of molecular docking has been raised in the context of drug discovery. We searched in Scopus using the word “docking” as a query, along with a selection of the most popular docking softwares according to Kroemer [6] (in the Search field: all fields “docking” and all fields “AutoDock” or “FlexX” or “DOCK” or “FRED” or “Glide” or “GOLD” or “Hammerhead” or “ICM” or “LigandFit” or “QXP” or “SLIDE” or “Surflex”). Figure 1 shows the results of this inquiry: research papers where molecular docking has been used have increased almost exponentially. Interestingly, the



Novel *N*-allyl/propargyl tetrahydroquinolines: Synthesis via Three-component Cationic Imino Diels–Alder Reaction, Binding Prediction, and Evaluation as Cholinesterase Inhibitors

Yeray A. Rodríguez¹, Margarita Gutiérrez^{1,*}, David Ramírez², Jans Alzate-Morales², Cristian C. Bernal³, Fausto M. Güiza³ and Arnold R. Romero Bohórquez^{3,*}

¹Laboratorio Síntesis Orgánica, Instituto de Química de Recursos Naturales, Universidad de Talca, Casilla 747, Talca 3460000, Chile

²Centro de Bioinformática y Simulación Molecular, Universidad de Talca, 2 Norte 685, Casilla 721, Talca 3460000, Chile

³Grupo de Investigación de Compuestos Orgánicos de Interés Medicinal (CODEIM), Parque Tecnológico Guatiguará, Universidad Industrial de Santander, A.A. 678, Piedecuesta, Colombia

*Corresponding authors: Margarita Gutiérrez, mgutierrez@utalca.cl; Arnold R. Romero Bohórquez, ararom@uis.edu.co

New *N*-allyl/propargyl 4-substituted 1,2,3,4-tetrahydroquinolines derivatives were efficiently synthesized using acid-catalyzed three components cationic imino Diels–Alder reaction (70–95%). All compounds were tested *in vitro* as dual acetylcholinesterase and butyryl-cholinesterase inhibitors and their potential binding modes, and affinity, were predicted by molecular docking and binding free energy calculations (ΔG) respectively. The compound 4af ($IC_{50} = 72 \mu M$) presented the most effective inhibition against acetylcholinesterase despite its poor selectivity ($SI = 2$), while the best inhibitory activity on butyryl-cholinesterase was exhibited by compound 4ae ($IC_{50} = 25.58 \mu M$) with considerable selectivity ($SI = 0.15$). Molecular docking studies indicated that the most active compounds fit in the reported acetylcholinesterase and butyryl-cholinesterase active sites. Moreover, our computational data indicated a high correlation between the calculated ΔG and the experimental activity values in both targets.

Key words: Alzheimer's disease, cationic imino Diels–Alder reaction, cholinesterase inhibitors, docking and MM-GBSA simulations, *N*-Allyl/Propargyl tetrahydroquinolines

Received 9 December 2015, revised 10 March 2016 and accepted for publication 5 April 2016

Alzheimer's disease (AD) is the most complex and common form of dementia in elderly people.

It is a neurodegenerative disease that causes progressive damage to the central nervous system, and is manifested with a cognitive deterioration, changes in brain function, including disordered behavior and impairment in language and comprehension (1). Currently, it is estimated that AD appears as the fourth leading cause of death afflicting more than seven million people worldwide (2).

According to the cholinergic hypothesis for AD pathogenesis, the decline of hippocampal and cortical levels of acetylcholine (ACh) leads to dysfunction of the cholinergic system and results in severe memory and learning deficits (3). At the neuronal level, ACh can be degraded by acetylcholinesterase (AChE) and butyrylcholinesterase (BChE), being the predominant AChE (80%). Therefore, it is important to know that the use of different biological entities, which are involved in the same pathology (AChE and BChE), is widely accepted and can be a good strategy to block the course of multifactorial diseases rather than just reducing their symptoms (4).

Acetylcholinesterase and BChE share 65% amino acid sequence homology and, even though being encoded by different genes on human chromosomes (5), both enzymes display a similar overall structure. Therefore, their active sites, composed of a catalytic triad and a choline-binding pocket, are both buried at the bottom of a $\sim 20 \text{ \AA}$ deep gorge. The two enzymes differ by the presence and extent of subdomains within the gorge, including a mid-gorge aromatic recognition site, a peripheral anionic site, and an acyl-binding site (6).

On the other hand, many kinds of heterocyclic derivatives have been reported with potent AChE and BChE inhibitory activity (7–11). However, many of them have showed adverse effects and problems of bioavailability (12,13). Therefore, it is necessary to develop new, safe, and efficient chemotherapeutic agents with potential applications for the treatment of AD.

Because of their remarkable biological applications, natural and synthetic quinoline compounds and their partially



CoaTx-II, a new dimeric Lys49 phospholipase A₂ from *Crotalus oreganus abyssus* snake venom with bactericidal potential: Insights into its structure and biological roles



J.R. Almeida^{a,b,e,*}, M. Lancellotti^b, A.M. Soares^{c,e}, L.A. Calderon^{c,e}, D. Ramírez^d,
W. González^{d,e}, S. Marangoni^b, S.L. Da Silva^{a,e}

^a IKIAM - Universidad Regional Amazónica, Km 7 Via Muyuna, Tena, Napo, Ecuador

^b Department of Biochemistry and Tissue Biology, Institute of Biology, Campinas State University (UNICAMP), Campinas, SP, Brazil

^c Oswaldo Cruz Foundation (FIOCRUZ), CEBio, Fiocruz Rondônia and Federal University of Rondônia, Porto Velho, RO, Brazil

^d Centro de Bioinformática y Simulación Molecular (CBSM), Universidad de Talca, 2 Norte 685, Casilla 721, Talca, Chile

^e International Network of Ecuadorian Snakes Venoms Studies (RIEVSE), Ecuador

ARTICLE INFO

Article history:

Received 21 June 2016

Received in revised form

5 August 2016

Accepted 11 August 2016

Available online 13 August 2016

Keywords:

Snake venom

Lys49 phospholipase A₂

Crotalus oreganus abyssus

Myotoxicity

Antibacterial effect

ABSTRACT

Snake venoms are rich and intriguing sources of biologically-active molecules that act on target cells, modulating a diversity of physiological functions and presenting promising pharmacological applications. Lys49 phospholipase A₂ is one of the multifunctional proteins present in these complex secretions and, although catalytically inactive, has a variety of biological activities, including cytotoxic, antibacterial, inflammatory, antifungal activities. Herein, a Lys49 phospholipase A₂, denominated CoaTx-II from *Crotalus oreganus abyssus*, was purified and structurally and pharmacologically characterized. CoaTx-II was isolated with a high degree of purity by a combination of two chromatographic steps; molecular exclusion and reversed-phase high performance liquid chromatography. This toxin is dimeric with a mass of 13868.2 Da (monomeric form), as determined by mass spectrometry. CoaTx-II is rich in Arg and Lys residues and displays high identity with other Lys49 PLA₂ homologues, which have high isoelectric points. The structural model of dimeric CoaTx-II shows that the toxin is non-covalently stabilized. Despite its enzymatic inactivity, *in vivo* CoaTx-II caused local muscular damage, characterized by increased plasma creatine kinase and confirmed by histological alterations, in addition to an inflammatory activity, as demonstrated by mice paw edema induction and pro-inflammatory cytokine IL-6 elevation. CoaTx-II also presents antibacterial activity against gram negative (*Pseudomonas aeruginosa* 31NM, *Escherichia coli* ATCC 25922) and positive (*Staphylococcus aureus* BEC9393 and Rib1) bacteria. Therefore, data show that this newly purified toxin plays a central role in mediating the degenerative events associated with envenomation, in addition to demonstrating antibacterial properties, with potential for use in the development of strategies for antivenom therapy and combating antibiotic-resistant bacteria.

© 2016 Elsevier Ltd. All rights reserved.

1. Introduction

Antimicrobial resistance is one of most serious and alarming public health problems, spreading faster than the discovery and introduction of new therapeutic molecules into clinical practice.

The prevalence of this bacterial resistance and the side effects of conventional antibiotics have prompted the search and development of more efficient strategies, as well as powerful and safe compounds to aid in the fight against infectious diseases (Ling et al., 2015; Sudharshan and Dhananjaya, 2015). As such, proteins and peptides from snake venoms represent valuable and attractive sources of bioactive molecules against Gram-positive and Gram-negative bacteria (Oliveira-Junior et al., 2013; Corrêa et al., 2016).

Snake venoms constitute a complex and natural library of proteins and peptides that present valuable structural and functional diversity (Calvete et al., 2007; McCleary and Kini, 2013). A deeper

* Corresponding author. IKIAM – Universidad Regional Amazónica, Km 7, via Muyuna, Tena, Napo, Ecuador.

E-mail addresses: rafaeldealmeida@ikiam.edu.ec, zerafaelbio@hotmail.com (J.R. Almeida).

9. CONCLUDING REMARKS

In conclusion, K_{2p} channels produce background K^+ currents that regulate cell excitability but not in a “passive way”, these channels are regulated by several and different physical and chemical signals; however the regulation mechanism remains unclear. It has recently been reported that these channels –which do not possess a canonical voltage-sensing domain– can be voltage gated by an ion check valve mechanism on the selectivity filter, similar to classical C-type inactivation in more extensively studied Kv and Kir channels. Besides, new structural and physiological evidence points to the possibility that the side-openings called here “fenestrations” could be related to blockade mechanism in K_{2p} channels. We strongly believe that these channels are modulated by the side-openings, as well as that the gated mechanism is formed by the selectivity filter and the fenestrations. This new and exciting hypothesis has high explanatory power, but more evidence is needed to clarify the mentioned mechanism. It is, however, necessary to take into account the fenestration role in all structure-based drug discovery processes targeting K_{2p} .

In the present work we studied the TASK potassium channels using both theoretical and experimental approaches. For the theoretical studies several TASK-1 and TASK-3 homology models were generated. All models exhibited a 3D-structure energetically stable. From this models as a starting point, using theoretical (virtual screening, docking, MM/GBSA, molecular dynamics) and experimental (electrophysiology measurements) approaches it was possible: 1) to study why Kv1.5 blockers inhibit preferentially TASK-1 channels; from these results we proposed TASK-1 channels as an unrecognized molecular target of Kv1.5 blockers in atrial fibrillation or obstructive sleep apnea; 2) to study the role of the fenestration for the binding of A1899 to TASK-1, and 3) to discover two novel TASK-3 modulators that exhibits an IC_{50} in the micromolar range. The computational protocol employed here is efficient and allows the identification in short time of novel modulators.

Finally, we conclude that TASK channels might represent novel drug targets for several disorders for which additional therapeutic options would be useful. Although further exploration of TASK channels is expected to yield additional insights into physiological roles of the different

members of this K_{2P} subfamily; our understanding of K_{2P} channels function and modulation would also benefit tremendously from identification of potent modulators by using dry and wet approaches.

10. REFERENCES

- Abagyan, R. & Totrov, M., 1994. Biased probability Monte Carlo conformational searches and electrostatic calculations for peptides and proteins. *Journal of molecular biology*, 235(3), pp.983–1002.
- Adasme-Carreño, F. et al., 2014. Performance of the MM/GBSA scoring using a binding site hydrogen bond network-based frame selection: the protein kinase case. *Physical Chemistry Chemical Physics*, 16(27), pp.14047–14058.
- Aryal, P. et al., 2014. A hydrophobic barrier deep within the inner pore of the TWIK-1 K2P potassium channel. *Nature Communications*, 5, pp.1–9.
- Bachmann, A. et al., 2001. Characterization of a novel Kv1.5 channel blocker in *Xenopus* oocytes, CHO cells, human and rat cardiomyocytes. *Naunyn-Schmiedeberg's archives of pharmacology*, 364(5), pp.472–478.
- Baxter, D.F. et al., 2002. A Novel Membrane Potential-Sensitive Fluorescent Dye Improves Cell-Based Assays for Ion Channels. *Journal of Biomolecular Screening*, 7(1), pp.79–85.
- Bayliss, D.A. et al., 2001. TASK-1 is a highly modulated pH-sensitive leak K⁺ channel expressed in brainstem respiratory neurons. *Respiration physiology*, 129(1), pp.159–174.
- Bayliss, D.A. & Barrett, P.Q., 2009. Emerging roles for two-pore-domain potassium channels and their potential therapeutic impact. In *Trends Pharmacol Sci*. pp. 566–575.
- Bayliss, D.A., Sirois, J.E. & Talley, E.M., 2003. The TASK family: two-pore domain background K⁺ channels. *Molecular Interventions*, 3(4), p.205.
- Bittner, S. et al., 2010. Upregulation of K2P5.1 potassium channels in multiple sclerosis. *Annals of neurology*, 68(1), pp.58–69.
- Bottegoni, G., Cavalli, A. & Recanatini, M., 2006. A comparative study on the application

- of hierarchical-agglomerative clustering approaches to organize outputs of reiterated docking runs. *Journal of Chemical Information and Modeling*, 46(2), pp.852–862.
- Bowers, K.J. et al., 2006. Scalable algorithms for molecular dynamics simulations on commodity clusters. In *SC 2006 Conference, Proceedings of the ACM/IEEE*. p. 43.
- Brendel, J. et al., 2004. Atrial-selective antiarrhythmic actions of novel I_{Kr} vs. I_{Ks}, and I_KACh class I_c drugs and beta blockers in pigs. *Medical Science Monitor Basic Research*, 10(7), p.BR221--BR228.
- Bressi, J.C. et al., 2001. Adenosine analogues as selective inhibitors of glyceraldehyde-3-phosphate dehydrogenase of Trypanosomatidae via structure-based drug design. *Journal of medicinal chemistry*, 44(13), pp.2080–2093.
- Brohawn, S., Campbell, E. & MacKinnon, R., 2013. Domain-swapped chain connectivity and gated membrane access in a Fab-mediated crystal of the human TRAAK K⁺ channel. *Proceedings of the National Academy of Sciences of the United States of America*, 110(6), pp.2129–34.
- Brohawn, S., Campbell, E. & MacKinnon, R., 2014. Physical mechanism for gating and mechanosensitivity of the human TRAAK K⁺ channel. *Nature*, 516(7529), pp.126–130.
- Brohawn, S., del Marmol, J. & MacKinnon, R., 2012. Crystal Structure of the Human K2P TRAAK, a Lipid- and Mechano-Sensitive K⁺ Ion Channel. *Science*, 335(6067), pp.436–441.
- Brohawn, S., Su, Z. & MacKinnon, R., 2014. Mechanosensitivity is mediated directly by the lipid membrane in TRAAK and TREK1 K⁺ channels. *Proceedings of the National Academy of Sciences of the United States of America*, 111(9), pp.3614–9.
- Bruner, J.K. et al., 2014. Identification of novel small molecule modulators of K2P18.1 two-pore potassium channel. *European journal of pharmacology*, 740, pp.603–10.
- Budde, T. et al., 2008. Reciprocal modulation of I_h and I_{TASK} in thalamocortical relay neurons by halothane. *Pflügers Archiv-European Journal of Physiology*, 456(6), pp.1061–1073.

- Burashnikov, A. et al., 2012. Atrial-selective prolongation of refractory period with AVE0118 is due principally to inhibition of sodium channel activity. *Journal of cardiovascular pharmacology*, 59(6), p.539.
- Campagna-Slater, V. et al., 2010. Pharmacophore screening of the protein data bank for specific binding site chemistry. *Journal of chemical information and modeling*, 50(3), pp.358–367.
- Caporuscio, F. et al., 2011. Structure-based design of potent aromatase inhibitors by high-throughput docking. *Journal of medicinal chemistry*, 54(12), pp.4006–4017.
- Chokshi, R.H. et al., 2015. Breathing Stimulant Compounds Inhibit TASK-3 Potassium Channel Function Likely by Binding at a Common Site in the Channel Pore. *Molecular pharmacology*, 88, pp.926–934.
- Christ, T. et al., 2008. Pathology-specific effects of the IKur/Ito/IK, ACh blocker AVE0118 on ion channels in human chronic atrial fibrillation. *British journal of pharmacology*, 154(8), pp.1619–1630.
- Clarke, C.E. et al., 2008. The M1P1 loop of TASK3 K2P channels apposes the selectivity filter and influences channel function. *The Journal of biological chemistry*, 283(25), pp.16985–92.
- Coburn, C. a et al., 2012. Discovery of a pharmacologically active antagonist of the two-pore domain potassium channel K2P9.1 (TASK-3). *ChemMedChem*, 7(1), pp.123–33.
- Cotten, J.F., 2013a. TASK-1 (KCNK3) and TASK-3 (KCNK9) Tandem Pore Potassium Channel Antagonists Stimulate Breathing in Isoflurane-Anesthetized Rats. *Anesthesia & Analgesia*, 116(4), pp.810–816.
- Cotten, J.F., 2013b. TASK-1 (KCNK3) and TASK-3 (KCNK9) Tandem Pore Potassium Channel Antagonists Stimulate Breathing in Isoflurane Anesthetized Rats. *Anesthesia & Analgesia*, 116(4), pp.810–816.
- Cotten, J.F. et al., 2006. The ventilatory stimulant doxapram inhibits TASK tandem pore (K2P) potassium channel function but does not affect minimum alveolar anesthetic concentration. *Anesthesia and analgesia*, 102(3), pp.779–85.

- Czirják, G. et al., 2000. TASK (TWIK--Related Acid-Sensitive K⁺ Channel) Is Expressed in Glomerulosa Cells of Rat Adrenal Cortex and Inhibited by Angiotensin II. *Molecular Endocrinology*, 14(6), pp.863–874.
- Czirják, G. & Enyedi, P., 2002. TASK-3 dominates the background potassium conductance in rat adrenal glomerulosa cells. *Molecular Endocrinology*, 16(3), pp.621–629.
- Czirják, G. & Enyedi, P., 2003. Ruthenium red inhibits TASK-3 potassium channel by interconnecting glutamate 70 of the two subunits. *Molecular pharmacology*, 63(3), pp.646–52.
- Czirják, G. & Enyedi, P., 2006. Zinc and mercuric ions distinguish TRESK from the other two-pore domain K⁺ channels. *Molecular pharmacology*, 69(3), pp.1024–1032.
- Decher, N. et al., 2006. Binding site of a novel Kv1.5 blocker: a “foot in the door” against atrial fibrillation. *Molecular pharmacology*, 70(4), pp.1204–1211.
- Decher, N. et al., 2004. Molecular Basis for Kv1.5 Channel block conservation of drug binding sites among voltage-gated K⁺ channels. *Journal of Biological Chemistry*, 279(1), pp.394–400.
- Decher, N. et al., 2010. RNA editing modulates the binding of drugs and highly unsaturated fatty acids to the open pore of Kv potassium channels. *The EMBO journal*, 29(13), pp.2101–2113.
- Dennington, R., Keith, T. & Millam, J., 2009. GaussView 5.0.8. *Semichem Inc.: Shawnee Mission, KS*.
- Dixon, S.L., Smondyrev, A.M. & Rao, S.N., 2006. PHASE: a novel approach to pharmacophore modeling and 3D database searching. *Chemical biology & drug design*, 67(5), pp.370–2.
- Dobrev, D. et al., 2005. The G protein--gated potassium current I_K, ACh is constitutively active in patients with chronic atrial fibrillation. *Circulation*, 112(24), pp.3697–3706.
- Dong, Y. et al., 2015. K2P channel gating mechanisms revealed by structures of TREK-2 and a complex with Prozac. *Science*, 347(6227), pp.1256–1259.
- Duprat, F. et al., 1997. TASK, a human background K⁺ channel to sense external pH

- variations near physiological pH. *The EMBO Journal*, 16(17), pp.5464–5471.
- Enyedi, P. & Czirják, G., 2010. Molecular background of leak K⁺ currents: two-pore domain potassium channels. *Physiological Reviews*, 90(2), pp.559–605.
- Ewing, T.J.A. et al., 2001. DOCK 4.0: search strategies for automated molecular docking of flexible molecule databases. *Journal of computer-aided molecular design*, 15(5), pp.411–428.
- Fedida, D. et al., 1993. Identity of a novel delayed rectifier current from human heart with a cloned K⁺ channel current. *Circulation research*, 73(1), pp.210–216.
- Feixas, F. et al., 2015. Exploring the Role of Receptor Flexibility in Structure-Based Drug Discovery. *Biophysical chemistry*, 186, pp.31–45.
- Flaherty, D.P. et al., 2014. Potent and selective inhibitors of the TASK-1 potassium channel through chemical optimization of a bis-amide scaffold. *Bioorganic and Medicinal Chemistry Letters*, 24(16), pp.3968–3973.
- Friesner, R.A. et al., 2004. Glide: a new approach for rapid, accurate docking and scoring. 1. Method and assessment of docking accuracy. *Journal of medicinal chemistry*, 47(7), pp.1739–1749.
- Frisch, M. et al., 2009. Gaussian 09, Revision A. 02, Gaussian. *Inc.*, Wallingford, CT, 200.
- Gardener, M.J. et al., 2004. Functional evidence of a role for two-pore domain potassium channels in rat mesenteric and pulmonary arteries. *British journal of pharmacology*, 142(1), pp.192–202.
- Gögelein, H. et al., 2004. Effects of the atrial antiarrhythmic drug AVE0118 on cardiac ion channels. *Naunyn-Schmiedeberg's archives of pharmacology*, 370(3), pp.183–192.
- Goldstein, M. et al., 2016. Functional mutagenesis screens reveal the “cap structure” formation in disulfide-bridge free TASK channels. *Scientific reports*, 6, p.19492.
- Goldstein, S. et al., 2001. Potassium leak channels and the KCNK family of two-P-domain subunits. *Nature Reviews Neuroscience*, 2(3), pp.175–184.
- González, W. et al., 2013. An extracellular ion pathway plays a central role in the cooperative gating of a K2P K⁺ channel by extracellular pH. *Journal of Biological*

- Chemistry*, 288(8), pp.5984–5991.
- González, W. et al., 2015. K2P channels in plants and animals. *Pflugers Archiv : European journal of physiology*, 467(5), pp.1091–1104.
- Gotter, A.L. et al., 2011. TASK-3 as a potential antidepressant target. *Brain research*, 1416(6), pp.69–79.
- Gray, K.A. et al., 2012. Genenames. org: the HGNC resources in 2013. *Nucleic acids research*, p.gks1066.
- Guagliardo, N.A. et al., 2012. TASK-3 channel deletion in mice recapitulates low-renin essential hypertension. *Hypertension*, 59(5), pp.999–1005.
- Halgren, T.A. et al., 2004. Glide: a new approach for rapid, accurate docking and scoring. 2. Enrichment factors in database screening. *Journal of medicinal chemistry*, 47(7), pp.1750–1759.
- Hecht, F.M. et al., 1998. Sexual transmission of an HIV-1 variant resistant to multiple reverse-transcriptase and protease inhibitors. *New England Journal of Medicine*, 339(5), pp.307–311.
- Heitzmann, D. et al., 2008. Invalidation of TASK1 potassium channels disrupts adrenal gland zonation and mineralocorticoid homeostasis. *The EMBO journal*, 27(1), pp.179–187.
- Hou, T. et al., 2012. Assessing the performance of the MM/PBSA and MM/GBSA methods: I. The accuracy of binding free energy calculations based on molecular dynamics simulations. *Journal of Chemical Information and Modeling*, 51(1), pp.69–82.
- Hou, T. & Yu, R., 2007. Molecular dynamics and free energy studies on the wild-type and double mutant HIV-1 protease complexed with amprenavir and two amprenavir-related inhibitors: mechanism for binding and drug resistance. *Journal of medicinal chemistry*, 50(6), pp.1177–1188.
- HUGO, 2014. Human Genome Organisation. Available at: <http://www.hugo-international.org/> [Accessed July 18, 2014].

- Humphrey, W., Dalke, A. & Schulten, K., 1996. VMD: visual molecular dynamics. *Journal of molecular graphics*, 14(1), pp.33–38.
- Innamaa, A. et al., 2013. Expression and prognostic significance of the oncogenic K2P potassium channel KCNK9 (TASK-3) in ovarian carcinoma. *Anticancer research*, 33(4), pp.1401–1408.
- Irwin, J.J. & Shoichet, B.K., 2005. ZINC-a free database of commercially available compounds for virtual screening. *Journal of chemical information and modeling*, 45(1), pp.177–182.
- IUPHAR, 2014. International Union of Basic and Clinical Pharmacology. Available at: <http://www.iuphar.org/> [Accessed July 18, 2014].
- Jain, A. & Trivedi, V., 2014. Docking and virtual screening to identify PKC agonists: potentials in anticancer therapeutics. *Current computer-aided drug design*, 10(1), pp.50–58.
- Jiang, Y. et al., 2002. Crystal structure and mechanism of a calcium-gated potassium channel. *Nature*, 417(6888), pp.515–522.
- Jorgensen, C. et al., 2016. Lateral fenestrations in K⁺ channels explored using MD simulations. *Molecular Pharmaceutics*, 13, pp.2263–2273.
- Jorgensen, W.L., 2006. QikProp. *Schrödinger LLC, New York*.
- Jorgensen, W.L., Maxwell, D.S. & Tirado-Rives, J., 1996. Development and testing of the OPLS all-atom force field on conformational energetics and properties of organic liquids. *Journal of the American Chemical Society*, 118(45), pp.11225–11236.
- Kaczmariski, J.A. & Corry, B., 2014. Investigating the size and dynamics of voltage-gated sodium channel fenestrations: A molecular dynamics study. *Channels*, 8(3), pp.264–277.
- Kaminski, G.A. et al., 2001. Evaluation and reparametrization of the OPLS-AA force field for proteins via comparison with accurate quantum chemical calculations on peptides. *The Journal of Physical Chemistry B*, 105(28), pp.6474–6487.
- Kelly, M.D. & Mancera, R.L., 2004. Expanded interaction fingerprint method for analyzing

- ligand binding modes in docking and structure-based drug design. *Journal of chemical information and computer sciences*, 44(6), pp.1942–1951.
- Kim, D., 2005. Physiology and pharmacology of two-pore domain potassium channels. *Current pharmaceutical design*, 11(21), pp.2717–2736.
- Kim, D. & Gnatenco, C., 2001. TASK-5, a New Member of the Tandem-Pore K⁺ Channel Family. *Biochemical and biophysical research communications*, 284(4), pp.923–930.
- Kincaid, V.A. et al., 2015. Virtual screening for UDP-galactopyranose mutase ligands identifies a new class of antimycobacterial agents. *ACS chemical biology*.
- Kindler, C.H. et al., 2003. Amide Local Anesthetics Potently Inhibit the Human Tandem Pore Domain Background K² Channel TASK-2 (KCNK5). , 306(1), pp.84–92.
- Kindler, C.H., Yost, S.C. & Gray, A.T., 1999. Local anesthetic inhibition of baseline potassium channels with two pore domains in tandem. *Anesthesiology*, 90(4), pp.1092–1102.
- Kiper, A.K. et al., 2015. Kv1.5 blockers preferentially inhibit TASK-1 channels: TASK-1 as a target against atrial fibrillation and obstructive sleep apnea? *Pflugers Archiv : European journal of physiology*, 467(5), pp.1081–1090.
- Knobloch, K. et al., 2002. Electrophysiological and antiarrhythmic effects of the novel I Kur channel blockers, S9947 and S20951, on left vs. right pig atrium in vivo in comparison with the I Kr blockers dofetilide, azimilide, d, l-sotalol and ibutilide. *Naunyn-Schmiedeberg's archives of pharmacology*, 366(5), pp.482–487.
- Koes, D.R. & Camacho, C.J., 2011. Pharmer: efficient and exact pharmacophore search. *Journal of chemical information and modeling*, 51(6), pp.1307–1314.
- Koes, D.R. & Camacho, C.J., 2012. ZINCPharmer: pharmacophore search of the ZINC database. *Nucleic acids research*, 40(Web Server issue), pp.W409-14.
- Kräutler, V., van Gunsteren, W.F. & Hünenberger, P.H., 2001. A fast SHAKE algorithm to solve distance constraint equations for small molecules in molecular dynamics simulations. *Journal of computational chemistry*, 22(5), pp.501–508.
- Kumar, A. et al., 2014. Identification of 1, 2, 5-Oxadiazoles as a New Class of SENP2

- Inhibitors Using Structure Based Virtual Screening. *Journal of chemical information and modeling*, 54(3), pp.870–880.
- Kun, A. et al., 2014. Neurogenic Contraction Induced by the Antiarrhythmic Compound, AVE 0118, in Rat Small Mesenteric Arteries. *Basic & clinical pharmacology & toxicology*, 115(4), pp.315–320.
- Laskowski, R.A. et al., 1993. PROCHECK: a program to check the stereochemical quality of protein structures. *Journal of applied crystallography*, 26(2), pp.283–291.
- Law, R. et al., 2005. Membrane protein structure quality in molecular dynamics simulation. *Journal of Molecular Graphics and Modelling*, 24(2), pp.157–165.
- Lazarenko, R.M. et al., 2010. Motoneuronal TASK channels contribute to immobilizing effects of inhalational general anesthetics. *The Journal of Neuroscience*, 30(22), pp.7691–7704.
- Lesage, F. et al., 1996. Dimerization of TWIK-1 K⁺ channel subunits via a disulfide bridge. *The EMBO journal*, 15(23), pp.6400–7.
- Lesage, F. & Lazdunski, M., 2000. Molecular and functional properties of two-pore-domain potassium channels. *American Journal Physiol Renal Physiol*, 279, pp.793–801.
- Li, G.-R. et al., 1996. Evidence for two components of delayed rectifier K⁺ current in human ventricular myocytes. *Circulation Research*, 78(4), pp.689–696.
- Li, J. et al., 2011. The VSGB 2.0 model: a next generation energy model for high resolution protein structure modeling. *Proteins: Structure, Function, and Bioinformatics*, 79(10), pp.2794–2812.
- Limberg, S.H. et al., 2011. TASK-1 channels may modulate action potential duration of human atrial cardiomyocytes. *Cellular Physiology and Biochemistry*, 28(4), pp.613–624.
- Lipinski, C.A. et al., 2012. Experimental and computational approaches to estimate solubility and permeability in drug discovery and development settings. *Advanced drug delivery reviews*, 64, pp.4–17.

- Lolicato, M. et al., 2014. Transmembrane Helix Straightening and Buckling Underlies Activation of Mechanosensitive and Thermosensitive K₂P Channels. *Neuron*, 84, pp.1198–1212.
- Long, S.B., Campbell, E.B. & MacKinnon, R., 2005. Crystal structure of a mammalian voltage-dependent Shaker family K⁺ channel. *Science*, 309(5736), pp.897–903.
- Lorenzen, S. & Zhang, Y., 2007. Identification of near-native structures by clustering protein docking conformations. *PROTEINS: Structure, Function, and Bioinformatics*, 68(1), pp.187–194.
- Lotshaw, D.P., 2007. Biophysical, pharmacological, and functional characteristics of cloned and native mammalian two-pore domain K⁺ channels. *Cell biochemistry and biophysics*, 47(2), pp.209–256.
- Maingret, F. et al., 2001. The endocannabinoid anandamide is a direct and selective blocker of the background K⁺ channel TASK-1. *The EMBO Journal*, 20(1–2), pp.47–54.
- Martyna, G.J., Tobias, D.J. & Klein, M.L., 1994. Constant pressure molecular dynamics algorithms. *The Journal of Chemical Physics*, 101(5), pp.4177–4189.
- Massova, I. & Kollman, P.A., 2000. Combined molecular mechanical and continuum solvent approach (MM-PBSA/GBSA) to predict ligand binding. *Perspectives in drug discovery and design*, 18(1), pp.113–135.
- Meadows, H.J. & Randall, A.D., 2001. Functional characterisation of human TASK-3, an acid-sensitive two-pore domain potassium channel. *Neuropharmacology*, 40(4), pp.551–559.
- Mena-Ulecia, K., Tiznado, W. & Caballero, J., 2015. Study of the Differential Activity of Thrombin Inhibitors Using Docking, QSAR, Molecular Dynamics, and MM-GBSA. *PloS One*, 10(11), p.e0142774.
- Meuth, S. et al., 2008. TWIK-related acid-sensitive K⁺ channel 1 (TASK1) and TASK3 critically influence T lymphocyte effector functions. *Journal of biological chemistry*, 283(21), pp.14559–14570.
- Meuth, S.G. et al., 2003. Contribution of TWIK-related acid-sensitive K⁺ channel 1

- (TASK1) and TASK3 channels to the control of activity modes in thalamocortical neurons. *The Journal of neuroscience*, 23(16), pp.6460–6469.
- Millar, J.A. et al., 2000. A functional role for the two-pore domain potassium channel TASK-1 in cerebellar granule neurons. *Proceedings of the National Academy of Sciences*, 97(7), pp.3614–3618.
- Miller, A. & Long, S., 2012. Crystal Structure of the Human Two-Pore Domain Potassium Channel K2P1. *Science*, 335, p.432.
- Miller, M.R. et al., 2013. Development of a Selective Chemical Inhibitor for the Two-Pore Potassium Channel, KCNK9.
- Mittal, A. et al., 2014. Pharmacophore based virtual screening, molecular docking and biological evaluation to identify novel PDE5 inhibitors with vasodilatory activity. *Bioorganic & medicinal chemistry letters*, 24(14), pp.3137–3141.
- Mu, D. et al., 2003. Genomic amplification and oncogenic properties of the KCNK9 potassium channel gene. *Cancer cell*, 3(3), pp.297–302.
- Murray, C.W. et al., 1997. PRO_SELECT: combining structure-based drug design and combinatorial chemistry for rapid lead discovery. 1. Technology. *Journal of computer-aided molecular design*, 11(2), pp.193–207.
- Nattel, S. et al., 2007. Arrhythmogenic ion-channel remodeling in the heart: heart failure, myocardial infarction, and atrial fibrillation. *Physiological reviews*, 87(2), pp.425–456.
- Nayak, T.K. et al., 2009. Inhibition of human two-pore domain K⁺ channel TREK1 by local anesthetic lidocaine: negative cooperativity and half-of-sites saturation kinetics. *Molecular pharmacology*, 76(4), pp.903–917.
- Niemeyer, M. et al., 2016. Gating, regulation and structure in K2P K⁺ channels: In varietate concordia? *Molecular pharmacology*, p.mol--116.
- Noriega-Navarro, R. et al., 2014. Novel TASK channels inhibitors derived from dihydropyrrolo[2,1-a]isoquinoline. *Neuropharmacology*, 79, pp.28–36.
- O'Connell, A.D., Morton, M.J. & Hunter, M., 2002. Two-pore domain K⁺ channels -

- molecular sensors. *Biochimica et Biophysica Acta (BBA)-Biomembranes*, 1566(1), pp.152–161.
- Ortega-Sáenz, P. et al., 2010. Carotid body chemosensory responses in mice deficient of TASK channels. *The Journal of general physiology*, 135(4), pp.379–392.
- Pan, J.-F., Chua, S.-J. & Huang, W., 2002. Conformational analysis (ab initio HF/3-21G*) and optical properties of poly (thiophene-phenylene-thiophene)(PTPT). *Chemical physics letters*, 363(1), pp.18–24.
- Pang, D.S.J. et al., 2009. An unexpected role for TASK-3 potassium channels in network oscillations with implications for sleep mechanisms and anesthetic action. *Proceedings of the National Academy of Sciences*, 106(41), pp.17546–17551.
- Patel, A.J. et al., 1999. Inhalational anesthetics activate two-pore-domain background K⁺ channels. *Nature neuroscience*, 2(5), pp.422–426.
- Pathak, M.M. et al., 2007. Closing in on the resting state of the Shaker K⁺ channel. *Neuron*, 56(1), pp.124–140.
- Payandeh, J. et al., 2012. Crystal structure of a voltage-gated sodium channel in two potentially inactivated states. *Nature*, 486(7401), pp.135–139.
- Pei, L. et al., 2003. Oncogenic potential of TASK3 (Kcnk9) depends on K⁺ channel function. *Proceedings of the National Academy of Sciences*, 100(13), pp.7803–7807.
- Petric, S. et al., 2012. In vivo electrophysiological characterization of TASK-1 deficient mice. *Cellular physiology and biochemistry*, 30(3), pp.523–537.
- Piechotta, P. et al., 2011. The pore structure and gating mechanism of K2P channels. *The EMBO journal*, 30(17), pp.3607–3619.
- Putzke, C. et al., 2007. The acid-sensitive potassium channel TASK-1 in rat cardiac muscle. *Cardiovascular research*, 75(1), pp.59–68.
- Rajan, S. et al., 2000. TASK-3, a novel tandem pore domain acid-sensitive K⁺ channel. An extracellular histidine as pH sensor. *The Journal of biological chemistry*, 275(22), pp.16650–7.
- Rapedius, M. et al., 2012. State-independent intracellular access of quaternary ammonium

- blockers to the pore of TREK-1. *Channels*, 6(6), pp.473–478.
- Rastelli, G. et al., 2010. Fast and accurate predictions of binding free energies using MM-PBSA and MM-GBSA. *Journal of computational chemistry*, 31(4), pp.797–810.
- Russell, R.B. & Barton, G.J., 1992. Multiple protein sequence alignment from tertiary structure comparison: assignment of global and residue confidence levels. *Proteins: Structure, Function, and Bioinformatics*, 14(2), pp.309–323.
- Sabogal-arango, A. et al., 2014. Computational Insights of the Interaction among Sea Anemones Neurotoxins and Kv1.3 Channel. *Bioinformatics and Biology Insights*, 8, pp.73–81.
- Šali, A. & Blundell, T.L., 1993. Comparative protein modelling by satisfaction of spatial restraints. *Journal of molecular biology*, 234(3), pp.779–815.
- Schewe, M. et al., 2016. A Non-canonical Voltage-Sensing Mechanism Controls Gating in K2P K⁺ Channels. *Cell*, 164(5), pp.937–949.
- Schrödinger, L., 2011. Desmond Molecular Dynamics System, version 3.0; Epik version 2.2; Glide, version 5.7; Impact, version 5.7; LigPrep, version 2.5; Phase, version 3.3; Prime, version 2.3; SiteMap, version 2.5; Virtual Screening Workflow. *New York, NY*.
- Shelke, S.M. et al., 2011. Exploration of new scaffolds as potential MAO-A inhibitors using pharmacophore and 3D-QSAR based in silico screening. *Bioorganic & medicinal chemistry letters*, 21(8), pp.2419–2424.
- Shenkin, P.S. & McDonald, D.Q., 1994. Cluster Analysis of Molecular Conformations. *Journal of computational Chemistry*, 15(8), pp.899–916.
- Singh, K.D. et al., 2012. Homology modeling, molecular dynamics, e-pharmacophore mapping and docking study of Chikungunya virus nsP2 protease. *Journal of Molecular Modeling*, 18(1), pp.39–51.
- Smart, O. et al., 1996. HOLE: a program for the analysis of the pore dimensions of ion channel structural models. *Journal of molecular graphics*, 14(6), pp.354–360.
- Streit, A.K. et al., 2011. A specific two-pore domain potassium channel blocker defines the structure of the TASK-1 open pore. *The Journal of biological chemistry*, 286(16),

pp.13977–13984.

- Strutz-Seebohm, N. et al., 2007. Comparison of potent Kv1.5 potassium channel inhibitors reveals the molecular basis for blocking kinetics and binding mode. *Cellular Physiology and Biochemistry*, 20(6), pp.791–800.
- Talley, E.M. et al., 2001. Cns distribution of members of the two-pore-domain (KCNK) potassium channel family. *The Journal of neuroscience : the official journal of the Society for Neuroscience*, 21(19), pp.7491–505.
- Talley, E.M. et al., 2000. TASK-1, a Two-Pore Domain K⁺ Channel, Is Modulated by Multiple Neurotransmitters in Motoneurons. *Neuron*, 25(2), pp.399–410.
- Talley, E.M. et al., 2003. Two-pore-Domain (KCNK) potassium channels: dynamic roles in neuronal function. *The Neuroscientist*, 9(1), pp.46–56.
- Talley, E.M. & Bayliss, D.A., 2002. Modulation of TASK-1 (Kcnk3) and TASK-3 (Kcnk9) potassium channels volatile anesthetics and neurotransmitters share a molecular site of action. *Journal of Biological Chemistry*, 277(20), pp.17733–17742.
- Tarasiuk, A. & Reuveni, H., 2013. The economic impact of obstructive sleep apnea. *Current opinion in pulmonary medicine*, 19(6), pp.639–644.
- Totrov, M. & Abagyan, R., 2008. Flexible ligand docking to multiple receptor conformations: a practical alternative. *Current Opinion in Structural Biology*, 18(2), pp.178–184.
- Trapp, S. et al., 2008. A role for TASK-1 (KCNK3) channels in the chemosensory control of breathing. *The Journal of Neuroscience*, 28(35), pp.8844–8850.
- Tubert-Brohman, I. et al., 2013. Improved docking of polypeptides with Glide. *Journal of chemical information and modeling*, 53(7), pp.1689–1699.
- Vega-Saenz de Miera, E. et al., 2001. KT3.2 and KT3.3, two novel human two-pore K⁺ channels closely related to TASK-1. *Journal of Neurophysiology*, 86(1), pp.130–142.
- Voelker, C. et al., 2010. Roles of tandem-pore K⁺ channels in plants--a puzzle still to be solved*. *Plant Biology*, 12(s1), pp.56–63.
- Van Wagoner, D.R. et al., 1997. Outward K⁺ current densities and Kv1.5 expression are

- reduced in chronic human atrial fibrillation. *Circulation research*, 80(6), pp.772–781.
- Walters, W.P., 2012. Going further than Lipinski's rule in drug design. *Expert opinion on drug discovery*, 7(2), pp.99–107.
- Wang, W. & Kollman, P.A., 2001. Computational study of protein specificity: the molecular basis of HIV-1 protease drug resistance. *Proceedings of the National Academy of Sciences*, 98(26), pp.14937–14942.
- Wang, Z., Fermini, B. & Nattel, S., 1993. Sustained depolarization-induced outward current in human atrial myocytes. Evidence for a novel delayed rectifier K⁺ current similar to Kv1.5 cloned channel currents. *Circulation research*, 73(6), pp.1061–1076.
- Whiteaker, K. et al., 2001. Validation of FLIPR Membrane Potential Dye for High Throughput Screening of Potassium Channel Modulators. *Journal of Biomolecular Screening*, 6(5), pp.305–312.
- Wickenden, A., Priest, B. & Erdemli, G., 2012. Ion channel drug discovery: challenges and future directions. *Future medicinal chemistry*, 4(5), pp.661–679.
- Wirth, K.J. et al., 2007. In vitro and in vivo effects of the atrial selective antiarrhythmic compound AVE1231. *Journal of cardiovascular pharmacology*, 49(4), pp.197–206.
- Wirth, K.J., Steinmeyer, K. & Ruetten, H., 2013. Sensitization of upper airway mechanoreceptors as a new pharmacologic principle to treat obstructive sleep apnea: investigations with AVE0118 in anesthetized pigs. *Sleep*, 36(5), p.699.
- Wolf, P.A. et al., 1998. Impact of atrial fibrillation on mortality, stroke, and medical costs. *Archives of internal medicine*, 158(3), pp.229–234.
- Zúñiga, L. et al., 2011. Gating of a pH-sensitive K₂P potassium channel by an electrostatic effect of basic sensor residues on the selectivity filter. *PloS one*, 6(1), p.e16141.

Abbreviations and Acronyms

A: Hydrogen bond acceptor.

AA: amino acids.

ADME: Absorption, distribution, metabolism and excretions.

AMS: Alanine mutagenesis screening.

At: *Arabidopsis thaliana*.

BD: Bottleneck diameter.

D: Hydrogen bond donor.

EIP: Extracellular ion pathway.

EIS: Experimental interaction score.

F: Fenestration.

FLIPR–MPA: Fluorometric imaging plate reader – Membrane potential assay.

Glide-XP: Extra precision Glide algorithm.

H: Hydrophobic group.

H-Bond: Hydrogen bond.

HRE: Halothane response element.

HTVS: High-throughput virtual screening.

IC₅₀: Half-maximal inhibitory concentration.

K⁺: Potassium ion.

K_{2p}: Two-pore domain potassium channel.

Kir: Inwardly rectifying potassium channels.

Kv1.5: Potassium voltage-gated channel

LCA: Last common ancestor.

LogP: Partition coefficient.

MDs: Molecular dynamics simulations.

MM/GBSA: Molecular Mechanics/Generalized Born Surface Area

M1-M4: Transmembrane domains.

N: Negative charged group.

OPLS: Optimized Potentials for Liquid Simulations.

P: Positive charged group.

PDB: Protein Data Bank.

POPC: Phosphatidyl oleoyl phosphatidylcholine.

P1-P2: Pore forming loops.

R: Aromatic ring.

RMSD: Root mean square deviation.

RMSF: Root mean square fluctuation.

RR: Red ruthenium.

SAR: Structure-activity relationship.

SASA: Solvent accessible surface area.

SF: Selectivity filter.

SPC: Single point charge – pre-equilibrated water molecules.

TASK: TWIK-related Acid Sensitive K⁺ channel.

TALK: TWIK-related Alkaline pH activated K⁺ channel.

TEA: Tetraethylammonium.

TEVC: Two-electrode voltage clamp

THPP: 5,6,7,8- Tetrahydropyrido [4,3-d] Pyrimidine.

THIK: Tandem pore domain Halothane Inhibited K⁺ channel.

TPK: Tandem-pore K⁺ channels.

TRAAK: TWIK-Related Arachidonic Acid stimulated K⁺ channel.

TREK: TWIK-Related K⁺ channel gene.

TRESK: TWIK-Related Spinal cord K⁺ channel.

TWIK: Tandem of P domains in a Weak Inwardly rectifying K⁺ channel.

T1treCC: Model of TASK-1 from TREK-2 in Closed-Closed fenestration state.

T1trCC: Model of TASK-1 from TRAAK in Closed-Closed fenestration state.

T1trCO: Model of TASK-1 from TRAAK in Closed-Open fenestration state.

T1twiOO: Model of TASK-1 from TWIK-1 in Open-Open fenestration state.

T3treCC: Model of TASK-3 from TREK-2 in Closed-Closed fenestration state.

T3trCC: Model of TASK-3 from TRAAK in Closed-Closed fenestration state.

T3trCO: Model of TASK-3 from TRAAK in Closed-Open fenestration state.

T3twiOO: Model of TASK-3 from TWIK-1 in Open-Open fenestration state.

VMD: Visual molecular dynamics.

Supplemental Information of Chapter II

12.1. Supplemental Tables.

Supplemental Table S1. Receptors grid information. Grid information for the receptor structures used for molecular docking simulations.

	Receptor	T1treCC	T1twiOO	T1trOO	T1trCO
Grid Box	x-Centre (Å)	-4.59	-5.75	-3.68	-3.68
	y-Centre (Å)	-19.23	-10.49	-10.43	-10.44
	z-Centre (Å)	23.99	23.50	24.69	24.69
	Outerbox (Å)	30.00	30.00	30.00	30.00

Supplemental Table S2. TASK-1 models interactions with A1899 poses from representative clusters.

Model	#	T 92		T 93		I 118		L 122		L 239		T 198		T 199		I 235		G 236		N 240		V 243		M 247		dG _{bind}	Score			
		Dis	Exp	Dis	Exp	Dis	Exp	Dis	Exp	Dis	Exp	Dis	Exp	Dis	Exp	Dis	Exp	Dis	Exp	Dis	Exp	Dis	Exp	Dis	Exp	kcal/mol	Interaction			
T1treCC	Clu: 1 Pop: 37	1	3.6	5.7	2.3	9.8	2.5	12.4	2.5	7.3	2.6	11.8	3.5	7.4	2.1	8.5			2.3	6.8	3.7	8.1	3.6	7.5			-70.2	85.3		
		2	3.4	5.7	2.2	9.8	2.6	12.4	2.5	7.3	2.7	11.8	3.5	7.4	2.4	8.5			2.2	6.8							-56.7	69.7		
		4			3.6	9.8			2.9	7.3	2.2	11.8	2.5	7.4	1.9	8.5			2.0	6.8	2.3	8.1	2.8	7.5			-54.6	67.3		
		11			2.1	9.8	2.1	12.4	2.7	7.3	2.6	11.8	3.0	7.4	2.1	8.5			2.3	6.8							-67.6	64.0		
		13			2.3	9.8	2.3	12.4	2.2	7.3	2.2	11.8	2.8	7.4	2.2	8.5			2.4	6.8							-62.3	64.0		
		14			2.2	9.8	2.5	12.4	2.7	7.3	2.8	11.8	2.9	7.4	2.1	8.5			3.9	6.8							-56.6	64.0		
		36	3.6	5.7	2.7	9.8	3.0	12.4	2.9	7.3	1.9	11.8	2.6	7.4	2.3	8.5			2.7	6.8	2.7	8.1					-53.5	77.8		
		37	3.2	5.7	2.1	9.8	2.5	12.4	2.6	7.3	2.4	11.8	3.0	7.4	2.1	8.5			2.3	6.8	3.7	8.1					-54.2	77.8		
		56	2.5	5.7	2.6	9.8	3.5	12.4	1.8	7.3	2.4	11.8	3.1	7.4	1.9	8.5			2.5	6.8	2.7	8.1					-54.9	77.8		
		60	3.2	5.7	3.5	9.8	3.3	12.4	2.1	7.3	2.1	11.8	3.1	7.4	1.9	8.5			2.4	6.8							-45.4	69.7		
		76			3.0	9.8			3.2	7.3	2.1	11.8	3.1	7.4	2.0	8.5	3.7	7.5	1.9	6.8	2.3	8.1	2.9	7.5					-55.6	74.8
		80	3.9	5.7	2.4	9.8	3.7	12.4	2.4	7.3	2.7	11.8	2.6	7.4	2.2	8.5												-46.1	62.9	
		99	3.7	5.7	2.6	9.8	3.3	12.4	3.3	7.3	1.9	11.8	2.8	7.4	2.2	8.5					3.0	6.8	3.0	8.1					-49.2	77.8
		105			3.7	9.8					2.5	11.8			2.5	8.5			2.4	6.8	2.4	8.1	1.9	7.5					NC	52.6
		106			3.8	9.8					2.5	11.8			2.4	8.5			2.3	6.8	2.4	8.1	1.9	7.5					-80.6	52.6
		108			2.2	9.8	3.8	12.4			2.0	11.8	2.7	7.4	2.9	8.5	3.1	7.5	2.2	6.8	2.3	8.1	3.9	7.5					-61.8	79.9
		109			3.7	9.8					2.6	11.8			2.2	8.5			2.6	6.8	2.7	8.1	2.0	7.5					-72.8	52.6
		119			3.3	9.8	3.0	12.4	2.0	7.3	2.3	11.8	3.5	7.4	3.1	8.5			2.3	6.8	2.3	8.1	2.5	7.5					-36.0	79.7
		121	2.7	5.7	3.1	9.8			1.9	7.3	2.7	11.8	3.8	7.4	2.1	8.5			2.7	6.8									-71.5	57.3
		122	2.7	5.7	3.1	9.8			1.9	7.3	2.7	11.8	3.6	7.4	2.1	8.5			2.7	6.8									-63.5	57.3
123			2.4	9.8	3.3	12.4	2.2	7.3	3.5	11.8	2.2	7.4	2.4	8.5			2.9	6.8	2.2	8.1	3.5	7.5					-50.2	79.7		

677			2.5 9.8	2.0 12.4	2.1 7.3	3.3 11.8			2.4 8.5			4.0 6.8					-42.3	56.7
681			3.7 9.8	2.4 12.4	2.3 7.3	2.4 11.8	3.0 7.4		3.4 8.5			3.1 6.8	3.3 8.1				-62.6	72.1
684	2.9 5.7		2.5 9.8	2.1 12.4	2.7 7.3	6.4 11.8			2.1 8.5								-89.2	55.5
688	2.5 5.7		2.3 9.8	2.0 12.4	2.5 7.3				2.6 8.5								-67.0	43.7
691			2.6 9.8	3.0 12.4	2.9 7.3	3.3 11.8	2.7 7.4		2.4 8.5			2.6 6.8					-56.0	64.0
693			3.5 9.8	2.1 12.4	2.2 7.3	2.9 11.8	2.7 7.4		2.7 8.5			2.6 6.8					-71.7	64.0
700	3.1 5.7		2.2 9.8	1.9 12.4	2.6 7.3				2.9 8.5								-58.2	43.7
705	3.9 5.7		1.9 9.8	2.0 12.4	2.3 7.3				3.1 8.5								-51.6	43.7
708	2.3 5.7		3.2 9.8	2.1 12.4	2.2 7.3				2.8 8.5								-53.1	43.7
709	2.3 5.7		2.6 9.8	1.9 12.4	2.0 7.3				2.6 8.5								-73.1	43.7
714			3.3 9.8	3.1 12.4	2.1 7.3	2.6 11.8	2.2 7.4		2.3 8.5			2.6 6.8					-61.3	64.0
716			2.9 9.8	3.1 12.4	2.2 7.3	2.5 11.8	2.3 7.4		2.3 8.5			2.7 6.8					-71.3	64.0
717			3.4 9.8	3.0 12.4	2.2 7.3	2.7 11.8	2.3 7.4		2.5 8.5			2.6 6.8					-77.2	64.0
721			3.4 9.8	2.7 12.4	2.3 7.3	2.2 11.8	2.5 7.4	3.1 8.5			2.7 6.8	4.1 8.1					-42.8	72.1
723			3.2 9.8	2.4 12.4	2.3 7.3	2.2 11.8	2.5 7.4	3.0 8.5			2.9 6.8	4.0 8.1					-31.4	72.1
724			3.0 9.8	2.8 12.4	2.2 7.3	2.2 11.8	2.5 7.4	3.1 8.5			2.7 6.8						-64.7	64.0
728			2.9 9.8	2.3 12.4	2.1 7.3	2.3 11.8	2.7 7.4	3.0 8.5			2.8 6.8	4.0 8.1					-47.7	72.1
729			2.4 9.8	2.2 12.4	2.3 7.3	2.0 11.8	2.5 7.4	2.7 8.5			2.8 6.8	4.0 8.1					-47.9	72.1
730	3.8 5.7		2.3 9.8	2.3 12.4	2.1 7.3	4.0 11.8	3.6 7.4	2.6 8.5			4.1 6.8						-59.2	69.7
735			2.9 9.8	2.2 12.4	2.7 7.3	2.1 11.8	2.2 7.4	2.7 8.5			3.0 6.8	3.7 8.1					-48.9	72.1
745			2.2 9.8	2.4 12.4	2.1 7.3	2.7 11.8	3.1 7.4	3.0 8.5			2.8 6.8						-42.3	64.0
746	2.2 5.7		2.8 9.8	2.1 12.4	2.1 7.3				2.6 8.5								-53.7	43.7
747			2.7 9.8	2.7 12.4	2.0 7.3	2.7 11.8	2.6 7.4	2.9 8.5	4.0 7.5		2.6 6.8						-28.3	71.6
751			3.3 9.8	2.4 12.4	3.3 7.3	2.4 11.8	3.4 7.4	3.8 8.5			3.1 6.8	3.0 8.1					-56.0	72.1
759	2.8 5.7		2.4 9.8	2.1 12.4	2.5 7.3			3.6 7.4	1.9 8.5								-76.7	51.1
760	2.5 5.7		2.8 9.8	2.1 12.4	2.3 7.3	3.8 11.8	4.0 7.4	1.8 8.5									-42.7	62.9
762			3.9 9.8	2.5 12.4	2.6 7.3	2.2 11.8	2.5 7.4	3.3 8.5			3.2 6.8						-61.1	64.0
763			3.2 9.8	2.3 12.4	2.5 7.3	2.1 11.8	2.6 7.4	3.3 8.5			3.5 6.8						-48.3	64.0
764			3.4 9.8	2.9 12.4	2.5 7.3	2.2 11.8	2.5 7.4	3.3 8.5			3.1 6.8						-54.0	64.0
765			3.4 9.8	2.0 12.4	2.7 7.3	2.1 11.8	2.3 7.4	3.1 8.5			3.1 6.8						-50.0	64.0
766			3.3 9.8	2.3 12.4	2.3 7.3	2.2 11.8	2.7 7.4	3.2 8.5			3.5 6.8						-53.5	64.0
767			3.5 9.8	2.3 12.4	2.5 7.3	2.5 11.8	2.3 7.4	2.9 8.5			2.5 6.8						-55.6	64.0
769	3.4 5.7		2.9 9.8	2.3 12.4	2.2 7.3	3.5 11.8	3.2 7.4	2.3 8.5									-53.4	62.9
772			3.3 9.8	2.3 12.4	3.6 7.3	2.6 11.8	2.5 7.4	3.3 8.5			2.9 6.8	3.9 8.1					-57.4	72.1
773			3.3 9.8	2.2 12.4	3.7 7.3	3.0 11.8	2.6 7.4	3.1 8.5			2.4 6.8						-54.9	64.0
774			3.3 9.8	2.4 12.4	3.6 7.3	2.8 11.8	2.5 7.4	3.1 8.5			2.8 6.8	4.1 8.1					-57.7	72.1
775	3.2 5.7		2.0 9.8	2.1 12.4	2.1 7.3				3.5 8.5								-57.1	43.7
776			2.3 9.8	2.1 12.4	2.1 7.3	2.6 11.8	3.3 7.4	2.7 8.5	3.9 7.5		3.4 6.8						-69.6	71.6
777			2.6 9.8	2.3 12.4	3.8 7.3	3.3 11.8	2.2 7.4	2.2 8.5			3.5 6.8						-70.3	64.0
778	2.8 5.7		2.4 9.8	2.1 12.4	2.2 7.3			3.6 7.4	1.8 8.5								-58.8	51.1
779			2.0 9.8	2.3 12.4	2.2 7.3	2.8 11.8	2.6 7.4	2.4 8.5			2.8 6.8						-50.2	64.0
781				2.1 12.4	3.0 7.3	2.9 11.8	3.1 7.4	2.6 8.5			2.6 6.8	4.0 8.1					-73.7	62.3
782				2.1 12.4	3.4 7.3	2.8 11.8	3.2 7.4	2.5 8.5			2.6 6.8	4.0 8.1					-81.9	62.3
783			3.8 9.8	2.0 12.4	3.6 7.3	3.0 11.8	3.1 7.4	2.6 8.5			2.6 6.8	4.0 8.1					-75.7	72.1
784			3.2 9.8	2.0 12.4		3.0 11.8	3.0 7.4	2.8 8.5			2.6 6.8						-71.9	56.8
785			3.3 9.8	2.0 12.4	3.3 7.3	2.7 11.8	2.9 7.4	2.8 8.5			2.8 6.8	3.9 8.1					-57.8	72.1
788			3.1 9.8	2.1 12.4		2.9 11.8	3.1 7.4	2.6 8.5			3.5 6.8						-77.9	56.8
794			2.7 9.8	1.8 12.4	2.3 7.3	3.1 11.8	3.2 7.4	2.3 8.5			2.8 6.8						-42.2	64.0
795	3.1 5.7		2.4 9.8	2.0 12.4	1.8 7.3			2.0 8.5									-55.0	43.7
796	3.0 5.7		2.0 9.8	2.1 12.4	2.3 7.3				2.3 8.5								-74.6	43.7
797			2.3 9.8	2.0 12.4	2.7 7.3				2.5 8.5								-66.1	38.0
798	3.2 5.7		3.0 9.8	2.0 12.4	2.5 7.3				2.5 8.5								-77.8	43.7
602			3.0 9.8	2.5 12.4	2.3 7.3	2.5 11.8	2.5 7.4		2.6 8.5								-43.0	57.2

Dis: Distance of interaction (Å), **Exp:** Interaction Scoring according with the experimental Alanine Scanning. **Clu:** Cluster. **Pop:** Population of the Cluster. **Red:** T1treCC. **Green:** T1twiOO. **Orange:** T1trOO. **Purple:** T1trCO. **Gray:** Cluster average structure. **Blue:** Poses with H-Bond interactions detected by measuring the distance between the atoms involved in the H-bond and analyzing the H-bond energetic contribution to the dG Bind . **NC:** Not Calculated.

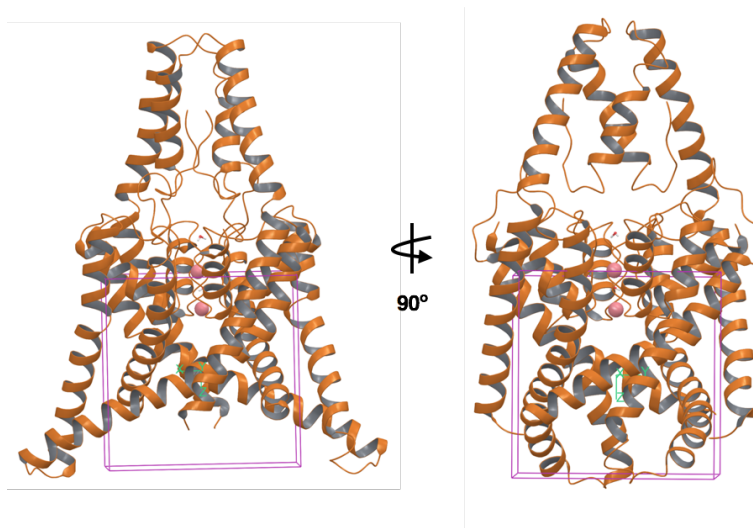
Supplemental Table S3. Clusters of A1899 poses.

T1treCC		T1twiOO		T1trOO		T1trCO	
No. Cluster	Pop.	No. Cluster	Pop.	No. Cluster	Pop.	No. Cluster	Pop.
1	37	17	67	36	26	57	93
2	31	18	45	37	26	58	16
3	23	19	25	38	20	59	13
4	23	20	15	39	18	60	12
5	19	21	9	40	17	61	11
6	14	22	7	41	15	62	7
7	11	23	6	42	12	63	5
8	10	24	5	43	11	64	5
9	8	25	4	44	10	65	5
10	7	26	4	45	9	66	3
11	7	27	4	46	7	67	3
12	6	28	2	47	6	68	3
13	1	29	1	48	5	69	2
14	1	30	1	49	5	70	2
15	1	31	1	50	3	71	2
16	1	32	1	51	3	72	2
		33	1	52	2	73	2
		34	1	53	2	74	1
		35	1	54	1	75	1
				55	1	76	1
				56	1	77	1
						78	1
						79	1
						80	1
						81	1
						82	1
						83	1
						84	1
						85	1
						86	1
						87	1
Pop. ave. = 12.50		Pop. ave. = 10.10		Pop. ave. = 9.52		Pop. ave. = 6.45	
$\delta = 11.2$		$\delta = 17.5$		$\delta = 8.0$		$\delta = 16.6$	

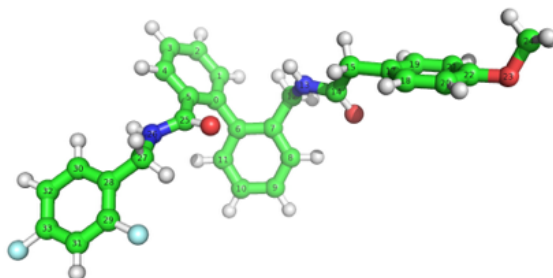
Pop.: Population; **Pop. ave.:** Population average; **δ :** Standard deviation

12.2. Supplemental Figures.

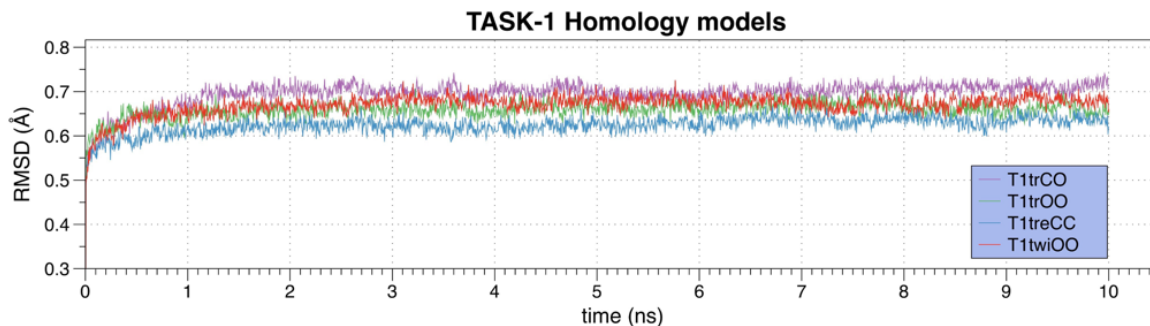
Supplemental Fig. S1. Grid box used in the docking simulations. T1twiOO homology model (orange cartoon representation) with K⁺ ions (pink sphere representation) and H₂O molecules (in CPK representation) in the selectivity filter. Grid box with the outer box edge setting as 30 Å.



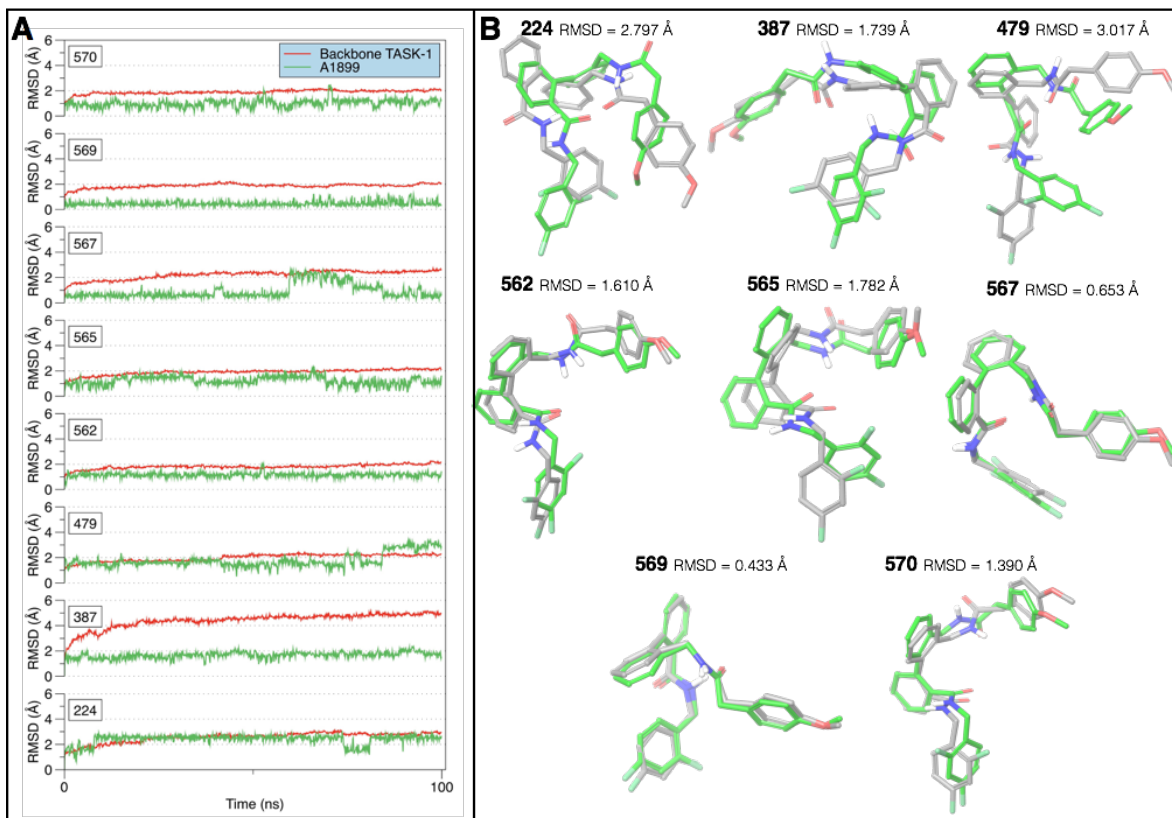
Supplemental Fig. S2. Chemical structure of A1899. 3D structure numbered according with the atoms used to calculate the RMSD matrix.



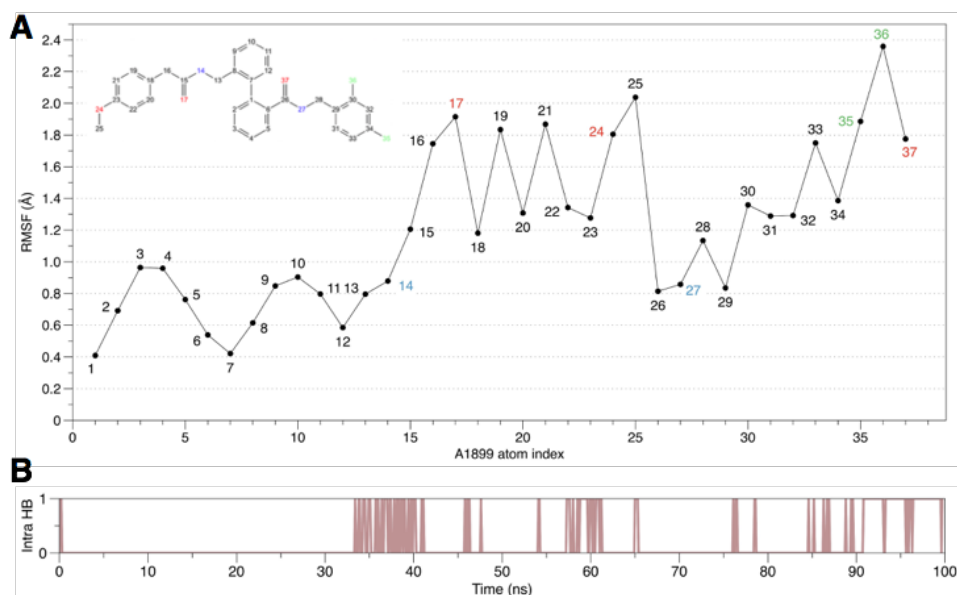
Supplemental Fig. S3. RMSD for backbones of TASK-1 models during the 10ns-MDs. RMSD for T1trCO, T1trOO, T1treCC and T1twiOO are represented in purple, green, blue and red respectively.



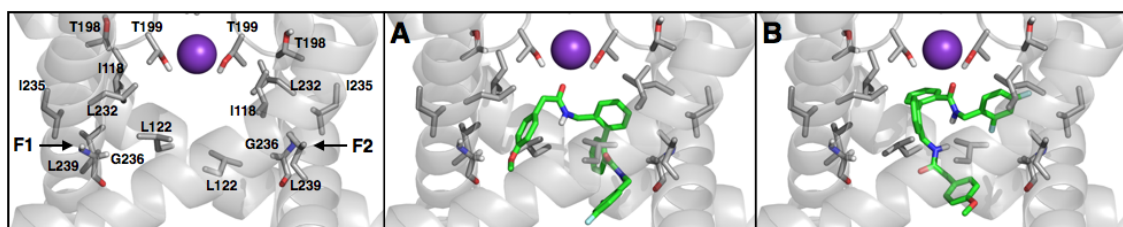
Supplemental Fig. S4. A. Time dependence of the RMSD for A1899 atoms (green) and TASK-1 backbone atoms (red) during the 100 ns unrestrained MDs for poses 224, 387, 469, 562, 565, 567, 579 and 570. Backbone atoms of the TASK-1 model interacting with the pose 387 exhibits a RMSD greater than the acceptable RMSD from the starting structure, which is about 3 Å (Law et al. 2005). **B.** Comparison between the starting conformations (gray) and the final conformations (green) of A1899 for poses 224, 387, 469, 562, 565, 567, 579 and 570 in the 100ns unrestrained MDs.



Supplemental Fig. S5. A1899 behavior during 100 ns unrestrained MDs (pose 479). **A.** *Root Mean Square Fluctuation (RMSF, black line) characterizes the internal atom fluctuations of A1899.* Only the fluorine atom (atom 36) exhibits a high RMSF (2.36 Å) indicating that A1899 remains in the binding site during the whole MDs. The number of the atoms are presented in the x-axis and in the structure. The RMSF is given in Å. **B.** *Number of internal Hydrogen Bonds (HB) within A1899.* A1899 presents one intra H-bond interaction between the Oxygen No. 17 and the Nitrogen No. 27. This interaction occurs 17% of the trajectory during the unrestrained MDs.



Supplemental Fig. S6. A1899 poses interacting with residues of the binding site placed in T1trOO at the fenestrations. A1899 and residues of the binding site are shown in stick representation, K^+ ion at S4 position is shown in sphere representation and T1trOO model in cartoon representation. Only segments M2 and M4 are display for better visualisation. A1899 pose nearest the centroid in: **A.** Cluster No. 36; **B.** Cluster No. 37; **C.** Cluster No. 38; **D.** Cluster No. 39 and **E.** Cluster No. 40.



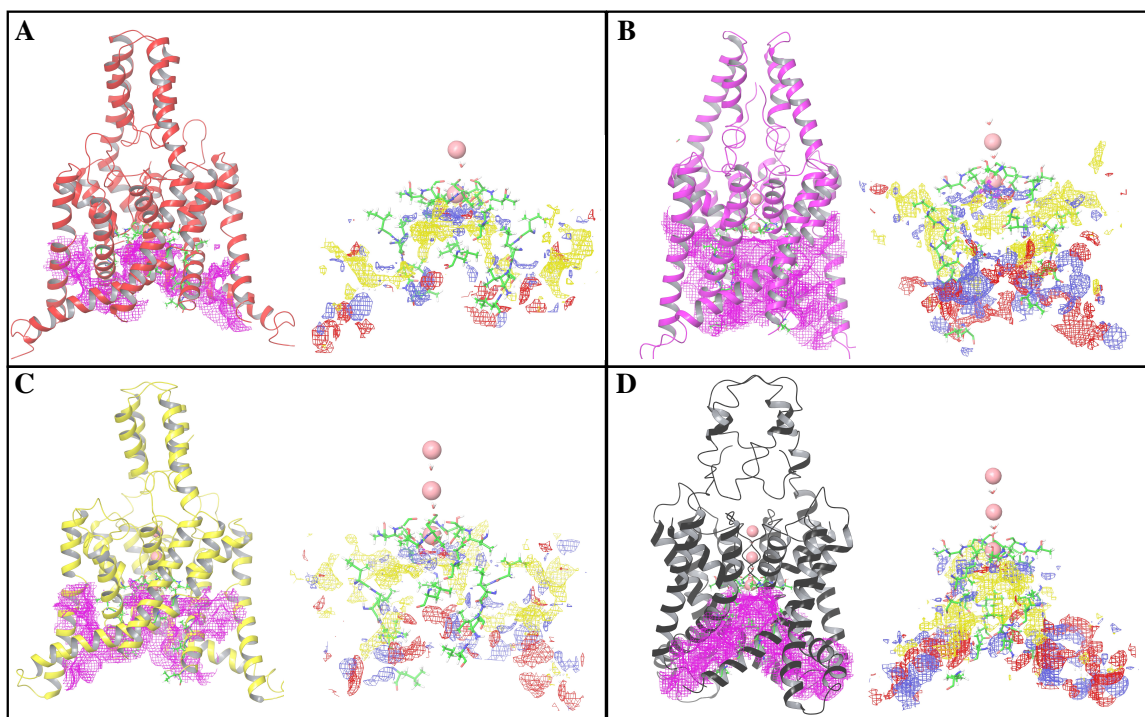
12.3. Supplemental References.

Law, R. et al., 2005. Membrane protein structure quality in molecular dynamics simulation.
Journal of Molecular Graphics and Modelling, 24(2), pp.157–165.

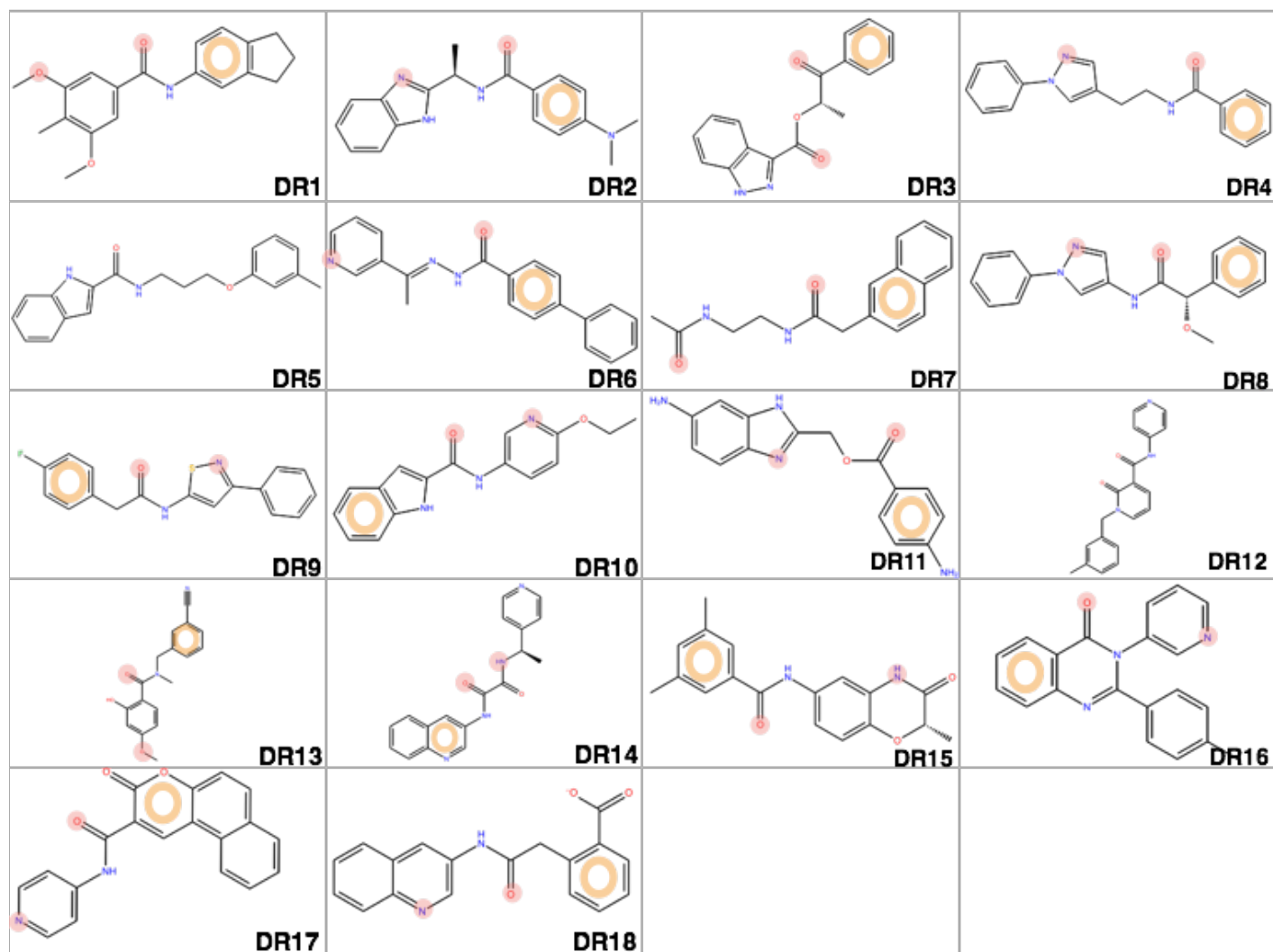
Supplemental Information of Chapter III

13.1. Supplemental Figures.

Supplemental Fig. S7. Active site prediction of TASK-3 models. Left: TASK-3 models with active site represented by mesh-magenta surface maps. The residues of A1899 binding site are shown in green sticks representation. Right: Zooms of the left ones, showing the entire predicted active site. The red-mesh surface is the H-bond acceptor area, the blue-mesh surface is the H-bond donor area, the yellow-mesh surface is the hydrophobic pocket and the magenta-mesh surface is the metal binding area. **A.** T3treCC, **B.** T3twiOO, **C.** T3trCO and **D.** T3trOO.



Supplemental Fig. S8. Identified hits ligands. The common pharmacophore is highlight as red circles (H-bond acceptor) and orange ring (aromatic ring).



Supplemental Fig. S9. Binding Site of A1899 in TASK-3 models. Residues of the binding site of A1899 integrate by T93, T199 of I118, L122, I235, G236, L239, N240, V243 and L247 (stick representation). For a better display of the residues, the models are rotated by 90° (right). Potassium ion is located in the S4 position in the selectivity filter showed in van der Waals representation **A.** T3treCC, **B.** T3twiOO, **C.** T3trCO and **D.** T3trOO.

